ADVANCES IN PHYSICS, 1989, VOL. 38, NO. 2, 89–188

Linear and nonlinear optical properties of semiconductor quantum wells

By S. SCHMITT-RINK
AT&T Bell Laboratories, Murray Hill, New Jersey 07974, U.S.A.

D. S. CHEMLA and D. A. B. MILLER
AT&T Bell Laboratories, Holmdel, New Jersey 07733, U.S.A.

[Received 14 January 1989]

Abstract

In this article we review the experimental and theoretical investigations of the linear and nonlinear optical properties of semiconductor quantum well structures, including the effects of electrostatic fields, extrinsic carriers and real or virtual photocarriers.

Contents

1. Introduction

The development of sophisticated growth techniques for layered semiconductor structures has stimulated a large body of new work in semiconductor physics over the last fifteen years or so. Undoubtedly, much of this interest was further stimulated by the possibility of novel physics and applications in electronic transport. New physical phenomena such as the integer and fractional quantum Hall effects have been discovered in inversion channels and heterostructures, and the first heterostructure electronic devices, such as modulation-doped field-effect transistors and heterojunction bipolar transistors, are now being commercially exploited. Linear optical spectroscopic techniques, such as absorption, luminescence and modulation spectroscopy, have for a long time been important tools in understanding the basic physics of semiconductor materials. Also over the last fifteen years or so, semiconductor optical and optoelectronic properties have become of increasing technological importance in their own right. The ever-growing application of semiconductor diode lasers and

related optoelectronic technology in communications and consumer products has helped to give yet further impetus to research on semiconductor optical properties. III–V semiconductor heterostructures have benefited particularly; direct band-gap materials and layered heterostructures are both essential for efficient laser diodes, even with 'bulk' semiconductor materials. Quantum well laser diodes, further enhanced by the quantum confinement in ultrathin layers, are now of serious practical interest also. The successes of semiconductor optoelectronics and promising physical mechanisms and novel devices using quantum-confined structures have, furthermore, enlivened the debate over possible applications of optics for other functions such as logic and switching in communications and computation.

This article reviews the physics of the optical properties of semiconductor microstructures, with emphasis on quantum wells and on the consequences of electric fields and carrier populations created either optically or by doping. The growth of interest in the physics of optical effects in confined semiconductors, especially over the last six years, is a result partly of the technological climate discussed above and also of a happy coincidence of several other factors including: the availability of high-quality, sophisticated, layered III–V structures; advances in the performance and convenience of short-pulse laser technology; and advances in physical understanding of many-body effects in semiconductors in general. The emphasis on quantum wells here is a reflection both of the availability of experimental samples, and of the fact that, being essentially a single-layer structure, the quantum well is one of the simplest structures showing clear quantum confinement effects. Quantum wells have therefore served as a useful model system for quantum confinement. Where possible, in this article we attempt to extrapolate to higher-dimensional confinement, although there is little experimental data here because of the lack of a suitable flexible and reproducible fabrication technology. Other structures with quantum confinement effects in one direction, such as superlattices with strong quantum-mechanical coupling between adjacent layers, are now starting to receive more interest for their optical properties, although the volume of work is still relatively small.

It is important to emphasize at the outset that quantum confinement and layered structures produce not only quantitative but also qualitative differences in physics from that in bulk structures, which is of course another major motivation for the interest in them. There are many examples of these differences. The optical absorption spectrum breaks up into a series of steps associated with the quantum-confined electron and hole levels. Excitonic effects become much stronger because of the quantum confinement, giving clear absorption resonances even at room temperature. The relative importance of direct Coulomb screening and exchange effects is quite different in quantum wells (the Coulomb screening is relatively much weaker), giving very different optical saturation behaviour. Modulation doping, which is only possible with layered structures, allows high concentrations of electrons without any impurity scattering, leading to the observation of Fermi-level correlation singularities, a phenomenon (to our knowledge) never clearly observed in bulk semiconductors. Electroabsorption is totally different from that in bulk semiconductors because of the confinement of the excitons, resulting in very large shifts of optical absorption peaks (the quantum-confined Stark effect). Semiconductors already offer an interesting laboratory to study hydrogenic systems at very high density and high electric fields through the nonlinear optics and electro-optics associated with excitons; quantum confined structures allow us to extend this laboratory to include confinement to within less than one hydrogenic diameter, a regime currently totally impossible with an actual hydrogen atom.

In this review, we start with a summary of the basic linear optical properties of quantum wells and related higher-dimensional structures, such as quantum 'wires' and 'dots' (or 'boxes') (section 2.1). We will concentrate throughout the article on the interband optical properties, although intersubband effects are now starting to receive more attention. Section 2.2 on the effects of electric fields on the linear optical properties requires a basic understanding of section 2.1, but otherwise can be read independently of the rest of the article because many-body effects are not involved here. It attempts to give a consistent picture of electroabsorption in quantum confined structures that can also be related to bulk electroabsorption. In sections 2.3 and 3.1, we have treated the effects of carrier populations on the optical properties in a unified manner, whether the carriers are of a single species created by (modulation) doping (section 2.3) or are created optically (section 3.1), because the physics is fundamentally linked by the many-body theory and effects, even although the doped effects are linear optics and the optically-created effects are nonlinear optics. Section 3.2 covers the effects of virtual populations (which can only be created optically) on the optical properties, continuing the many-body formalism and showing that, except for relaxation, virtual populations behave and obey the same physics as real ones. Finally in section 3.3, we examine nonlinear optical effects in the presence of an electric field, including both 'real' and 'virtual' population phenomena. We draw our conclusions in section 4.

2. Linear optical properties

2.1. *Excitons in semiconductor quantum wells*

In this article, we are mainly interested in III–V heterostructures that interact strongly with photons of energy close to their band gap. Hence we shall consider only so-called type-I structures, for which the bottom of the conduction band and the top of the valence band occur in the same material. Furthermore, since we are interested in the effects of reduced dimensionality on the optical properties, we shall concentrate on optical processes involving electronic excitations which are well confined in the low-gap material. Such a strong confinement occurs for large band-gap discontinuities at the hetero-interfaces and for low-gap layers spatially well separated. We shall call the low-gap layers quantum wells (QWs) and the large-gap layers, barrier layers (BLs). A sketch of a multilayer structure that consists of a stack of alternate QWs and BLs is shown in figure 1. For the case of strong confinement, which we are considering, the interaction between the lowest energy states of adjacent QWs is negligible. Thus, for the most relevant optical processes in the vicinity of the gap, it is possible to consider the QWs as independent. In direct gap semiconductors, the optical transitions close to the fundamental gap are governed by excitonic effects, that is, the final-state interaction between photoexcited electrons and holes plays an important role. The correct description of optical processes in type-I structures should therefore account for both excitonic and confinement effects. This is a very difficult task, which has not yet been completed, but numerous experimental investigations have been performed yielding a large amount of reliable data, so that the main features of linear optical effects in type-I structures are relatively well known. They have been explained with satisfactory accuracy by models based on the effective mass approximation (EMA). To introduce the main results as physically as possible we shall proceed as follows. Since exciton wavefunctions are built up from combinations of electron and hole single-particle wavefunctions, we first summarize the effects of confinement on the single-particle states. Then we will consider excitonic effects in the ideal limit of

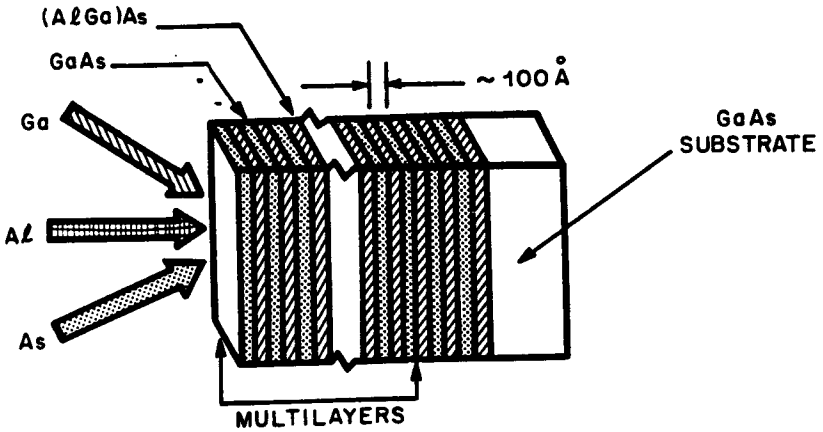

Figure 1. Schematic of a GaAs/AlGaAs multiple quantum well structure.

a pure two-dimensional motion of electrons and holes with a $1/r$ Coulomb interaction. Finally, we will consider the case of real QW structures; we will present some typical experimental data and discuss how the two idealized situations described first must be combined and amended to explain the experimental results.

In QWs the electrons (e) and holes (h) are free to move in the plane of the layers (x, y) whereas their motion along the normal to the layers (z) is strongly affected by the potential discontinuities at the interfaces. Although in the best current heterostructures the band gap can experience large discontinuities over distances of the order of the primitive cell parameters, it is found that the single-particle states are well described within the EMA. According to this approximation, the carrier dynamics are determined by the band parameters of the bulk compounds, such as the effective masses. When the Coulomb interaction is neglected, the motions in the plane and along the normal are independent.

To get a general insight into the effects of confinement on the single-particle states, it is useful to consider first the idealized case of a cuboidal sample limited by infinitely high potential barriers. The sample dimensions L_x, L_y and L_z are comparable to the characteristic lengths governing the carrier dynamics; namely the de Broglie wavelength or Bohr radius. It is customary to call such a sample a quantum box (QB) because quantum size effects occur in all directions. We will derive the energy structure of a QB and follow the evolution to higher dimensions by letting the length, width and height go to infinity. The electron and hole wavefunctions are sinusoidal inside the sample and vanish outside; they can be written as

$$\psi^{e,h}_{n_x,n_y,n_z} = \psi^{e,h}_{n_x}(x)\psi^{e,h}_{n_y}(y)\psi^{e,h}_{n_z}(z), \tag{2.1.1}$$

with $\psi^{e,h}_{n_z}(z) = (2/L_z)^{1/2}\sin(k_z z)$ and similar expressions in the other two directions. The wavenumbers are quantized according to $k_j = \pi n_j/L_j$, $j = x, y, z$, both for electrons and holes. They form a complete orthogonal set with a discrete spectrum,

$$E^{e,h}_{n_x,n_y,n_z} = \tfrac{1}{2}E_g + E^{e,h}_{n_x} + E^{e,h}_{n_y} + E^{e,h}_{n_z}, \tag{2.1.2}$$

where E_g is the band gap and the confinement energies in the three directions are $E^{e,h}_{n_j} = (\pi n_j/L_j)^2/(2m_{e,h})$, m_e and m_h being the electron and hole effective masses (in the

j direction if the medium is anisotropic). (Throughout the article $\hbar = k_B = 1$ is used.) Owing to the orthogonality of the wavefunctions, optical transitions obey the selection rule that the electron and hole quantum numbers must be identical, that is, only transitions with $(n_x, n_y, n_z)^e = (n_x, n_y, n_z)^h$ are allowed. The corresponding zero-dimensional (0D) joint density of states (DOS) consists of a series of δ-functions,

$$\varrho^{0D}(\omega) = 2 \sum_{n_x,n_y,n_z} \delta(\omega - E^e_{n_x,n_y,n_z} - E^h_{n_x,n_y,n_z}), \tag{2.1.3}$$

where the factor 2 in front of the sum accounts for spin degeneracy. The above formulae are used in elementary text books to discuss energy levels in periodic media. A one-dimensional (1D) sample or 'quantum wire' is obtained by letting the length, say L_y, go to infinity. Then the wavenumbers, k_y, span a continuum and the energy associated with it becomes $E^{e,h}_{n_y} \to k_y^2/(2m_{e,h})$. The resulting one-dimensional DOS per unit length is

$$\varrho^{1D}(\omega) = \frac{1}{2\pi}(2m)^{1/2} \sum_{n_x,n_z} (\omega - E_g - E^e_{n_x} - E^e_{n_z} - E^h_{n_x} - E^h_{n_z})^{-1/2}, \tag{2.1.4}$$

where m is the electron–hole reduced mass ($m^{-1} = m_e^{-1} + m_h^{-1}$). $\varrho^{1D}(\omega)$ exhibits van Hove singularities at the onset of each transition. For a 'quantum well' sample, one has to let in addition the width of the sample, say L_x, go to infinity. Now k_x and k_y span a two-dimensional continuum and $E^{e,h}_{n_x} + E^{e,h}_{n_y} \to (k_x^2 + k_y^2)/(2m_{e,h})$. The two-dimensional (2D) DOS per unit area is

$$\varrho^{2D}(\omega) = \frac{m}{\pi} \sum_{n_z} \theta(\omega - E_g - E^e_{n_z} - E^h_{n_z}), \tag{2.1.5}$$

where $\theta(E)$ is the Heaviside function ($\theta = 0$ for $E < 0$, $= 1$ for $E > 0$). The 2D DOS has a step-like structure with constant plateaus for each of the allowed $n_z^e = n_z^h$ transitions. Finally, the usual three-dimensional (3D) behaviour is obtained when the height goes to infinity as well. Then $\mathbf{k} = (k_x, k_y, k_z)$ spans a 3D continuum and the e and h energies are simply $E^{e,h}_{n_x,n_y,n_z} \to E_g/2 + k^2/(2m_{e,h})$. The 3D DOS takes on the well known form

$$\varrho^{3D}(\omega) = \frac{1}{2\pi^2}(2m)^{3/2}(\omega - E_g)^{1/2}. \tag{2.1.6}$$

The evolution of the joint DOS from 0D to 3D is clear. The discrete lines of the 0D system become more and more densely packed as one of the sample dimensions becomes larger. When the sample becomes infinite in one direction, the corresponding states finally merge to form a continuum. (An example of this evolution as it affects the absorption spectrum is given below in figure 16 for a GaAs-like quantum box (Miller *et al.* 1988).) In figure 2 we show an example of a 2D and a 3D DOS. In this simplified case, at the onset of each transition, the 2D DOS is equal to the 3D DOS.

Let us now consider the case of real semiconductor QWs for which the confinement potential corresponding to the conduction and valence band discontinuities, $\Delta E_{c,v}$, is finite. The wavefunctions can now penetrate the barriers and in each band there is only a limited number of confined states with energies smaller than $\Delta E_{c,v}$. The wavefunctions are sinusoidal in the QW and exponentially decreasing in the BL (Ando *et al.* 1982). In analogy with the infinitely confined case, these states can still be labelled by a 'normal motion' quantum number, $n_z = 1, 2, \ldots$. There are also states with energy larger than the band discontinuities. They form extended (3D)

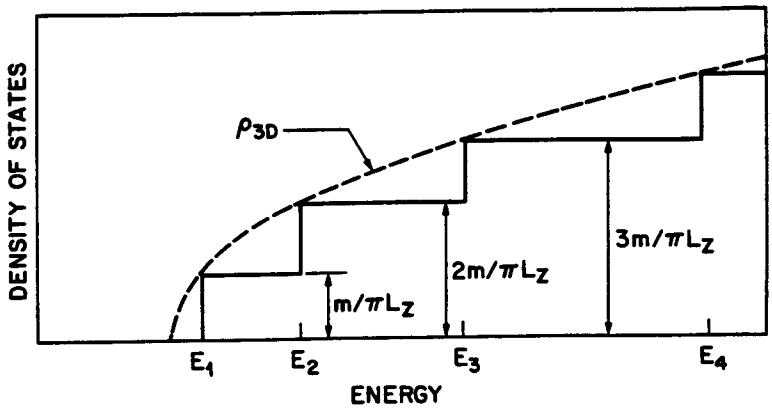

Figure 2. Single-particle density of states in 3D and in an infinite quantum well with thickness L_z.

continua in which the density of states shows resonances at specific energies analogous to resonances of an optical cavity (Bastard 1984).

The wavefunctions in the z direction, $\psi_{n_z}^{e,h}$, obey the 1D Schrödinger equation,

$$-\frac{\partial}{\partial z_{e,h}}\frac{1}{2m_{e,h}}\frac{\partial \psi_{n_z}^{e,h}}{\partial z_{e,h}} + V_{e,h}(z_{e,h})\psi_{n_z}^{e,h} = E_{n_z}^{e,h}\psi_{n_z}^{e,h}, \tag{2.1.7}$$

where $V_{e,h}(z_{e,h})$ is the structural potential that describes the band discontinuities. In equation (2.1.7) the masses $m_{e,h}$ depend on z since they are not the same in the QW and in the BL. The resulting boundary conditions describe the conservation of the probability density and probability current across the hetero-interfaces (Bastard and Brum 1986). The solution of equation (2.1.7) is straightforward. The quantum number n_z which labels the states of the discrete spectrum has a simple interpretation. It determines the number of nodes, $(n_z - 1)$, of the wavefunctions $\psi_{n_z}^{e,h}$. These states are less bound than the corresponding states of the infinite well and their number is equal to one plus the number of states of the infinite well with energy smaller than $\Delta E_{c,v}$. A sketch of the potential variation in the z direction and of a set of corresponding wavefunctions is shown in figure 3.

The motion in the plane of the QW is very simple for the electrons which originate from the non-degenerate Γ minimum of the bulk conduction band. For them, the in-plane wavefunctions are plane waves with a parabolic dispersion corresponding to the bulk effective mass, m_e. The behaviour of the holes is much more complicated. In bulk III–V compounds the top of the valence band consists of a $J = \frac{3}{2}$ upper valence band multiplet and a $J = \frac{1}{2}$ lower valence band which is depressed by the spin–orbit splitting (Luttinger and Kohn 1955, Dresselhaus *et al.* 1955). The $J = \frac{3}{2}$ bands are degenerate at the zone centre, but are separated for $k > 0$ because of the smaller curvature of the $J_z = \pm\frac{3}{2}$ (heavy hole; hh) component as compared with that of the $J_z = \pm\frac{1}{2}$ (light hole; lh) one. A correct description of the holes should treat on equal footing the $\mathbf{k}\cdot\mathbf{p}$ perturbation and the confinement. This can be done only numerically. Sticking to our approach, we will proceed by successive approximations to get an insight into the physics involved and only then will we give the results of some full numerical treatments.

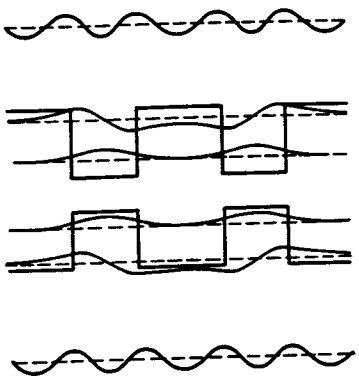

Figure 3. Potential variation and single-particle wavefunctions normal to the quantum well plane.

Near the zone centre, the dispersion of the $J = \frac{3}{2}$ multiplet is described by the Luttinger Hamiltonian (Luttinger 1956),

$$H = \frac{1}{2m_0}[(\gamma_1 + 5\gamma_2/2)k^2 - 2\gamma_2(k_x^2J_x^2 + k_y^2J_y^2 + k_z^2J_z^2) - 4\gamma_3((k_xk_y + k_yk_x)(J_xJ_y + J_yJ_x)) + \ldots], \quad (2.1.8)$$

where $\gamma_{1,2,3}$ are the Luttinger parameters and m_0 is the free electron mass. For most of the III–V heterostructure growth, the epilayers are such that the normal is along one of the bulk crystal axis (used as substrate), that is $z \parallel [001]$. One sees from equation (2.1.8) that in this direction the masses in the bulk corresponding to the $J_z = \pm\frac{1}{2}$ and $J_z = \pm\frac{3}{2}$ components are $m_z = m_0/(\gamma_1 \pm 2\gamma_2)$ respectively. If one uses these masses in equation (2.1.7) to calculate the energies of the holes in the z direction, it is found that the confinement lifts the degeneracy of the upper multiplet giving two separate bands, a $J_z = \pm\frac{3}{2}$ hh subband with $m_{z,\mathrm{hh}} = m_0/(\gamma_1 - 2\gamma_2)$ and a $J_z = \pm\frac{1}{2}$ lh subband with $m_{z,\mathrm{lh}} = m_0/(\gamma_1 + 2\gamma_2)$. For example, in the case of an infinite well, the energies of the first hh and lh states at $k_{x,y} = 0$ are $E_1^{\mathrm{hh}} = (\pi/L_z)^2/(2m_{z,\mathrm{hh}})$ and $E_1^{\mathrm{lh}} = (\pi/L_z)^2/(2m_{z,\mathrm{lh}})$. To gain insight into the origin of the complex in-plane behaviour, let us first neglect the effects of the confinement on the dispersion and assume for a moment that the hh and lh do not interact. Then, putting $k_z = k_y = 0$ and $k_x \neq 0$ in equation (2.1.8), one finds from the Luttinger Hamiltonian that the lh and hh have a parabolic dispersion with a reversal of curvature. The corresponding masses are $m_{xy,\mathrm{lh,hh}} = m_0/(\gamma_1 \mp \gamma_2)$, that is, in the plane the light hole ($J_z = \pm\frac{1}{2}$) is heavier than the heavy hole ($J_z = \pm\frac{3}{2}$). Within this oversimplified approximation, the two bands will cross for some $k_{x,y} > 0$. Again for the infinite well, the results can be expressed analytically. In this case the band crossing occurs at $k = \pi\sqrt{2}/L_z$. This situation is of course unphysical and, when one accounts for the $\mathbf{k}\cdot\mathbf{p}$ terms and the confinement potential, the crossing is removed. The resulting anti-crossing produces a strongly non-parabolic in-plane dispersion with rather flat hh bands and band mixing (Chang and Schulman 1983), that is, in each band the character of the hole close to $k = 0$ is reversed for $k \gg \pi\sqrt{2}/L_z$. The full diagonalization of the hole Hamiltonian is complicated but straightforward and must be carried out numerically

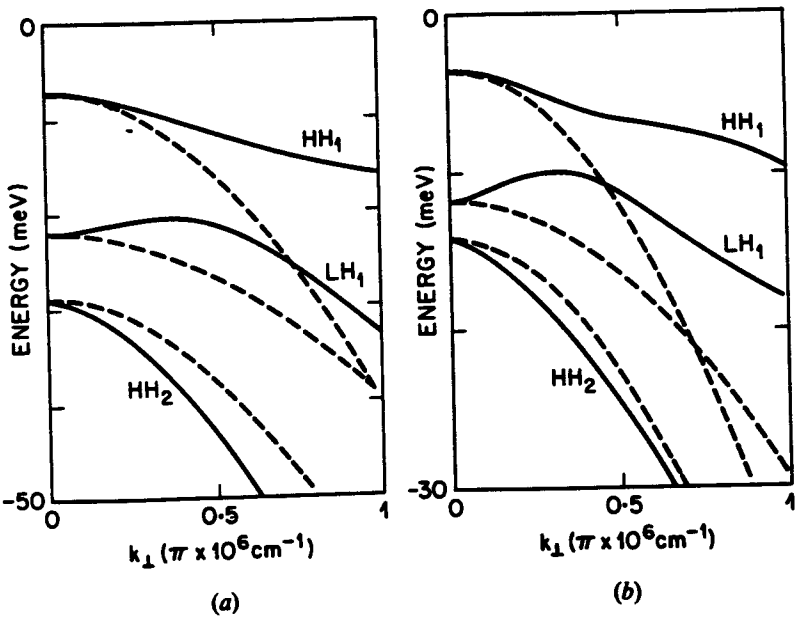

Figure 4. In-plane valence band dispersion against wave-vector for two GaAs/$Al_{0.3}Ga_{0.7}As$ quantum wells (L_z = 100, (*a*) and 150 Å, (*b*)). The dashed lines show the dispersion when band mixing is neglected. (After Bastard and Brum (1986).)

(Ekenberg and Altarelli 1984, Broido and Sham 1985, 1986, Bastard and Brum 1986). The main results confirm the above intuitive discussion. This is shown in figure 4 where valence band in-plane dispersion curves of 100 and 150 Å GaAs QWs calculated by Bastard and Brum (1986) are presented. The solid lines give the non-parabolic behaviour of the $n_z = 1$ hh and lh and the $n_z = 2$ hh. It is seen how the $n_z = 1$ hh band is flattened; furthermore, because of the strong effect of the $n_z = 2$ hh band, the $n_z = 1$ lh band exhibits a camel-back shape (Ekenberg and Altarelli 1984). The dashed lines indicate the parabolic dispersion and show the band crossing that would occur if the hole subbands did not interact.

The strength of optical transitions is given by the product of the square of the interband dipole matrix element ($|er_{cv}|^2$), the e–h envelope function overlap integral and the joint DOS, $\varrho(\omega)$. Thus, within the single-particle picture, the absorption spectrum consists of a set of continua corresponding to transitions between the various valence and conduction subbands. For a 2D parabolic dispersion valid close to $k = 0$, we can use equation (2.1.5) for the joint DOS. The absorption spectrum comprises a series of steps for the hh $\rightarrow$ e and lh $\rightarrow$ e transitions with height m/π, where m is the proper reduced e–h mass ($m^{-1} = m_e^{-1} + m_{hh,lh}^{-1}$). Close to $k = 0$, where the hh and lh character is well defined, the squares of the interband dipole matrix elements from the hh and lh subbands to the e subbands are proportional to $\frac{3}{4}$ and $\frac{1}{4}$ respectively, when the optical field is polarized parallel to the plane of the QW, and proportional to 0 and 1 for a field normal to it. Owing to the difference of masses, the e and h wavefunctions do not penetrate equally into the barriers, causing a breakdown of the $\Delta n_z = 0$ selection rule. However, the $n_{e,z} \neq n_{h,z}$ transitions usually remain weak. They are often referred to as 'forbidden transitions'.

The absorption spectrum is of course modified by the e–h Coulomb interaction. In bulk semiconductors, this interaction produces a hydrogenic series of excitonic peaks below the band edge, and a correlation enhancement in the continuum above it. The exact description of excitons in confined structures is complicated and a number of simplifying approximations are necessary to make the problem tractable. Throughout this article we shall use natural units of energy and length which we will express in terms of the 3D Rydberg $R = (e^4 m)/(2\epsilon_0^2)$ and Bohr radius $a_B = \epsilon_0/(me^2)$, where ϵ_0 is the static dielectric constant of the medium and m is the e–h reduced mass.

As in the case of single-particle states, we will first make some general comments on the effects of reduced dimensionality on the electrostatic interaction before specializing to QW. Let us note first that the form of the Coulomb potential itself may be substantially modified if the microstructure is embedded in a medium with a very different dielectric constant. These local field or image force effects can be important if the dielectric discontinuity is large (Bottcher 1973, Brus 1986). The general expression of the Coulomb interaction between two charges in a layer thinner than the 3D Bohr radius has been discussed by Keldysh (1979). He showed that its functional form is significantly affected if the dielectric constant of the layer and the surrounding medium are very different. However, if they are close, the Coulomb interaction varies indeed like r^{-1}, except for very short distances. Luckily the QWs fabricated up to now consist of alternate layers (QW and BL) of materials with very close dielectric constants. In this case there is no dielectric confinement, only the particle motion is modified. Consequently, we will limit ourselves to the ideal case of e and h interacting through an $I(r) = e^2/(\epsilon_0 r)$ potential, assuming that the QW is surrounded by a medium with identical dielectric constant.

For a cuboidal sample of dimension L, the Coulomb energy varies as L^{-1} whereas the confinement energy varies as L^{-2}. Hence, as the size decreases the Coulomb energy becomes relatively negligible. In the limit of microscopic cuboids the Coulomb interaction is too weak to affect the wavefunctions which are almost completely governed by the confinement (Brus 1986, Schmitt-Rink *et al.* 1987, Bryant 1987, 1988). It is natural to call this situation the 'regime of strong confinement'. In addition, when the Coulomb force produces bound states one can view the bound e–h pairs as 'Coulomb confined' systems. The notion of strong confinement results then from the comparison of the Coulomb confinement with that due to the crystal potential. If we consider now the cases where the particles are free to move in 1D, 2D or 3D, the Coulomb attraction is fully effective in these directions and even if the other directions are in the strong confinement regime, there will be excitonic effects. The Coulomb potential is singular at $r = 0$; therefore if e and h have a non-zero probability to be at the same point in space, the energy is infinite. As shown below, this singularity can be dealt with in 2D and 3D but it produces some difficulties in the 1D case. If the e–h relative motion is described by the wavefunction $\phi(r)$, the radial probability to have the e and the h at a relative distance r is $P(r)\,dr = |\phi(r)|^2\,d_{nD}r$, where $d_{nD}r$ is the element of volume in $n = 1$, 2 and 3D. In 2D and 3D this gives $P_{2D}(r) = 2\pi r|\phi(r)|^2$ and $P_{3D}(r) = 4\pi r^2|\phi(r)|^2$ respectively. Therefore, even if $\phi(r = 0) \neq 0$, the probability of having the two particles at the same place vanishes. This explains why the binding energy of hydrogenic s states is finite in 2D and 3D. Conversely, in 1D the element of volume does not appear in the relative probability distribution, $P_{1D}(x) = |\phi(x)|^2$, giving an infinite binding energy for s states (Loudon 1959, Haines and Roberts 1969). To avoid this difficulty one has to remove the singularity of the Coulomb potential

by introducing a cut-off in the potential, namely $I(x) \to 1/(x + x_0)$ (Loudon 1959). It is then found that the binding energy and wavefunction of the ground state depend critically on the cut-off distance x_0 (Haines and Roberts 1969). Luckily such difficulties do not appear in 2D which we consider now.

The theory of excitons in 3D semiconductors is extremely well documented (Knox 1963, Dimmock 1967); it turns out that for the case of a pure 2D motion and $I(r) = e^2/(\epsilon_0 r)$, the e–h interaction can also be solved exactly (Shinada and Sugano 1966). It is found that the 2D and 3D cases are formally similar. In the next paragraphs, in order to follow the effects of reduction of dimensionality on the exciton structure, we will discuss the general framework of the formalism and establish parallels between the most relevant quantities in the two cases.

Excitonic states can be expressed as a linear combination of e–h pair states

$$|\text{pair}\rangle = c_e^+(\mathbf{k}_e)c_h^+(\mathbf{k}_h)|g\rangle, \tag{2.1.9}$$

where $c_{e,h}^+(\mathbf{k}_{e,h})$ are electron and hole creation operators and $|g\rangle$ is the crystal ground state with an empty conduction band and a full valence band. To discuss optical transitions, it is convenient to make a transformation to the centre of mass and relative motions. This introduces the wave-vector of the centre of mass, $\mathbf{K} = \mathbf{k}_e + \mathbf{k}_h$, that is, the 'total' momentum of the pair, and $\mathbf{k} = (m_h\mathbf{k}_e - m_e\mathbf{k}_h)/(m_h + m_e)$ which is the Fourier conjugate of the relative distance coordinate ($r = r_e - r_h$). In optical transitions we can neglect the photon momentum, so that for photogenerated excitons $\mathbf{K} = 0$, $\mathbf{k} = \mathbf{k}_e = -\mathbf{k}_h$, and we can write for the exciton wavefunction

$$|X_n\rangle = \sum_{\mathbf{k}} \phi_n(\mathbf{k})c_e^+(\mathbf{k})c_h^+(-\mathbf{k})|g\rangle. \tag{2.1.10}$$

To simplify the notations we do not mention explicitly spin composition and indices. $\phi_n(\mathbf{k})$ is the exciton wavefunction in k-space; it obeys the Schrödinger–Wannier equation describing the e–h relative motion in k-space (Haug and Schmitt-Rink 1984),

$$E_n\phi_n(\mathbf{k}) = (\epsilon_{ek} + \epsilon_{hk})\phi_n(\mathbf{k}) - \sum_{\mathbf{k}'} I(\mathbf{k} - \mathbf{k}')\phi_n(\mathbf{k}'), \tag{2.1.11a}$$

where E_n is the relative motion energy, $\epsilon_{e,hk} = E_g/2 + k^2/(2m_{e,h})$ are the single-particle energies, and $I(q)$ is the bare e–h Coulomb interaction expressed in k-space, $I_{3D}(q) = 4\pi e^2/\epsilon_0 q^2$ and $I_{2D}(q) = 2\pi e^2/\epsilon_0 q$, screened only by the static dielectric constant of the material, ϵ_0. The expressions for $I(q)$ differ in the two cases because of the dependence of Fourier transforms on dimensionality. The index n runs over the discrete (bound states) as well as over the continuous (scattering states) spectrum. To prepare the discussion on nonlinear optical processes, let us rewrite equation (2.1.11a) in a slightly different form. We introduce the unperturbed Hamiltonian describing the relative e–h motion, $H^0_{\mathbf{k},\mathbf{k}'} = [\epsilon_{ek} + \epsilon_{hk}]\delta_{\mathbf{k},\mathbf{k}'} - I(\mathbf{k} - \mathbf{k}')$, and write

$$\sum_{\mathbf{k}'} [H^0_{\mathbf{k},\mathbf{k}'} - E_n\delta_{\mathbf{k},\mathbf{k}'}]\phi_n(\mathbf{k}') = 0. \tag{2.1.11b}$$

In most of the theoretical texts on linear absorption of excitons (Knox 1963, Dimmock 1967) one returns to the r-space representation at this point of the discussion. This is done by a Fourier transformation of the exciton wavefunction and the Schrödinger equation. In real space the exciton wavefunction is $\phi_n(r)$,

$$\phi_n(r) = \sum_{\mathbf{k}} \exp(i\mathbf{k}\cdot\mathbf{r})\phi_n(\mathbf{k}). \tag{2.1.12}$$

$\phi_n(r)$ obeys the well known hydrogenic Schrödinger equation and all discussion is usually limited to the r-space representation where the analogy with the hydrogen atom can be fully exploited. Of course, the two representations have the same physical content and, as shown in the next sections, it is better to stay in k-space for treating the nonlinear optical processes and many-body effects associated with large densities of carriers. The reason for this is that in crystals only k is a 'good quantum number' so that the exclusion principle and other fundamental mechanisms that affect the excitons are more naturally expressed in k-space. For example, let us consider the excitonic effects on the strength of optical transitions. They are determined by the square of the matrix element of the dipole operator

$$\hat{r} = \sum_{\mathbf{k}} r_{vc}(\mathbf{k}) c_e(\mathbf{k}) c_h(-\mathbf{k})$$

between the crystal ground state and the exciton state,

$$|\langle g|\hat{r}|X_n\rangle|^2 = \sum_{\mathbf{k}} \phi_n(k) r_{vc}(k) \sum_{\mathbf{k}'} \phi_n^*(k') r_{vc}^*(k'). \tag{2.1.13a}$$

It is customary to assume that $r_{cv}(k)$ is a slowly varying function of k (i.e. $R \ll E_g$) that can be taken out of the sum in equation (2.1.13*a*),

$$|\langle g|\hat{r}|X_n\rangle|^2 \sim |r_{cv}|^2 \sum_{\mathbf{k}} \phi_n(k) \sum_{\mathbf{k}'} \phi_n^*(k') = |r_{cv}|^2 |\phi_n(r=0)|^2. \tag{2.1.13b}$$

Although the form of equation (2.1.13*b*) given in the last line is the most commonly used, it is very difficult to generalize it to the case of band occupation by carriers due to doping or photoexcitation. On the contrary, as shown in the next sections the form given in the first line is most suitable for natural extensions.

Using equation (2.1.13*b*) to calculate the linear optical susceptibility, χ, one obtains the well known Elliott formula (Elliott 1957),

$$\chi = 2e^2 |r_{cv}|^2 \sum_n \frac{|\phi_n(r=0)|^2}{E_n - \omega - i\delta}. \tag{2.1.14}$$

The absorption coefficient is obtained from the imaginary part of χ through $\alpha(\omega) = [4\pi\omega]/[cn(\omega)] \operatorname{Im} \chi$, where $n(\omega)$ is the refractive index. This implies that the e–h correlation produces strong peaks in the absorption spectrum, at the energies of the s exciton states with zero angular momentum for which $|\phi_n(r=0)|^2 \neq 0$. The usual interpretation of this result is that the absorption is enhanced by the e–h correlation in proportion to the increased probability of finding the electron and hole at the same site. The optical spectrum is thus directly determined by the energies and wavefunctions of the s states. The solution of the hydrogenic Schrödinger equation in 2D gives for the bound state energies $E_n^{2D} = E_g - R/(n - \frac{1}{2})^2$ (Shinada and Sugano 1966) as compared with the 3D result $E_n^{3D} = E_g - R/n^2$. The wavefunction of the 1s state which determines the onset of absorption is

$$\phi_{1s}^{2D} = \left(\frac{2}{\pi}\right)^{1/2} \frac{2}{a_B} \exp\left(-\frac{2r}{a_B}\right) \tag{2.1.15a}$$

in r-space and

$$\phi_{1s}^{2D}(k) = \frac{(2\pi)^{1/2}(a_B/2)}{[1 + (a_B k/2)^2]^{3/2}} \tag{2.1.15b}$$

in k-space. Let us recall for comparison that in 3D the corresponding functions are

$$\phi_{1s}^{3D}(r) = \frac{1}{(\pi)^{1/2} a_B^{3/2}} \exp\left(-\frac{r}{a_B}\right), \tag{2.1.16a}$$

$$\phi_{1s}^{3D}(k) = \frac{8(\pi)^{1/2} a_B^{3/2}}{[1 + (a_B k)^2]^2}. \tag{2.1.16b}$$

Several points are worth noting:

(i) in 2D the first (1s) exciton is more bound ($E_{1s}^{2D} = E_g - E_0 = E_g - 4R$) then in 3D ($E_{1S}^{3D} = E_g - R$), hence the 1s-excitonic enhancement is larger.
(ii) conversely, the e–h overlap at $r = 0$ in the excited states ($n > 1$) decreases more rapidly in 2D than in 3D since $|\phi_n(0)|^2 = (2n - 1)^{-3}|\phi_{1s}(0)|^2$ in 2D, whereas in 3D $|\phi_n(0)|^2 = (n)^{-3}|\phi_{1s}(0)|^2$.
(iii) the 2D Bohr radius of the exciton determined by the wavefunction equation (2.1.15) is $a_0 = a_B/2$ so that $E_0 \times a_0^2 = (2m)^{-1} = R \times a_B^2$ as in 3D.
(iv) in 2D the charge density maximum occurs at $a_{2D} = a_B/4$ whereas in 3D it occurs at $a_{3D} = a_B$, so that in both cases $2E_0 \times a_{2D} = 2R \times a_{3D} = e^2/\epsilon_0$.

This shows that in both dimensions the position of the maximum charge density is determined by the equilibrium between electrostatic and kinetic energies (i.e. the virial theorem).

The excited states merge into a quasi-continuum ($n \gg 1$) that continuously connects to the true continuum of unbound states. The wavefunctions of these unbound states can also be determined exactly; they describe the residual e–h correlation in the scattering states above the ionization limit ($n = \infty$). The complete expressions are quite complicated, but they reduce for the quantities of interest for the optical spectra to

$$|\phi_k^{2D}(r = 0)|^2 = \frac{2}{[1 + \exp(-2\pi/a_B k)]}, \tag{2.1.17}$$

$$|\phi_k^{3D}(r = 0)|^2 = \frac{2\pi/a_B k}{[1 - \exp(-2\pi/a_B k)]}. \tag{2.1.18}$$

Let us note that the dimensionless e–h relative momentum $a_B k$ also measures the normalized detuning from the gap, $a_B k = (\omega - E_g)/R$. The effects of correlation at and above the gap are very important. In 2D, for $\omega = E_g$, $|\phi_k^{2D}(r = 0)|^2 = 2$, and even 10 Ryd above the gap, $(\omega - E_g)/R = 10$, $|\phi_k^{2D}(r = 0)|^2$ is still 30% above the single-particle limit.

Putting together the theoretical descriptions of ideal cases that we have analysed so far, we can infer that the absorption spectrum of QW structures consists of two series of steps with flat density of states corresponding respectively to the hh → e and lh → e transitions from the valence subbands to the conduction subbands. Each transition exhibits exciton peaks at its onset and a correlation enhanced continuum above (Dingle *et al.* 1974). Unfortunately, if one wishes to go beyond this general picture and determine quantitatively such parameters as the exciton binding energy and lineshape, these models are too oversimplified to be useful. Strictly speaking they do not apply quantitatively to real semiconductor QWs. However, for a number of reasons they are a good starting point.

There are a number of difficulties in rigorously treating excitons in real QWs. The first one is related to the e–h interaction in QWs with finite well width for which the

correct expression of the Coulomb force is $-e^2/(\epsilon_0[r^2 + (z_e - z_h)^2]^{1/2})$. This shows that the Coulomb interaction couples the motions along the normal and in the plane of the layer, that is, the different conduction and valence subbands. It is customary to neglect this coupling among the various subbands and in particular the coupling between the light and heavy hole. This is justified in the regime of strong confinement perpendicular to the layers, that is, as long as the energy separation between subbands is much larger than the exciton binding energy. Thus, this approximation holds for the subbands with different n_z and narrow wells, but it is questionable when applied to light and heavy holes of the same series. As discussed above, in the strong confinement regime the motion of the particles along the normal is governed by the confinement potential and the Coulomb interaction mainly affects the motion in the plane.

The second difficulty is related to the holes; we have seen that their degeneracy is lifted, giving two series of well separated subbands. Correspondingly, at the onset of each transition exciton resonances appear associated with the heavy hole (hh) and the light hole (lh) respectively. The problem of choosing in-plane masses for each hole to describe the relative e–h motion has not been solved. The usual approach is to 'average' the valence subband dispersion (over the distribution $\phi(k)$) to define a 'mean effective mass' for each hole, and to use a parabolic dispersion in the exciton Wannier equation to describe the e–h correlation. The corresponding values of the hole masses found in the literature are quite often a matter of personal taste.

Most of the theoretical determinations of the exciton binding energy performed so far use variational calculations, starting from well behaved wave functions to minimize the e–h Hamiltonian (Lee and Lin 1979, Miller *et al.* 1981b, Bastard *et al.* 1982, Greene and Bajaj 1983, Greene *et al.* 1984, Bauer and Ando 1987, Miller *et al.* 1985a). In the infinite well depth approximation, if trial wavefunctions inseparable in $z_{e,h}$ and $(x, y)_{e,h}$ are used, a smooth variation of the binding energy from $4R$ to R is found for L_z/a_B varying from 0 to ∞, in good agreement with physical intuition. In practice, this does not apply to real QWs because, in the case of finite well depth, the penetration of the e and h wavefunctions into the barrier material increases as $L_z/a_B \to 0$, so that for very thin wells the exciton tends toward the 3D exciton of the barrier material or of the superlattice formed by the thin layers embedded in the barrier material. Then the binding energy tends toward the corresponding Rydberg, (Greene and Bajaj 1983, Greene *et al.* 1984). Nevertheless a significant enhancement of the QW exciton binding energy is predicted, with a maximum in the range $3R < E_0 < 2R$ for $\frac{1}{4} < L_z/a_B < 1$. Figure 5 shows an example of the dependence of the hh and lh exciton binding energy on well thickness in $GaAs/Al_xGa_{1-x}As$ QWs calculated by Greene and Bajaj (1983) and Greene *et al.* (1984) for three well depths. The curves for the infinite well show a monotonic increase as $L_z \to 0$; conversely, the curves for $\Delta E_c \sim 228$ and 114 meV and $\Delta E_v \sim 152$ and 76 meV, corresponding to aluminium contents in the BL $x \sim 0{\cdot}3$ and $0{\cdot}15$, have a maximum at $E_0 \sim 2R$ (i.e. $E_0 \sim 9$ meV) for $L_z/a_B \sim 0{\cdot}4$ (i.e. $L_z \sim 50$ Å).

It is time to examine some experimental results. In figure 6, the absorption spectrum of a high quality GaAs sample 1 μm thick is compared with the spectrum of a GaAs QW structure. The QW structure consists of 50 periods of 100 Å GaAs QWs and 100 Å $Al_{0{\cdot}3}Ga_{0{\cdot}7}As$ BLs. The difference is striking. The spectrum of the GaAs sample shows a steep edge, with a bump which is the remnant of the exciton peak at 300 K, and a smooth continuum above. The spectrum of the QW sample shows the onset of absorption shifted by the confinement followed by three plateaus that

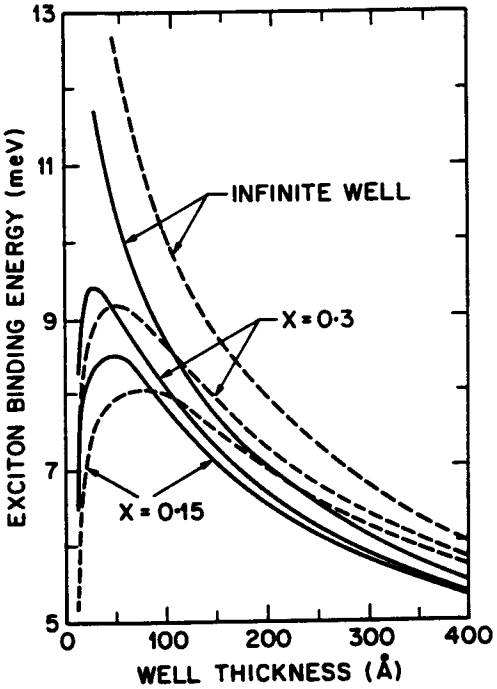

Figure 5. Variation of the exciton binding energy in a GaAs/$Al_xGa_{1-x}As$ quantum well, as a function of quantum well thickness. The solid lines correspond to the heavy-hole exciton and the dashed lines to the light-hole exciton. Curves for the three well depths are shown: an infinite well; $\Delta E_g \sim 190$ meV and $\Delta E_g \sim 380$ meV corresponding to $x \sim 0{\cdot}15$ and $0{\cdot}3$ respectively. (After Greene *et al.* (1984).)

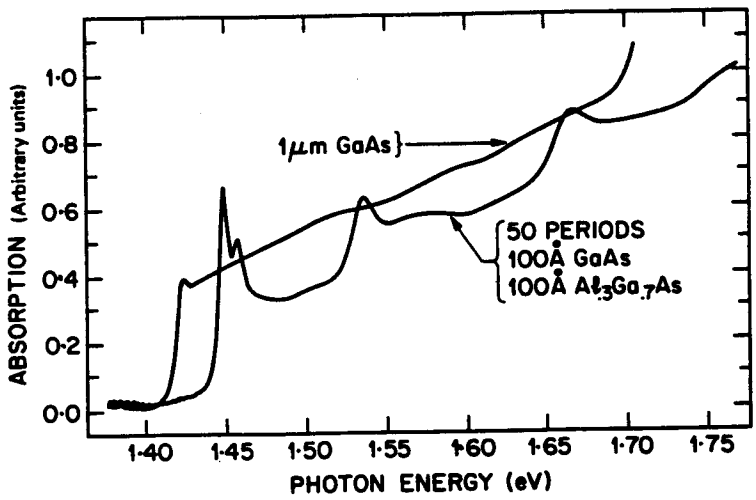

Figure 6. Comparison of the room-temperature absorption spectra of high-quality bulk and $L_z = 100$ Å quantum well GaAs samples. The bump at the onset of the bulk spectrum is the remnant of the exciton resonance. The quantum well spectrum shows the onset of absorption shifted by the confinement, followed by excitons and plateaus corresponding to $n_z = 1$, 2 and 3. The $n_z = 1$ hh and lh excitons peaks are remarkably well resolved.

correspond to the $n_z = 1$, 2 and 3 transitions. Before each plateau exciton resonances are seen. For $n_z = 1$ the hh and lh exciton peaks are remarkably resolved at this temperature, the $n_z = 2$ and 3 hh excitons are still well resolved but the $n_z = 2$ lh resonance appears just as a bump above the hh peak and the $n_z = 3$ is not resolved. In the $n_z = 1$ continuum just before the $n_z = 2$ exciton one can distinguish a kink which corresponds to a forbidden transition. It is worth noting that the total thickness of active material in the QW sample is half that of the GaAs sample showing the enhancement of the absorption strength due to the confinement. The rather wide width of the resonances is not only due to the high temperature, but it has also contributions that originate from imperfections. This is shown in figure 18 (*a*) where the absorption spectra of an $In_{0.48}Ga_{0.52}As/In_{0.47}Al_{0.53}As$ quantum well structure measured at 12, 200 and 300 K are presented. This structure consists of 100 periods of 100 Å QWs and 100 Å BLs grown lattice-matched on an InP substrate. The spectra show how the resonances sharpen and increase as the temperature is lowered. At the lowest temperature the exciton peaks are still broad. This is due to unavoidable imperfections such as monoatomic fluctuations in the layer thickness, strain due to small lattice mismatch, interface defects and suchlike which produce the inhomogeneous broadening seen at low temperature (Weisbuch *et al.* 1981, Hegarty and Sturge 1985). For not too narrow wells ($L_z \sim 100$ Å) the absorption profile is well fitted by exciton peaks with Gaussian lineshape and broadened 2D Sommerfeld enhanced continua (Chemla *et al.* 1984). Investigation of the temperature dependence of the broadening of the hh-exciton (Chemla *et al.* 1984, Weiner *et al.* 1985a, Livescu *et al.* 1988) shows that its width varies as the density of LO phonons,

$$\Gamma(T) = \Gamma_0 + \frac{\Gamma_{LO}}{\exp(\omega_{LO}/T) - 1}. \tag{2.1.19}$$

In equation (2.1.19), Γ_0 is the width due to the inhomogeneous broadening and Γ_{LO} measures the interaction with polar LO phonons which are therefore identified as the dominant temperature mechanism reducing the exciton lifetime. The very large width of the $n_z > 1$ excitons, and in particular of the $n_z = 2$ lh exciton, is most likely due to intersubband coupling. Because these resonances are above the continuum of the $n_z = 1$ excitons, their lifetime is reduced by any intersubband scattering such as Coulomb interaction or phonon scattering. The coupling to a continuum of states can induce a Fano lineshape as discussed recently by Broido *et al.* (1988).

It is interesting to note that excitons are still resolved at room temperature even in InGaAs QWs, although the gap of bulk InGaAs is half that of GaAs. This is a consequence of the increasing binding energy even in this low-gap material and a remarkable compensation of two effects. The 3D exciton binding energy scales roughly with the gap owing to the dependence of the effective masses on E_g. This gives a binding energy of the exciton in bulk InGaAs ($\sim 2{\cdot}8$ meV) about twice smaller than in GaAs ($\sim 4{\cdot}2$ meV) and correspondingly it is very difficult to observe excitons in bulk InGaAs even at low temperature. However, as noted in a previous paragraph, the binding energy is inversely proportional to the Bohr radius. Since the dielectric constant, ϵ_0, is roughly the same, the Bohr radius in InGaAs (~ 300 Å) is thus about twice that in GaAs (~ 140 Å). The confinement in QWs of the same thickness is thus more effective for the low-gap compound and the increase in binding energy due to the confinement compensates for the reduction due to the lower gap. Typical values are $E_0 \sim 6$ meV in InGaAs and $E_0 \sim 9$ meV in GaAs for $L_z = 100$ Å.

Finally, it is worth noting that the excitons at room temperature are very ephemeral. If one interprets the temperature dependent broadening as a reduction of life time due to collisions with LO-phonons, one finds that excitons live only 400 fs in GaAs QWs and 250 fs in InGaAs QWs. The interpretation of this short life time is that because the LO phonon energy (~ 36 meV in both materials) is much larger than the exciton binding energy every collision ionizes the exciton, releasing an e–h pair with a substantial excess energy. At high temperatures the large density of LO phonons increases the collision frequency, hence the functional form of the exciton linewidth given by equation (2.1.13). At room temperature the absorption of a photon thus creates an exciton which almost immediately collides with an LO-phonon producing a free e–h pair. This sequence of events causes unusual dynamics in the ultrafast nonlinear optical response of QW structures which will be discussed in section 3.1.

2.2. *Effects of electric fields*

It is well known that electric fields affect the linear optical properties of bulk semiconductors near the optical absorption edge. For example, the first and best known mechanism was the Franz–Keldysh effect (FK) (Franz 1958, Keldysh 1958), which correctly predicts the growth of a weak absorption tail at photon energies below the nominal bandgap energy with applied electric field. It is natural to ask therefore what will be the electroabsorption effects in QWs and other confined structures, and what relation will they bear to the mechanisms already known for bulk semiconductors. In the discussion that follows, we will see that, just as in the bulk, the inclusion of excitonic effects is crucial for the understanding of the electroabsorption, both from quantitative and qualitative points of view, and current understanding does explain the basic electroabsorption effects, at least in QWs.

QW electroabsorption differs from that of the bulk in several ways; most importantly, the mechanisms are very different depending on whether the electric field is parallel or perpendicular to the QW layers, with qualitatively different behaviour for the perpendicular field case (the quantum-confined Stark effect (QCSE)) (Miller *et al.* 1984a, 1985a, Brum and Bastard 1985). The QCSE has received a lot of attention for devices (Miller 1987) because it is a very large electroabsorption effect even at room temperature, allowing low-energy optical modulators and switches, and it operates under technologically convenient conditions; it is compatible with laser diodes and semiconductor electronics in wavelengths, powers, voltages and materials. We will not discuss devices at any length here, concentrating instead on the physics. In this section, we will attempt to explain the physical mechanisms of electroabsorption in quantum wells and to relate them to bulk effects (Miller *et al.* 1986a). We will attempt to summarize some of the recent work in this active research area. We will also extend the theory to confinement in quantum 'wires' and quantum 'boxes' or 'dots' (QD) (Miller *et al.* 1988).

To understand the QW theory, we will try to present a consistent theoretical picture that can explain electroabsorption in bulk semiconductors, quantum wells and more highly-confined structures. We start by noting that the optical absorption, that is, the imaginary part of the optical susceptibility, can be represented rather generally by a relation of the form

$$\mathrm{Im}\,\chi \propto \sum_n |\langle g|\hat{r}|X_n\rangle|^2 \delta(\omega - E_n), \tag{2.2.1}$$

as discussed for equation (2.1.13-14). In all cases, the evaluation of the absorption can be reduced to:

(i) solving for all possible electron–hole pair states $|X_n\rangle$ and their energies E_n by solving the relevant Schrödinger equation (which in the present case will also include an applied electric field);
(ii) evaluating the dipole matrix elements as above; and
(iii) summing as above.

We state this explicitly to emphasize that this is a complete prescription within our approximations, and we can use it to solve for electroabsorption in all dimensions, with or without inclusion of excitonic effects; this is true even although the qualitative explanations of various electroabsorptions are often explained most easily using apparently different descriptions (e.g. the Franz–Keldysh effect is often explained as photon-assisted tunnelling between bands (Franz 1958)) that are formally equivalent to this prescription. Treating only Wannier excitons, we may remove $|r_{cv}|^2$ as essentially a constant in equations (2.2.1) or (2.1.14), and we will henceforth omit it in this section.

For three dimensions we transform to centre of mass and relative motion coordinates and obtain

$$\operatorname{Im}\chi \propto \sum_n |\phi_n(r = 0)|^2 \delta(\omega - E_n), \tag{2.2.2}$$

as in equation (2.1.14). Note that this standard transformation already simplifies the problem because the centre of mass motion is always zero from momentum conservation in direct optical transitions; this remains true even in the presence of field since the field does not affect the centre of mass motion because the pair is neutral overall.

To treat the Franz–Keldysh effect, we have to solve the Schrödinger equation for an electron–hole pair in a static electric field, neglecting the electron–hole Coulomb interaction (i.e. no exciton effects); this neglect decouples the motion in the direction of the field (say the z direction) from that in the other coordinate directions, leaving those motions as plane waves, and the only non-trivial equation to be solved is for the relative motion in the direction of the field, giving

$$\left(-\frac{1}{2m}\frac{\partial^2}{\partial z^2} + eFz\right)\phi(z) = E\phi(z), \tag{2.2.3}$$

where $z = z_e - z_h$ and F is the electric field. This equation may be solved exactly (Tharmalingam 1963), giving a continuous spectrum of energies with Airy functions as the wavefunctions, and an explicit formula can be obtained for the Franz–Keldysh absorption. Although it is not obvious, this treatment is equivalent to the description of the Franz–Keldysh effect as photon-assisted tunnelling between valence and conduction bands tilted by the field. This correctly predicts the growth of a weak absorption tail below the bandgap energy, and oscillations in the spectrum above the bandgap energy, although the absolute magnitude of the absorption is significantly underestimated (Dow and Redfield 1970).

We can proceed to include excitonic effects by adding the Coulomb interaction. As before, the centre of mass motion may be neglected, but now all directions of relative motion are coupled. Now we must solve

$$\left[-\frac{\nabla^2}{2m} - \frac{e^2}{\epsilon_0 r} + eFz\right]\phi(\mathbf{r}) = E\phi(\mathbf{r}). \tag{2.2.4}$$

This equation can be solved using numerical or WKB techniques (Ralph 1968, Dow and Redfield 1970, Blossey 1970, 1971, Merkulov and Perel 1973, Merkulov 1974). Important conclusions from such an analysis are:

(i) a weak absorption tail below the bandgap and oscillations above the bandgap are retained, as in the Franz–Keldysh effect;
(ii) additionally, the exciton line is broadened strongly by the field, for fields of the order of the classical ionization field of the exciton, and dominates the electroabsorption near the bandgap;
(iii) the magnitude of the absorption spectrum near the edge is much larger than predicted by the Franz–Keldysh effect.

The broadening of the exciton line can be understood as an uncertainty principle effect (Merkulov and Perel 1973, Merkulov 1974); soon after the exciton is created, it is destroyed by field ionization, and hence its energy resonance is broadened by lifetime broadening. There is a small shift of the peak of the exciton line to lower energy, but this is restricted to $\sim 10\%$ of the binding energy before the broadening becomes very severe (Dow and Redfield 1970, Schultheis *et al.* 1987). The three-dimensional case is thus well understood both with and without excitonic effects.

In moving to the situation in quantum wells, we cannot usefully transform to centre of mass and relative motion coordinates in the direction perpendicular to the layers, because now the absolute position of electron and holes is relevant since we have introduced 'walls' and associated absolute position boundary conditions. The centre of mass description was more useful in three dimensions because the crystal is implicitly assumed infinite in all directions, and absolute position is irrelevant. Even without field, there is no analytic solution for the exciton wavefunction in a finite quantum well. If, however, we are in the strong confinement approximation as discussed in section 2.1, where the confinement energies of the electron and the hole are large compared with the Coulomb energy (a reasonable approximation for quantum wells significantly narrower than the three-dimensional exciton Bohr diameter), then we can approximately separate the wavefunction into a product (Miller *et al.* 1985a)

$$\phi(\mathbf{r}) = \psi^{e}_{p_z}(z_e)\psi^{h}_{q_z}(z_h)\phi^{xy}_{n_{xy}}(\mathbf{r}_{xy}), \tag{2.2.5}$$

where $\psi^{e}_{p_z}(z_e)$ and $\psi^{h}_{q_z}(z_h)$ are the electron and hole particle-in-a-box wavefunctions in the z direction and $\phi^{xy}_{n_{xy}}(\mathbf{r}_{xy})$ is the relative motion electron–hole wavefunction in the plane of the quantum wells. (In this section, we will explicitly use $\mathbf{r}$ as the three-dimensional electron–hole separation and $\mathbf{r}_{xy}$ to refer to the in-plane separation). The wavefunction separation is possible because we assume that the Coulomb attraction between electron and hole is not strong enough to perturb the motion in the z direction. We can still transform to centre of mass and relative motion coordinates in the quantum well plane because the crystal is still assumed infinite in this direction, with the centre of mass motion still being irrelevant for optically created excitons by momentum conservation. Now the absorption can be written

$$\operatorname{Im}\chi \propto \sum_{p_z,q_z,n_{xy}} |\langle\psi^{e}_{p_z}|\psi^{h}_{q_z}\rangle|^2 |\phi^{xy}_{n_{xy}}(r_{xy}=0)|^2 \delta(\omega - E^{e}_{p_z} - E^{h}_{q_z} - E^{xy}_{n_{xy}} - E_g), \tag{2.2.6}$$

where $E^{e}_{p_z}$ and $E^{h}_{q_z}$ are the single-particle electron and hole confinement energies for the (p_z)th and (q_z)th states respectively, $E^{xy}_{n_{xy}}$ is the sum of Coulomb and in-plane kinetic energies for the (n_{xy})th in-plane relative motion state of the electron-hole pair (loosely

speaking, the 'binding energy' of the exciton (Miller *et al.* 1985a)), and E_g is the bandgap energy which we have now explicitly separated out for clarity. This is therefore a sum over all the in-plane exciton states for each possible combination of electron and hole states perpendicular to the layers.

The case of electroabsorption for fields parallel to the layers has been solved numerically for the extreme case of a totally two-dimensional system (Lederman and Dow 1976) (where the exciton behaviour is also exactly solvable without field). The behaviour is qualitatively similar to the case of three-dimensional excitonic electroabsorption because the same physical processes are operating. Franz–Keldysh-like oscillations are found above the band edge, a weak absorption tail is created below the edge, and the exciton lines broaden with field because of field ionization. Miller *et al.* (1985a) also estimated the field ionization time for the quantum well case. The experimental results (Miller *et al.* 1985a, Knox *et al.* 1986b) for the quantum well case also confirm the same general qualitative behaviour; the primary consequence of electric fields in the plane is to broaden the exciton lines, at least for moderate fields, as is shown in figure 7. Characteristic fields for this process are fields such that the potential drop across one exciton diameter is comparable to the binding energy.

It is for fields perpendicular to the layers that the quantum well electroabsorption shows behaviour qualitatively different from bulk electroabsorption, and the majority of the rest of this section will be devoted to this situation. For pedagogical purposes, it is useful to start by neglecting excitonic effects, even although the different behaviour of the excitons in this case is particularly important in understanding perpendicular field electroabsorption in quantum wells. For reasons that will become obvious presently, we will refer to this model as the quantum-confined Franz–Keldysh effect (QCFK) (Miller *et al.* 1986a).

Neglecting excitonic effects, the electron and hole wavefunctions in the plane again become plane waves, and we may perform the summations over these plane wave

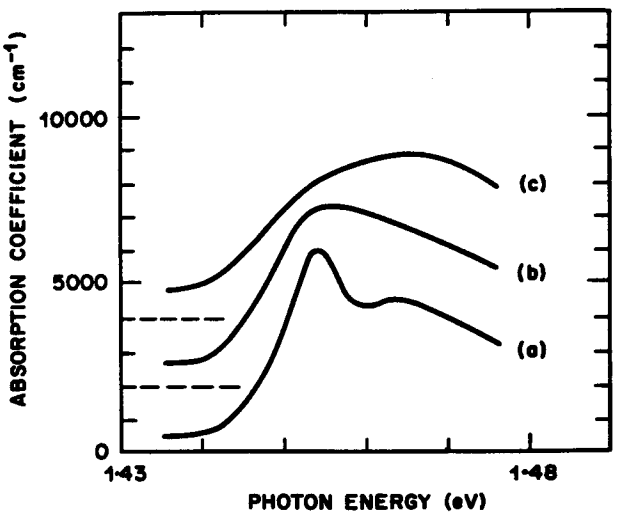

Figure 7. Electroabsorption for fields in the plane of quantum well layers. Fields are (*a*) $0\,V\,cm^{-1}$, (*b*) $1{\cdot}6 \times 10^4\,V\,cm^{-1}$ and (*c*) $4{\cdot}8 \times 10^4\,V\,cm^{-1}$. The quantum wells are 95 Å GaAs with AlGaAs barriers. The zeros have been displaced for clarity as shown by the dashed lines. (After Miller *et al.* (1985a).)

states in equation (2.2.6) (i.e. over the index n_{xy}) to obtain

$$\mathrm{Im}\,\chi \propto \sum_{p_z,q_z} |\langle \psi^{e}_{p_z} | \psi^{h}_{q_z} \rangle|^2 \theta(\omega - E^{e}_{p_z} - E^{h}_{q_z} - E_g), \tag{2.2.7}$$

where $\theta(E)$ ($=0$ for $E < 0$, $=1$ for $E > 0$) is the Heaviside ('step') function. For the case without field, this is simply a formal statement that the quantum well absorption is a series of steps, corresponding essentially to one step for each allowed transition ($p_z = q_z$). When the field is applied, we now have to solve the Schrödinger equations

$$\left[-\frac{1}{2m_{e,h}} \frac{\partial^2}{\partial z^2_{e,h}} \pm eFz_{e,h} + V_{e,h}(z_{e,h}) \right] \psi^{e,h}(z_{e,h}) = E^{e,h} \psi^{e,h}(z_{e,h}), \tag{2.2.8}$$

where e and + refer to electrons in the conduction band, and h and − to holes in the valence band, to find all the possible electron and hole states. When the structural potentials $V_{e,h}$ are step-like as in equation (2.1.7) (e.g. as in simple rectangular wells), the solutions of this equation are Airy functions. The simplest case to consider is that of infinite potential barriers (Miller *et al.* 1986a). Illustrative calculations are shown in figure 8 for a strong field case. Figure 9 shows the resulting absorption calculated with field using equation (2.2.7).

Figures 8 and 9 show several features of this electroabsorption. The energy of the lowest ($p_z = 1$, $q_z = 1$) transition is reduced by the application of the field, and the electron and hole in these states are pulled to opposite sides of the well by the field. This energy shift is approximately quadratic at low fields, and corresponds primarily to the polarization energy of the polarized electron–hole pair in the electric

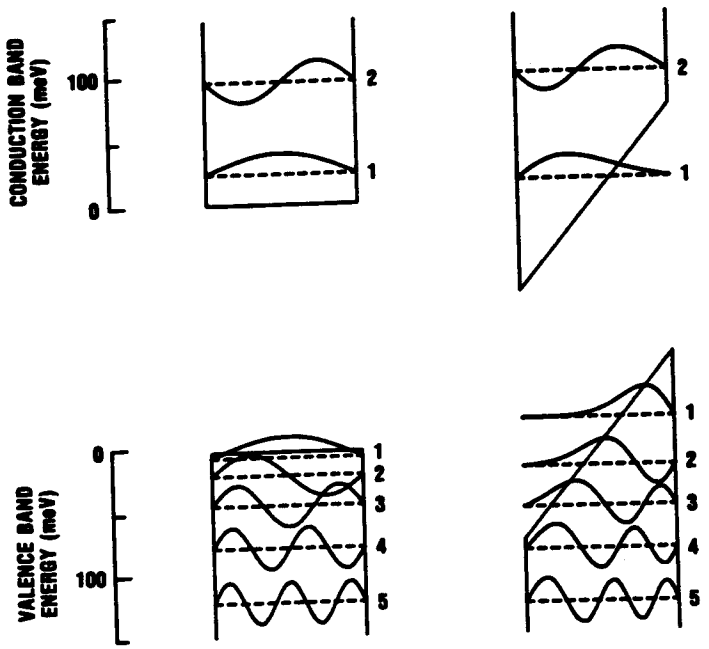

Figure 8. Calculated wavefunctions and energy levels for a 150 Å thick two-band GaAs-like quantum well with infinite barriers at 0 and $10^5\,\mathrm{V\,cm^{-1}}$. (After Miller *et al.* (1986a).)

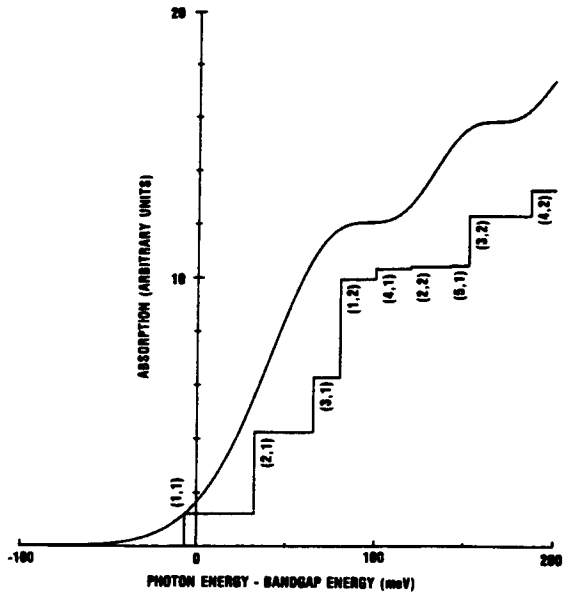

Figure 9. Calculated absorption of a 150 Å thick two-band GaAs-like quantum well at $10^5\,V\,cm^{-1}$ neglecting excitonic effects (the quantum-confined Franz–Keldysh approximation). The individual transitions are labelled (n_v, n_c) where n_v (n_c) is the valence (conduction) subband number. (After Miller *et al.* (1986a).) The smooth line is the calculated Franz–Keldysh effect for bulk material.

field. At higher fields, this is partly offset by the fact that the kinetic energy of the electron and hole is increased as they are squeezed towards the walls of the wells. As the electron and hole are pulled apart, the overlap integral between electron and hole wavefunctions decreases, reducing the step height for this transition; in the particular case of figure 9, this loss of step height is substantial for the (1,1) transition; this strong loss is associated with the fact that the shift of the hole state in particular is much larger than its initial confinement energy. The shift of these heavy-hole states in general is larger than that of the electrons, because particles with larger mass are more easily perturbed because of their lower confinement energies. For the case of the infinite well, the problem can be recast in dimensionless units in which the energy is expressed in units of the lowest confinement energy at zero field, and the field is expressed in units corresponding to a potential drop of one energy unit across the well width. The shifts of the higher levels are not so large, and do not follow the simple intuition of the lowest states. The second state, for example, starts by moving up in energy relative to the centre of the well as field is applied. Another very important point that is clear from figure 9 is that the 'forbidden' transitions ($p_z \neq q_z$) are becoming strong. This is simply because the electron and hole wavefunctions are no longer sinusoidal, and all the overlap integrals are in general non-zero. In the strong field case of figures 8 and 9 the 'forbidden' transitions are in some cases stronger than the 'allowed' transitions.

The relation of this quantum well electroabsorption model to the Franz–Keldysh effect is interesting; it has been shown analytically that, in the limit as the well

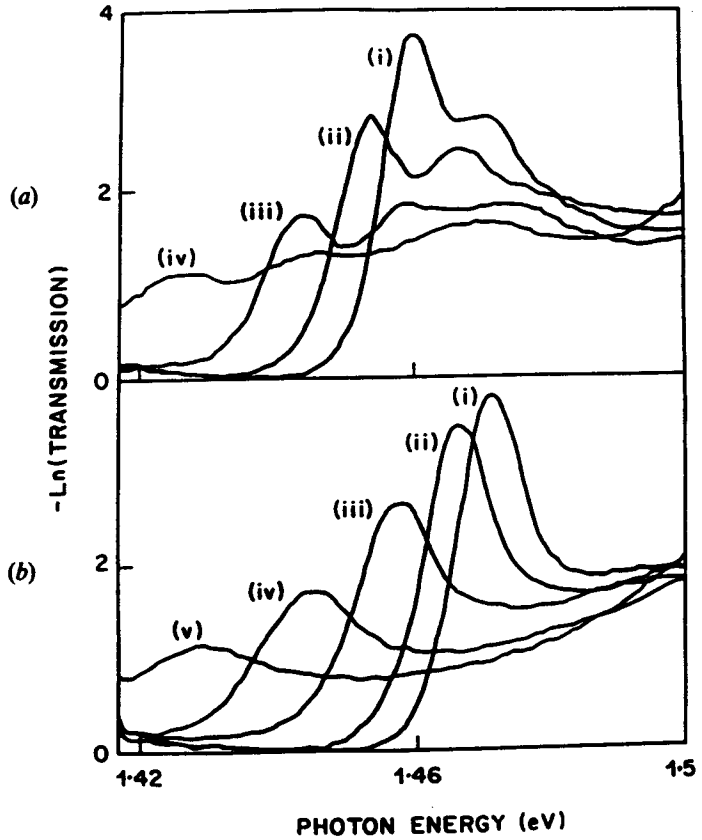

Figure 10. Experimental spectra for electric fields perpendicular to the quantum well layers with 94 Å GaAs quantum wells. (*a*) Incident polarization parallel to the plane of the layers for estimated fields of (i) 0 V cm^{-1}, (ii) 6 × 10^4 V cm^{-1}, (iii) 1·0 × 10^5 V cm^{-1}, and (iv) 1·5 × 10^5 V cm^{-1}. (*b*) Incident polarization perpendicular to the plane of the layers for estimated fields of (i) 0 V cm^{-1}, (ii) 6 × 10^4 V cm^{-1}, (iii) 1·1 × 10^5 V cm^{-1}, (iv) 1·5 × 10^5 V cm^{-1}, and (v) 2·0 × 10^5 V cm^{-1}. (After Weiner *et al.* (1985c), Miller *et al.* (1986b).)

thickness becomes infinite, this model becomes formally identical with the Franz–Keldysh effect (Miller *et al.* 1986a, Ikonic *et al.* 1987a) correctly predicting bulk electroabsorption neglecting excitons, hence the title QCFK. In fact, this transition is rather rapid with increasing well size (Miller *et al.* 1986a); for example, for a 300 Å thick layer, the electroabsorption in this model is practically almost identical to the Franz–Keldysh effect at 10^5 V cm^{-1}. Conversely, for thinner wells (e.g. 100 Å) the electroabsorption is apparently very different in character from the Franz–Keldysh effect at such fields, corresponding mostly to a shift of the lowest, (1,1), transition, without the growth of a weak absorption tail.

As mentioned above, the behaviour of the excitons is very different in the QWs for fields perpendicular to the layers. Experimental spectra (figure 10) (Weiner *et al.* 1985c, Miller *et al.* 1986b) clearly show that the excitons do not broaden strongly with field, and the peaks shift substantially; the behaviour of bulk (and in-plane QW)

electroabsorption is exactly the opposite, showing much broadening and little shift. To analyse this QW case formally, we must finally add the electron–hole Coulomb attraction into the Schrödinger equation (Miller *et al.* 1984a, 1985a, Brum and Bastard 1985)

$$\left[-\frac{1}{2m_{xy}}\nabla_{xy}^2 - \frac{1}{2m_e}\frac{\partial^2}{\partial z_e^2} - \frac{1}{2m_h}\frac{\partial^2}{\partial z_h^2} - \frac{e^2}{\epsilon_0 r} \pm eFz_{e,h} + V_{e,h}(z_{e,h})\right]\phi(\mathbf{r}) = E\phi(\mathbf{r}), \tag{2.2.9}$$

where ∇_{xy} refers to the in-plane directions only and m_{xy} is the in-plane reduced mass. So far, there is no complete solution of this equation, but it has been treated approximately for the specific case of the lowest electron–hole pair state using the strong confinement approximation, equation (2.2.5). In this case, we first solve for the single-particle states in the presence of the field, and then solve variationally for the motion in the plane by presuming a two-dimensional 1s-like Bohr orbital as in equation (2.1.15) but with a variationally adjustable radius instead of a_B.

Before proceeding to calculations of energy shifts, it is important to understand qualitatively why the exciton absorption resonances still exist at the very high fields that can be used in the experiments; in bulk GaAs, the excitonic absorption is very strongly broadened for fields $\sim 10^3\,\mathrm{V\,cm^{-1}}$, whereas the QW exciton lines are still clearly resolved at $\sim 10^5\,\mathrm{V\,cm^{-1}}$. Furthermore, the shift can be many times the 'binding energy' of the exciton in the perpendicular field QW case (this is not unphysical since the energy of the electron–hole pair is decreasing with field, not increasing), whereas it is almost negligible in the bulk case. The key physical reason for the persistence of the excitonic resonance in the perpendicular field QW case is that the walls of the quantum well prevent the field ionization of the exciton. As field is applied, the electron and hole (in the lowest confined states) are pulled to opposite sides of the well, but they are restrained by the walls from going any further. Thus the exciton is not 'ripped apart' by the field; it is very strongly polarized by the field with the electron and hole orbits being partly separated spatially, but it can still complete several classical orbits, just as it could without field, before being destroyed. Consequently, it is still a well defined particle with a well resolved optical absorption resonance without additional lifetime-broadening effects. This description requires some quantitative justification; we must show that the electron and hole do not tunnel too rapidly out of the well. (In principle the electron–hole Coulomb attraction helps to hold the particle together also, but this is usually negligible by comparison with the effect of the barriers for GaAs). We require that the tunnelling time is significantly longer than the lifetime of the exciton from other causes (e.g. phonon ionization as discussed in section 2.1). This is indeed the case for QWs showing this electroabsorption effect. It is also intuitively clear that this suppression of field ionization will no longer be effective if the well is made much larger than the bulk exciton diameter, because then the exciton could be effectively field-ionized just by pulling electron and hole to opposite sides of the thick well, so it is necessary to stay with moderately thin layers to see this effect clearly. It is also of course possible to design wells in which the tunnelling is rapid, either by making the barrier lower or thinner, or by making the well itself thin, thereby pushing the confined energy level higher so that it can tunnel more easily through the barrier. This is relevant to the discussion of luminescence quenching below.

It is clear that equation (2.2.9) is the Schrödinger equation for a confined hydrogenic system with an electric field perpendicular to the confinement direction. Consequently,

this mechanism is often referred to as the quantum-confined Stark effect (QCSE) (Miller *et al.* 1984a, 1985a, 1986b). The shift that we calculate here would be the shift in the ground state energy of such a hydrogenic system. To see this effect with an actual hydrogen atom would require that we confined it between 'walls' < 1 Å apart with applied fields 10^{10}–10^{11} V cm^{-1}.

The first stage in modelling the QCSE with the separation equation (2.2.5) is to solve for the single-particle states as in the QCFK (i.e. equation (2.2.8)). To obtain quantitative comparison with situations of experimental interest requires inclusion of the effects of finite barrier heights, both in the values of the energy levels and in the possibility of tunnelling out of the wells. Simple calculation methods that neglect this tunnelling include both infinite well calculations (either variationally (Mendez *et al.* 1982, Bastard *et al.* 1983, Miller *et al.* 1985a, Sanders and Bajaj 1987a), perturbationally (Bastard *et al.* 1983), or exactly using Airy functions (Miller *et al.* 1985a, Matsuura and Kamizato 1986)) and effective infinite well calculations (using a well width corrected to account approximately for the penetration into the finite barriers) (Miller *et al.* 1984a, 1985a, Ahn and Chuang 1987a). Strictly, because of the possibility of tunnelling, there are no bound states in a system with uniform electric field. There are many ways of approaching this problem mathematically. The tunnelling can be included by using the simple tunnelling resonance technique that allows calculation of the quasi-bound states and their energy widths for arbitrary structures. These techniques are adequate for calculating the behaviour of the lower confined states in most quantum well structures, and were used in the original QCSE calculations (Miller *et al.* 1984a, 1985a); contrary to some confusion in the subsequent literature, these calculations did include the effects of tunnelling explicitly in the energy levels and their widths. In situations where the tunnelling is not so rapid as to lifetime-broaden the transitions beyond their width from other causes, the effect of the tunnelling on the position of the energy levels is essentially negligible. Other calculations have been performed by tunnelling resonance and related techniques (Harwit *et al.* 1986, Klipstein *et al.* 1986, Hiroshima and Lang 1986). One important point about the tunnelling is that it becomes much stronger with field, since the effective height and

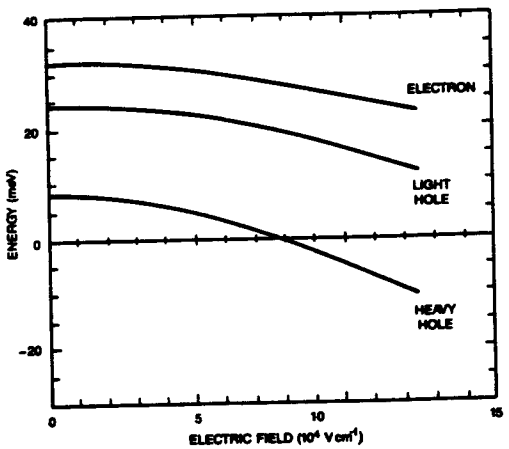

Figure 11. Theoretical energies of the first electron, heavy-hole, and light-hole states (relative to the potentials at the centre of the well) for a 95 Å GaAs quantum well with AlGaAs barriers. (After Miller *et al.* (1985a).)

thickness of the barrier are reduced as the structure is tilted by the field. A set of calculated single-particle energies as a function of field is shown in figure 11.

Many other techniques have also been proposed to handle the quasi-bound nature of the states including: phase-shift analysis (Austin and Jaros 1985a, 1985b, 1986, 1987); Monte Carlo variational method (Singh 1986, Singh and Hong 1986, Hong and Singh 1987); continuum spectrum approach (Ikonic *et al.* 1987a,b); complex eigenenergy (Ahn and Chuang 1986a); Gram-Schmidt orthogonalization (Ahn and Chuang 1986b); stabilization method (Borondo and Sanchez-Dehesa 1986); and an *R*-matrix technique (Schwartz 1987). Recently, electron–phonon coupling has also been included in a quantum well calculation, giving some predicted corrections to the energy shifts (Xu *et al.* 1988).

Calculations that stop at the point of the single-particle states are effectively QCFK calculations. However, as mentioned above, the behaviour of the exciton is crucial. Only the lowest exciton states have been calculated in the presence of perpendicular field, and these calculations include the Coulomb attraction variationally using the separation in equation (2.2.5) after solving for the single-particle states by variational or other means (Miller *et al.* 1984a, 1985a, Brum and Bastard 1985, Sanders and Bajaj 1987, Matsuura and Kamizato 1986, Hong and Singh 1987, Hong *et al.* 1987, Nojima 1988). For the case of strong electron–hole Coulomb effects, as might be encountered in wider gap II–VI semiconductors, a correction can be evaluated variationally for the effect of the Coulomb attraction on the z wavefunctions (Wu and Nurmikko 1987). All such calculations evaluate a radius with field and also a change in exciton binding energy E_{1s}^{xy} that is the sum of the total Coulomb energy for the mutual attraction of electron and hole and the in-plane kinetic energy. A set of such calculations is shown in figure 12. The exciton becomes significantly larger as the field is applied; this is because the Coulomb attraction is weaker when the electron and hole are pulled apart by the field. There is a significant decrease in the magnitude of the 'binding energy' as the field is applied, which is the net effect of a reduction in in-plane kinetic energy and a reduction (in magnitude) of the Coulomb attraction. The absolute magnitude of the energy shift from the 'binding energy' is not very

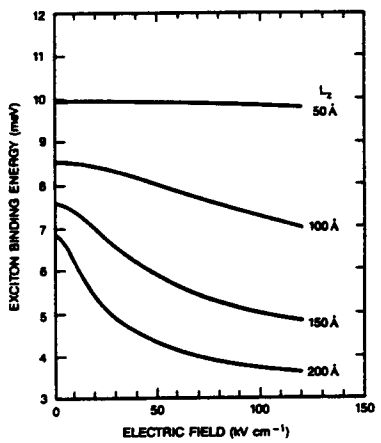

Figure 12. Calculated heavy-hole exciton binding energy for 50, 100, 150 and 200 Å thick GaAs quantum wells as a function of applied field perpendicular to the layers. (After Nojima (1988).)

significant compared with the shift of the single-particle states, but the increase in size can result in a significant change in the electron–hole overlap, reducing the absorption strength of the exciton line. The calculated energy shifts under such QCSE models agree remarkably well with experiment for the lower-lying energy levels.

A variety of different techniques can be used to observe the QCSE. The most direct is optical absorption spectroscopy for light propagating perpendicularly through the layers (Wood *et al.* 1984, Miller *et al.* 1985a) or in waveguides (Tarucha *et al.* 1985, Weiner *et al.* 1985c, Miller *et al.* 1986b). The waveguide has the additional feature that the spectra for optical electric vector in the plane and perpendicular to the plane can both be observed, as in the spectra in figure 10. These are different because of the microscopic selection rules as discussed above in section 2.1. The most prominent consequence near the band edge is that the heavy-hole absorption is forbidden for the optical electric vector perpendicular to the layers; note that this selection rule is not a consequence of the applied field, although it is not destroyed by it.

The technique that is apparently used most to observe the QCSE is photocurrent spectroscopy, especially for GaAs/AlGaAs QWs (Miller *et al.* 1984b, 1985a, Larsson *et al.* 1985, Yamanaka *et al.* 1986, Collins *et al.* 1986a,b, Vina *et al.* 1986, Whitehead *et al.* 1988). It has the advantage that it does not require that any light be transmitted, and is therefore very convenient for structures grown on opaque substrates. The diode used to apply the field to the quantum wells can very efficiently collect the photogenerated carriers, especially at room temperature, although the precise mechanism by which the carriers leave the wells to be collected is not yet entirely clear, especially at low temperatures (Collins *et al.* 1986b). It can therefore give a reasonably good quantitative measure of the absorption (Miller *et al.* 1985a,b). It is common however for the collection efficiency to be less than perfect at low voltages, probably because either the depletion region does not extend throughout the entire quantum well region of the diode or the carriers require the presence of a substantial field to cause them to be emitted from the wells.

Photoluminescence has also been successfully used to monitor the shifts and loss of overlap of the lowest transition in the QCSE (Polland *et al.* 1985, Klipstein *et al.* 1986, Vina *et al.* 1986, Juang *et al.* 1986, Vina *et al.* 1987a, Naganuma *et al.* 1987, Fu *et al.* 1987, Shorthose *et al.* 1987). Such photoluminescence techniques can work well for moderately thick wells (e.g. $\gtrsim 100$ Å), in which case the change in the luminescence intensity or lifetime with field can usually be ascribed to the separation of the electron and hole within the well by the field. This has led to interesting device concepts whereby luminescence of a light source could be turned on and off rapidly simply by separating the carriers within the well with an applied field (Yamanishi and Suemune 1983, Yamanishi *et al.* 1985, Kan *et al.* 1985, 1986, Ogura *et al.* 1987, Takeoka *et al.* 1987). For thinner wells (e.g. ~ 30 Å), the luminescence quenching is very rapid with field, and shifts are barely visible (Mendez *et al.* 1982). The explanation of this quenching is that the electrons and holes are removed from the wells by tunnelling before they can recombine, and has essentially nothing to do with the QCSE (Kash *et al.* 1985, Horikoshi *et al.* 1985, Naganuma *et al.* 1987, Shorthose *et al.* 1987). There are also some effects on luminescence that can be seen at low temperatures associated with the electric field changing the amount of impurity luminescence (Miller and Gossard 1983, Yu *et al.* 1985).

Photoluminescence excitation can also be used to measure the electroabsorption, subject to the possible field-dependence of the luminescence efficiency discussed above, and can provide information similar to the photocurrent spectroscopy. This

technique has been used by several authors (Klipstein *et al.* 1986, Collins *et al.* 1987, Chen *et al.* 1987). Electroreflectance has been used (Alibert *et al.* 1985) and analysed (Klipstein and Apsley 1986). Finally, the QCSE has also been seen in electroluminescence (Levi *et al.* 1987).

It is clear from the electroabsorption spectra (figure 10) that there is some broadening of the excitonic peaks as they are shifted. There are various possible mechanisms that could give broadening. One obvious one, a lifetime broadening from tunnelling of electrons and holes out of the wells, is not a likely cause for most situations showing QCSE, as can be verified by calculating these tunnelling rates. Another mechanism which certainly will exist is due to the fact that, in multiple well samples, the electric field is not the same in all the wells because of the finite impurity concentration in the depletion region of the diodes used (Newson and Kurobe 1987). For the spectra shown in figure 10, this is also unlikely because these spectra were taken with only two quantum wells in the sample. The most likely remaining mechanism for GaAs/AlGaAs QWs in high quality samples appears to be interface disorder (Hong and Singh 1986, 1987, Hong *et al.* 1987). It is well known that a strong contribution to the exciton absorption line width is from the non-uniformity of the quantum well thickness, giving different confinement energies in different regions of the sample, with width fluctuations of the order of one atomic layer being common. As the field is applied, the particles are pushed closer to the walls, squeezing the wavefunctions, and the fluctuations in the wall positions become ever more important because they become progressively larger compared with the thickness of the wavefunction, giving progressively larger confinement energy variations and correspondingly larger exciton spectral widths. One final mechanism, which has been suggested as a possible line broadening in poorer quality samples and in some alloy quantum wells, is due to the presence of ionized impurities in the depletion region of the diode (Bar-Joseph *et al.* 1987). Under reverse bias, any impurities will tend to ionize, but there is no free carrier density to screen the random field that results from these randomly distributed point charges. The resulting random field fluctuations will have components in the plane of the quantum well layers. Any such components, even if they are about ten times weaker than the field perpendicular to the layers, will tend to broaden the exciton line by field ionization in the plane, as discussed above for parallel field QW electroabsorption. This mechanism depends directly on the sample purity, and is predicted to be a problem at $\sim 10^{16}\,\mathrm{cm}^{-3}$ impurity density. It may explain the correlation that is sometimes observed between samples that show strong broadening with field and those in which the overall magnitude of the photocurrent signal depends strongly on voltage; both effects could be explained by a large impurity concentration in the quantum well region.

Electroabsorption for fields perpendicular to the layers has also been observed in a number of QW materials systems other than GaAs/AlGaAs on GaAs. These materials include: InGaAs/InGaAlAs (Wakita *et al.* 1985a); InGaAs/InAlAs (Wakita *et al.* 1985b,c, 1986, 1987); GaSb/AlGaSb (Miyazawa *et al.* 1986, Wood *et al.* 1987a); InGaAs/GaAs strained QWs on GaAs substrates (Van Eck *et al.* 1986); InGaAs/InP (Bar-Joseph *et al.* 1987, Moseley *et al.* 1987, Shorthose *et al.* 1987, Nojima *et al.* 1987); InGaAsP/InP (Temkin *et al.* 1987); ZnSe/(Zn,Mn)Se (Fu *et al.* 1987); and GaAs/AlGaAs on InP (Lee *et al.* 1987). Some of these measurements show clear shifts in absorption spectra with sharp exciton peaks retained at high fields (the GaSb/AlGaSb work, InGaAs/GaAs, some of the InGaAs/InP work (Bar-Joseph *et al.* 1987)). In some of the rest of the work, the spectra show considerable broadening with field that may

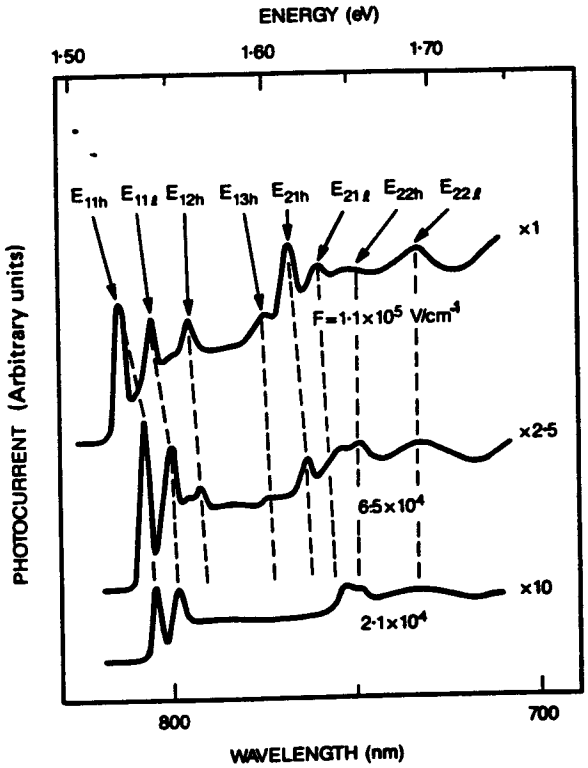

Figure 13. Photocurrent spectra at 77 K for 105 Å GaAs quantum wells, showing the growth of forbidden transitions with field. E_{nmh} refers to the transition between the nth electron state and the mth heavy-hole state, and similarly with l instead of h for the light-hole states. (After Yamanaka *et al.* (1986).)

be due to the random impurity field model discussed above. There has also been a theoretical prediction that the electroabsorption of copolymers would also show behaviour similar to the QCSE (Seel *et al.* 1988). Another interesting prediction is that there is a 'built-in' QCSE in strained superlattices grown on the [111] crystallographic direction, because substantial piezoelectric fields (e.g. $10^5\,\mathrm{V\,cm^{-1}}$) will exist because of the strain (Smith 1986, Mailhiot and Smith 1986, 1987, Smith and Mailhiot 1987).

It is apparent from the discussion of the QCFK above and from the form of equation (2.2.6) that one of the features of the QCSE is the appearance of 'forbidden' transitions as the field is applied. These can be seen quite clearly in experimental spectra (figure 13) (Yamanaka *et al.* 1986, Iwamura *et al.* 1985, Miller *et al.* 1986b, Collins *et al.* 1987a), and can be used to deduce the band offsets. The first forbidden transition (heavy-hole 2 to electron 1) is also apparent in figure 10 as the third, (highest energy) peak appearing at high field in the spectra for optical electric vector parallel to the layers. In general, the shifts associated with higher subbands are smaller, because these higher energy states are more difficult to perturb; the directions of these shifts can also vary. For a specific discussion, see also Ikonic *et al.* (1987b).

It is also possible to see the consequences of the shifts of the subbands with field in the transitions between subbands within one band. The selection rules here require an optical electric vector perpendicular to the layers, and at zero field in a symmetric

quantum well only transitions between states of the opposite parity are allowed (e.g. between state 1 and state 2). This has been examined experimentally by absorption in doped quantum wells (Harwit and Harris 1987) and by Raman scattering (Bajema *et al.* 1987) with further theoretical work by Ahn and Chuang (1987a,b). 'Forbidden' transitions should also become partly allowed when the symmetry is broken by an applied field perpendicular to the layers (e.g. between state 1 and state 3) (Ahn and Chuang 1987a).

Another consequence of the forbidden transitions for interband absorption is sum rules (Miller *et al.* 1986b, Whitehead *et al.* 1988). It is apparent from the spectra of figure 10 for optical electric vector perpendicular to the layers, for example, that, although the absorption of the lowest heavy-hole transition is weakened by the field, the absorption at higher photon energies (above the 'forbidden' third peak) is essentially unchanged. This is because the 'forbidden' transition has acquired the absorption lost by the allowed transition. This is the third of three sum rules that can be proved quite generally (Miller *et al.* 1986b), which are:

(1) the field-induced absorption change integrated over the entire spectrum is zero (this is generally true even for bulk materials);
(2) the integrated absorption over the excitonic lines associated with a given valence subband to conduction subband transition is (approximately) proportional to the square of the z overlap integral (i.e. proportional to the height of the step);
(3) the sum of the heights of the steps (z overlap integrals squared) from any one conduction (valence) subband to all the valence (conduction) subbands is conserved.

Sum rule (1) has been tested experimentally over a large spectral range with agreement within less than 1%. Sum rule (2) allows us to make a meaningful quantitative comparison between theory and experiment for the z overlap integral without having to evaluate all the in-plane excitonic orbital motions. Figure 14 shows the comparison of the calculated squared z overlap integral with the experimental area under the

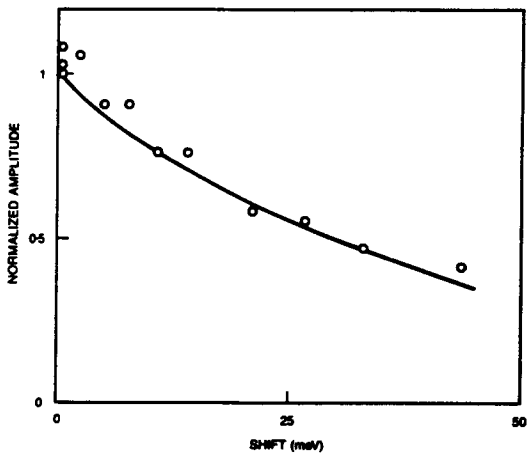

Figure 14. Comparison of experimental exciton absorption peak area with calculated squared z overlap integral. (After Miller *et al.* (1986b).)

excitonic absorption peak in the spectra with optical electric vector perpendicular to the layers in figure 10 (Miller *et al.* 1986b).

The changes in absorption associated with the QCSE must also, of course, result in changes in refractive index. For symmetric quantum wells, these refractive index changes must be even order (e.g. quadratic) with field (e.g. Kerr effect), in contrast to the more usual linear electro-optic effect (Pockels effect). This has received considerable theoretical (Yamamoto *et al.* 1985, Weiner *et al.* 1987a, Hiroshima 1987, Guy *et al.* 1987) and experimental (Glick *et al.* 1985, 1986, 1987, Nagai *et al.* 1986a,b, Kan *et al.* 1987, Koren *et al.* 1987, Wakita *et al.* 1987, Wood *et al.* 1987b, Zucker and Hendrikson 1988) attention. Inclusion of the excitons is very important for any quantitatively correct estimate of the magnitude of the effect. Most of the calculations proceed essentially by Kramers–Krönig transformation of theoretical or experimental absorption spectra. All such experimental spectra only cover a finite spectral range and some method must be found to handle this since the Kramers–Krönig transform is theoretically over infinite limits. The sum rules can be of some help here (Weiner *et al.* 1987a) in preventing unphysical answers. A calculated electrorefraction spectrum is shown in figure 15. The resulting changes in index can be large, although it is still difficult to contemplate induced changes in optical path of the order of half a wavelength in less than one absorption length (which would be very interesting from a device point of view) without total path lengths through the quantum wells $\gtrsim 100\,\mu m$, thus making refractive devices operating with light perpendicular to the layers difficult.

Thus far, we have discussed the electroabsorption as if the light holes and heavy holes were totally distinct kinds of particles. In reality, this is not true once their momentum is finite as discussed in section 2.1. Variational calculations incorporating valence band mixing (Sanders and Bajaj 1987a) show field-induced band 'crossings' and forbidden transitions, and also lifting of the Kramers degeneracy, giving split

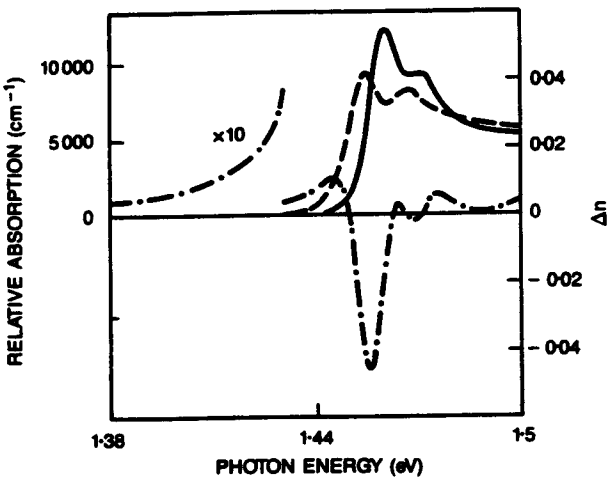

Figure 15. Calculation of the change in refractive index induced by a field perpendicular to a 95 Å GaAs quantum well. The solid and dashed lines show the absorption spectra at $0\,V\,cm^{-1}$ and $6{\cdot}4 \times 10^4\,V\,cm^{-1}$ respectively, and the dot-dashed line shows the calculated change of refractive index. (After Weiner *et al.* (1987a).)

excitons with field. Experimental observations of band mixing effects include observation of a field-induced coupling of heavy-hole exciton excited states and the light-hole exciton ground state (Vina *et al.* 1987b). Evidence of Γ–X mixing was also obtained through an anticrossing seen with electric field (Meynadier *et al.* 1988).

Most of the discussion so far has concerned simple 'rectangular' quantum wells. The mechanisms and models can also be extended to more complex structures. Islam *et al.* (1987) and also Chen *et al.* (1987) examined coupled quantum wells (i.e. two identical wells separated by a thin barrier) experimentally, with good agreement with theory for shifts and overlap integrals for the first few transitions (Islam *et al.* 1987). These coupled wells also show evidence of valence band mixing especially for higher transitions. Asymmetric coupled wells have also been investigated experimentally (Le *et al.* 1987, Little *et al.* 1987). Graded wells have received some theoretical attention (Sanders and Bajaj 1987b, Nishi and Hiroshima 1987, Hiroshima and Nishi 1987). These asymmetric structures have an effect similar in some ways to pre-biasing a symmetric structure with an additional field; certainly the response is no longer symmetric in the field. Parabolic wells have also been considered theoretically (Yang Qing and Yang Chu-liang 1987).

It is worth mentioning here the electroabsorption of superlattices with strong coupling between adjacent wells, although the mechanisms may be rather different from the QCSE because of the strong tunnelling. There have been some theoretical calculations on electroabsorption in superlattices (Jogai and Wang 1987, Austin and Jaros 1987, McIlroy 1986, Bleuse *et al.* 1988) although the theory of Jogai and Wang (1987) does not agree with subsequent work (Bleuse *et al.* 1988). Bleuse *et al.* (1988) make an interesting prediction of electric-field-induced localization resulting in an effective blue shift of the absorption edge (Mendez *et al.* 1988). One electroreflectance measurement has been reported for a superlattice (Behn and Gobsch 1987) showing quenching of the exciton as in bulk material without any measurable shift. In spatially indirect superlattices, the absorption can blue-shift with field due mainly to simple electrostatics; the electron and hole are spatially separated and hence acquire an ever higher energy as the field increases. The separation of electron and hole is caused by the structure, and is in the opposite direction to any field-induced effects, hence the difference in the sign of the shift compared to the QCSE (Danan *et al.* 1987).

Finally we will briefly discuss the theory of electroabsorption in more highly confined structures (Miller *et al.* 1988, Schmitt-Rink *et al.* 1987). To study this situation we can consider a cuboidal box with infinitely high potential barriers, and will take the QCFK approach of neglecting the Coulomb interaction for the moment. When this is done, we obtain a set of six completely separated Schrödinger equations of the form of equation (2.2.8), one for each coordinate direction and particle, because there is no coupling between the particles or directions. This problem is exactly solvable for all field directions. Equation (2.2.1) now becomes

$$\operatorname{Im}\chi \propto \sum_{p_z,q_x,r_y,s_z,t_x,u_y} |\langle \psi^{e}_{p_z,q_x,r_y} | \psi^{h}_{s_z,t_x,u_y} \rangle|^2 \times \delta(\omega - E^{e}_{p_z} - E^{e}_{q_x} - E^{e}_{r_y} - E^{h}_{s_z} - E^{h}_{t_x} - E^{h}_{u_y} - E_g), \quad (2.2.10)$$

where $\psi^{e}_{p_z,q_x,r_y} = \psi^{e}_{p_z}\psi^{e}_{q_x}\psi^{e}_{r_y}$ with $\psi^{e}_{p_z}$, $\psi^{e}_{q_x}$ and $\psi^{e}_{r_y}$ as the eigenfunctions and $E^{e}_{p_z}$, $E^{e}_{q_x}$, and $E^{e}_{r_y}$ as the eigenenergies of the individual Schrödinger equations for the z, x and y coordinate directions for the electron, and similarly for the hole.

If we assign a broadening to the δ functions to remove the mathematical singularities, we can obtain calculated spectra for boxes of different dimensions as shown

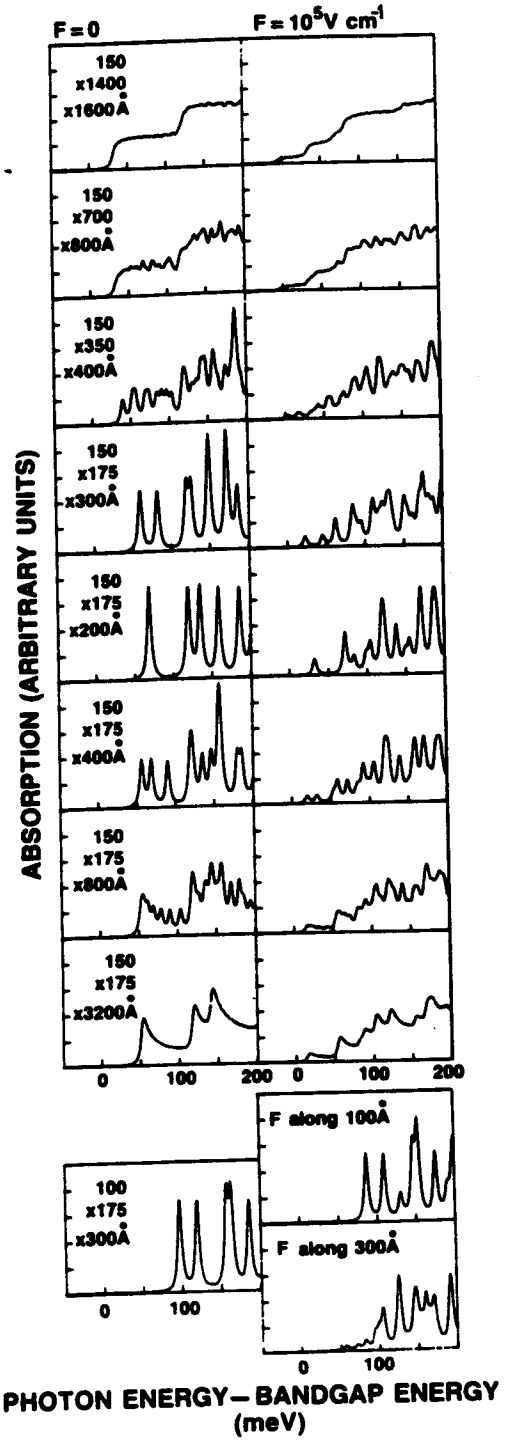

Figure 16. Absorption with and without field, F, calculated for a GaAs-like semiconductor box in the quantum-confined Franz–Keldysh approximation. A line broadening of 3 meV half-width has been used. Field F is along the 150 Å direction except as noted. (After Miller *et al.* (1988).)

in figure 16. Proceeding from top to bottom of figure 16 we see first essentially QW-like behaviour, changing to quantum box behaviour with isolated lines as two of the dimensions are decreased, and changing to quantum wire behaviour as one of them is increased again. Finally, we see anisotropic behaviour; fields along the short direction give strongly quantum-confined behaviour, with discrete lines shifting, whereas fields along the long direction give a smeared behaviour with the absorption strength distributed among many weak transitions especially in the absorption tail, just as in thick QWs.

In the limit of a small quantum box (i.e. much smaller than the exciton diameter in all directions) the Coulomb effect becomes negligible anyway compared with the quantum confinement, and this kind of calculation becomes again a QCSE calculation.

The shifts of the transitions in the quantum box are exactly the same as those of a QW of the same thickness. One intriguing possibility is that, if such structures could be made, we would be able to shift a much larger absorption for the same field because the absorption is concentrated into discrete lines.

2.3. *Effects of doping*

Modulation-doped heterostructures (Dingle *et al.* 1978, Gossard and Pinczuk 1985) provide an excellent means for the realization of a 2D electron or hole gas and have shown many remarkable new physical phenomena, such as the fractional quantum Hall effect (Tsui *et al.* 1982). They are also extremely attractive from the device point of view.

Much of their significance derives from the fact that—unlike in doped bulk semiconductors—the carriers are spatially separated from the dopants, which results in extremely high carrier mobilities (up to several $10^6\,cm^2\,V^{-1}\,s^{-1}$). Figure 17 shows the structure of a typical (n-type) modulation-doped quantum well structure (MDQW). During growth, the dopants are restricted to the barrier material. In order

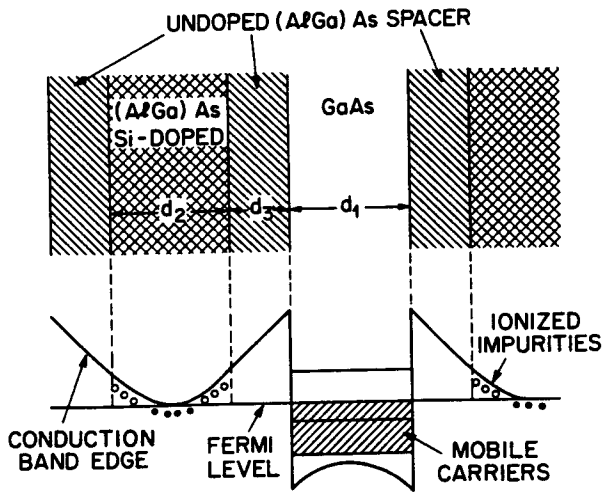

Figure 17. Sequence of layers and relative position of the conduction band edges in Si modulation-doped GaAs/AlGaAs quantum well structures. (After Gossard and Pinczuk (1985).)

to maintain a constant Fermi energy throughout the sample, they ionize with the free carriers migrating to the lower-energy quantum well(s).

The charge transfer creates significant electric fields. In single-interface structures, these fields confine the carriers at the heterojunction, in much the same way as in inversion layers (Ando *et al.* 1982, Stern and Das Sarma 1984). In the framework of density functional theory, the Kohn–Sham (1965) potential, V_{KS}, felt by a carrier consists of several parts

$$V_{KS}(z) = V(z) + V_H(z) + V_{XC}(z). \tag{2.3.1}$$

The first term, V, is the same as in equation (2.1.7), it describes the band offset. The Hartree potential, V_H, consists of the electrostatic potentials due to the ionized impurities and free carriers (including the respective image forces). Through Poisson's equation, it depends in turn on the local carrier density and thus has to be determined self-consistently. It gives rise to the band bending shown in figure 17. For example, for n-type MDQWs and electrons (figure 17), one has (neglecting image forces)

$$\frac{d^2}{dz^2} V_H(z) = -\frac{4\pi e^2}{\epsilon_0}[\varrho_e(z) - \varrho_d(z)], \tag{2.3.2}$$

where ϱ_e and ϱ_d are the electron and ionized donor densities respectively. If ϱ_e is approximated by a homogeneous density, N/L_z, this yields (inside the QW)

$$V_H(z) \sim -\frac{2\pi N e^2}{\epsilon_0 L_z} z^2, \quad -\frac{L_z}{2} \leqslant z \leqslant \frac{L_z}{2}, \tag{2.3.3}$$

that is, the band bending varies roughly like a parabola (Ploog and Doehler 1983). Finally, V_{XC} is the so-called exchange-correlation potential, it describes the residual many-body effects (see below).

Variational and numerical calculations of the electronic structure of MDQWs have been performed by Ando and Mori (1979) and Bauer and Ando (1985, 1986a,b), using the local density approximation (LDA). In this approximation, V_{XC} is replaced by the exchange-correlation part of the chemical potential, μ_{XC}^{3D}, of a homogeneous electron (hole) gas with the same local carrier concentration. The results of these calculations have been favourably compared with luminescence data of Pinczuk *et al.* (1984). The agreement is somewhat surprising, because the Kohn–Sham orbitals and energies obtained from equation (2.3.1) are ground state properties that have no direct physical meaning. The failure of interpreting these quantities in terms of quasi-particle ('electrons' and 'holes') properties is well documented, resulting in band gaps in semiconductors and insulators being generally underestimated by 30–50% (Sham and Schlüter 1983). Besides, μ_{XC}^{3D} is quite different from μ_{XC}^{2D}, the relevant quantity to compare with experiments, which for narrow MDQWs casts some doubts on the validity of the LDA itself.

The proper way to describe many-body effects is to start from the Hartree solution and incorporate exchange and correlation effects through self-energy corrections, as done by Bauer and Ando (1985, 1986a,b) and Kleinman and Miller (1985). This method, however, faces the difficulty that in two dimensions and (more so) in one dimension, most many-body systems become automatically strongly correlated ones, with the renormalizations being dominated by Coulomb repulsion rather than by random-phase-approximation (RPA)-type collective effects (for a $1/r$ interaction, two is the 'upper critical dimension'). This fact was recognized very early in studies of the classical 2D electron plasma (Totsuji 1975) and inversion layers (Ando *et al.* 1982),

but little progress has been made since then. We shall describe what has actually been done and why the quantitative problem is still open (like most of the other many-body problems addressed in this review).

In the presence of many-body interactions and (for ease of discussion) in the isotropic EMA, the Schrödinger equation for the electron or hole envelope functions $\psi(\mathbf{r}, z)$ takes on the form

$$\left[-\frac{\nabla^2}{2m_{e,h}} + \frac{E_g}{2} + V(z) + V_H(z)\right]\psi(\mathbf{r}, z) + \int d^2r'\,dz'\,\Sigma(\mathbf{r} - \mathbf{r}', z, z', E)\psi(\mathbf{r}', z') = E\psi(\mathbf{r}, z), \tag{2.3.4}$$

where $\mathbf{r}$ is the in-plane coordinate and Σ the self-energy. (Here and in the next few paragraphs, we omit the indices e and h.) Owing to the presence of the interfaces, Σ is non-local in z. Additionally, it is non-local in energy, because the renormalization of a particle depends on how fast it moves through its environment. A fast particle feels less of other carriers than a slow one, that is, its renormalization is smaller.

In superlattices and in multiple quantum well structures, the long-range Coulomb interaction couples different wells, which provides an additional source of nonlocality (Visscher and Falicov 1971, Fetter 1973, 1974). The physics associated with such local field effects is beyond the scope of this article and shall not concern us here. We will restrict ourselves to mentioning some of the important consequences.

Let $\psi_\alpha^0(\mathbf{r}, z)$, E_α^0 be the Hartree solutions of equation (2.3.4),

$$\left[-\frac{\nabla^2}{2m_{e,h}} + \frac{E_g}{2} + V(z) + V_H(z)\right]\psi_\alpha^0(\mathbf{r}, z) = E_\alpha^0\psi_\alpha^0(\mathbf{r}, z), \tag{2.3.5}$$

where the quantum number α comprises the in-plane momentum and subband index. The renormalized quasi-particle energies are then given by the solutions of the equation

$$\det[(E_\alpha^0 - E)\delta_{\alpha,\beta} - \Sigma_{\alpha\beta}(E)] = 0, \tag{2.3.6}$$

where

$$\Sigma_{\alpha\beta}(E) = \int d^2r\,dz \int d^2r'\,dz'\,\psi_\alpha^{0*}(\mathbf{r}, z)\Sigma(\mathbf{r} - \mathbf{r}', z, z', E)\psi_\beta^0(\mathbf{r}', z'). \tag{2.3.7}$$

Note that the self-energy equation (2.3.7) is diagonal in both the 2D and 3D limits.

Extensive studies of the 3D homogeneous electron gas have shown that both in the non-degenerate, classical and in the degenerate, metallic limit most of the renormalizations are accounted for by short-range exchange and long-range Coulomb correlations, as described by the so-called random phase approximation (RPA) to Σ and variations thereof. In the non-degenerate, classical limit, the RPA becomes exact, because of the long-range nature of the r^{-1} interaction in 3D. This is no longer true in 2D and 1D, where short-range Coulomb correlations play an important role as well, in much the same way as in Fermi systems with a hard core repulsion, such as ^{3}He. This is as expected, because the lower the dimension, the more the discreteness of the individual particles is pronounced.

The theoretical description of such short-range correlations is complicated and the subject of extensive research. Consistent, exchange-symmetric approaches were formulated mainly in the context of liquid ^{3}He, for example, by Pfitzner and Wölfle (1987). They usually involve the summation of so-called parquet diagrams in the

coupled particle-particle and (two) particle-hole channels. For the degenerate 2D homogeneous electron gas, a somewhat simpler point of view was adopted by Nagano *et al.* (1984). Neglecting long-range correlations altogether, they calculated the effective electron–electron interaction from the forward scattering T matrix, as determined by the Bethe–Goldstone equation. Their results for the correlation energy compare very well with variational Monte Carlo data (Ceperley 1978), which—together with Totsuji's (1975) exact results for the non-degenerate, classical case—suggests a satisfactory description of 2D Coulomb systems in terms of a 'screened ladder approximation'. The main physical feature of such a scheme is the (expected) cut-off of screening at distances corresponding to the closest approach of like particles, as given by the size of the exchange-correlation hole. We are not aware of any corresponding calculations, except for Jonson's (1976) application of the STLS approach (Singwi *et al.* 1968) to inversion layers. As in other instances, this simple, self-consistent scheme works better than one would *a priori* expect, as far as total energies are concerned.

With the exception of the above papers, most of the theoretical work on exchange-correlation effects has been preoccupied with extensions of RPA-type schemes from 3D to 2D. The comparison with exact and variational Monte Carlo results shows that the error involved can be significant. Finite well or layer size effects soften the Coulomb interaction at distances small compared with L_z, so that the 'figure of merit' is the ratio of L_z to the exchange-correlation hole of the strictly 2D system (which in turn is bounded by the 2D mean particle distance, $N^{-1/2}$). Only if this ratio is 'large', can RPA-type calculations be trusted.

Given these caveats, and before turning to experiments, we shall now discuss briefly the physics of the RPA-type approach to exchange-correlation effects. For ease of discussion, we assume a homogeneous 2D system. This allows for a direct comparison with 3D; the extension to the non-local, finite L_z case is trivial (but tedious). Among other things, it involves the multiplication of the bare 2D Coulomb interaction, $I(q) = (2\pi e^2)/(\epsilon_0 q)$, by charge density form factors

$$\int \mathrm{d}z \int \mathrm{d}z' \, e^{-q|z-z'|} \psi_n^{0*}(z) \psi_m^{0*}(z) \psi_l^0(z') \psi_o^0(z'), \tag{2.3.8}$$

where $\psi_\alpha^0(\mathbf{r}, z) = \exp(\mathrm{i}\mathbf{k}\cdot\mathbf{r})\psi_n^0(z)$. Within the $n_z = 1$ subspace, equation (2.3.8) is of course equivalent to the separable *Ansatz* for the exciton ground state wavefunction, discussed in section 2.1.

Within the RPA, the self-energy, Σ, can be split into a 'screened exchange' (sx) and a 'Coulomb hole' (Ch) term, $\Sigma = \Sigma_{\mathrm{sx}} + \Sigma_{\mathrm{Ch}}$. On the energy shell, one finds

$$\Sigma_{\mathrm{sx}}(k) = -\sum_{k'} I_s(\mathbf{k} - \mathbf{k}', \epsilon_k - \epsilon_{k'}) f(k'), \tag{2.3.9}$$

$$\Sigma_{\mathrm{Ch}}(k) = \sum_{k'} \int_{-\infty}^{+\infty} \frac{\mathrm{d}\omega}{\pi} \frac{\mathrm{Im}\, I_s(\mathbf{k} - \mathbf{k}', \omega) g(-\omega)}{\epsilon_k - \epsilon_{k'} - \omega + \mathrm{i}\delta}, \tag{2.3.10}$$

where $\epsilon_k = k^2/(2m_{\mathrm{e,h}}) +$ constant are the Hartree energies and $f(k)$ is the Fermi distribution,

$$N = 2\sum_k f(k) = 2\sum_k \frac{1}{\exp[(\epsilon_k - \mu)/T] + 1}, \tag{2.3.11}$$

and $g(\omega)$ the Bose distribution,

$$g(\omega) = \frac{1}{\exp(\omega/T) - 1}. \tag{2.3.12}$$

Finally, $I_s(q, \omega)$ is the screened Coulomb interaction,

$$I_s(q, \omega) = I(q) \frac{\epsilon_0}{\epsilon(q, \omega)}, \tag{2.3.13}$$

where $\epsilon(q, \omega)$ is the RPA dielectric function, given by the Lindhard formula

$$\epsilon(q, \omega) = \epsilon_0 \left[1 - 2I(q) \sum_{\mathbf{k}} \frac{f(k) - f(\mathbf{k} + \mathbf{q})}{\omega + i\delta + \epsilon_k - \epsilon_{k+q}} \right]. \tag{2.3.14}$$

Expressions (2.3.9) and (2.3.10) are both negative and therefore lead to a lowering of the quasi-particle energies, usually called band gap renormalization (BGR). Σ_{sx} describes the energy that parallel-spin, like particles gain by avoiding each other, while Σ_{Ch} describes the energy gain due to charge polarization of the medium. An elegant evaluation of the respective ground state energy of the 2D homogeneous electron gas was given by Ioriatti and Isihara (1981).

For computational purposes, equation (2.3.14) can be simplified considerably by replacing the total RPA excitation spectrum by a single effective plasmon mode ω_q (Lundqvist 1967 a,b, Overhauser 1970, Vinter 1976),

$$\frac{1}{\epsilon(q, \omega)} = \frac{1}{\epsilon_0} \left[1 + \frac{\omega_p^2(q)}{(\omega + i\delta)^2 - \omega_q^2} \right]. \tag{2.3.15}$$

$\omega_p(q)$ is the 2D plasma frequency, $\omega_p^2(q) = (2\pi N e^2 q)/(\epsilon_0 m_{e,h})$, which in contrast to 3D has a square-root dispersion; in 2D the r^{-1} interaction is not long-ranged enough to push $\omega_p(q)$ to a finite value. ω_q is the frequency of the effective plasmon mode,

$$\omega_q^2 = \omega_p^2(q) \left[1 + \frac{q}{\kappa} \right] + \left[\frac{q^2}{2m_{e,h}} \right]^2, \tag{2.3.16}$$

where $\kappa = [-4\pi e^2 \Sigma_k \partial f(k)/\partial \epsilon_k]/\epsilon_0$ is the 2D screening wavenumber. Another choice for ω_q is

$$\omega_q^2 = \omega_p^2(q) \frac{\epsilon(q, 0)}{\epsilon(q, 0) - \epsilon_0}, \tag{2.3.17}$$

with $\epsilon(q, 0)$ obtained from equation (2.3.14). For short and long wavelengths expressions (2.3.16) and (2.3.17) coincide. Similar relations hold in 3D.

The model in equation (2.3.15) is constructed in such a way that the most important sum rules are satisfied. These are the *f*-sum rule, the conductivity sum rule, the perfect screening sum rule and the compressibility sum rule. The dispersions in equations (2.3.16) and (2.3.17) reproduce the correct RPA screening behaviour at long wavelengths and simulate the individual particle–hole excitations at short wavelengths. Lattice dynamics can be readily incorporated. For $T \to 0$, the 2D screening wavenumber, κ, reduces to a constant, $\kappa = (2m_{e,h}e^2)/\epsilon_0$, due to the constant density of states, while in the non-degenerate, classical limit it takes on the value $\kappa = (2\pi N e^2)/(\epsilon_0 T)$.

Except for very high densities (see below), the Coulomb hole self-energy usually dominates. At $T = 0$, the resulting BGR varies like $N^{1/3}$. This can be easily seen

(Schmitt-Rink and Ell 1985) by using an argument due to Thuselt (1983). Replacing ω_q in equation (2.3.15) by its asymptotic forms (see equation (2.3.16)), $\omega_q = \omega_p(q)$ for $q \leqslant q_0$ and $\omega_q = q^2/(2m_{e,h})$ for $q \geqslant q_0$, with $\omega_p(q_0) = q_0^2/(2m_{e,h})$, one readily finds $\Sigma_{Ch} \sim q_0 \sim N^{1/3}$. In 3D, the same calculation yields $\Sigma_{Ch} \sim N^{1/4}$ (Thuselt 1983). At very high densities, the exchange self-energy, $\Sigma_x \sim N^{1/2}$, dominates. In this context, it should be noted that for finite L_z and $N^{1/2}L_z \sim O(1)$, a cross-over to 3D behaviour occurs, namely $\Sigma_x \sim N^{1/3}$. For $T = 0$ and in a real system, a cubic root behaviour is thus always expected. All the physics is contained in the (L_z-dependent) prefactor. The comparison with variational Monte Carlo results (Ceperley 1978) shows that in 2D this prefactor is overestimated by the RPA. The reported almost exact agreement of experiment and theory (Bauer and Ando 1985, 1986a, Kleinman and Miller 1985) thus comes as a surprise (see also section 3.1).

In superlattices and multiple quantum well structures, strong 3D screening is partially restored by local field effects (Visscher and Falicov 1971, Fetter 1973, 1974). As shown by Harwrylak (1987), this leads to a lowering of Σ and presumably to a deviation from the $N^{1/3}$ behaviour.

The breakdown of the RPA in 2D is most easily demonstrated by considering the non-degenerate, classical limit, in which equation (2.3.10) reduces to

$$\Sigma_{Ch} = \frac{1}{2}\sum_q [I_s(q) - I(q)], \tag{2.3.18}$$

where $I_s(q) = I_s(q, 0) \sim (2\pi e^2)/[\epsilon_0(q + \kappa)]$, with $\kappa = (2\pi N e^2)/(\epsilon_0 T)$. Obviously, Σ_{Ch} diverges logarithmically. As discussed above and shown by Totsuji (1975), this divergence is due to the neglect of Coulomb repulsion. The latter ensures that screening is cut off at distances corresponding to the closest approach of like particles, $q_c^{-1} \sim e^2/(\epsilon_0 T)$ for particles of energy T. The resulting Coulomb hole self-energy varies like $N \log N$, characteristic of dilute strongly repulsive 2D systems. Multilayer screening and finite thickness effects partially restore the validity of equation (2.3.18), with of course suitably modified interactions (Dahl 1988). In 3D, equation (2.3.18) is exact and identical to the Debye shift. The same is true in the 2D Coulomb gas (May 1967) above the Kosterlitz–Thouless (1973) transition. In the latter system, the electromagnetic field is confined too, so that the Coulomb interaction varies only smoothly like $\log r$ (Keldysh 1979).

The renormalized quasi-particle energies are given by

$$E_k = \epsilon_k + \Sigma(k), \tag{2.3.19}$$

with different renormalizations for electrons and holes and different subbands. For example, in an n-type material, electrons experience exchange and correlation effects, while holes experience correlation (Coulomb hole) effects only. Additionally, inter-subband renormalization, the renormalization induced in excited subbands by carriers in lower subbands, is small. This is due to the fact that different normal motion quantum numbers, n_z, correspond to large differences in velocities perpendicular to the interface. The notion of a rigid shift of all subbands must clearly be rejected.

The momentum dependence of Σ is sometimes neglected and the self-energy replaced by the exchange-correlation part of the chemical potential, μ_{XC}. A suitable definition of μ_{XC} for arbitrary temperatures is (Roesler *et al.* 1984)

$$\mu_{XC} = \sum_k \frac{\partial f(k)}{\partial \epsilon_k} \Sigma(k) \Big/ \sum_k \frac{\partial f(k)}{\partial \epsilon_k}. \tag{2.3.20}$$

At zero temperature, equation (2.3.20) reduces to the well known relation $\mu_{XC} = \Sigma(k_F)$, where $k_F = (2\pi N)^{1/2}$ is the Fermi wavenumber.

For purpose of illustration, we shall sometimes make use of Σ_{Ch}, equation (2.3.18), and the corresponding unretarded Σ_{sx},

$$\Sigma_{sx}(k) = -\sum_{k'} I_s(\mathbf{k} - \mathbf{k}')f(k'). \tag{2.3.21}$$

Equations (2.3.18) and (2.3.21) constitute a simple static approximation, which in 3D has been proven to be very powerful (Zimmermann *et al.* 1981, Loewenau *et al.* 1982, Schweizer *et al.* 1983, Haug and Schmitt-Rink 1984, 1985). Here I_s should be pictured as some suitably chosen effective interaction, and not as the overscreened static RPA I_s.

This concludes our brief discussion of the theory of exchange-correlation effects in modulation-doped heterostructures. Again, in our opinion, these effects are quantitatively not understood. This is even more true for the optical spectra, except that the difficulties are of a more fundamental nature and not related to dimensionality (Gavoret *et al.* 1969, Ruckenstein and Schmitt-Rink 1987).

The modulation-doped heterostructures most widely studied are GaAs wells with AlGaAs barriers, as well as InGaAs wells with InP or InAlAs barriers. The experimental techniques include luminescence, luminescence excitation (Pinczuk *et al.* 1984, Miller and Kleinman 1985, Sooryakumar *et al.* 1985, 1987, Ruckenstein *et al.* 1986, Meynardier *et al.* 1986, Skolnick *et al.* 1987, Delalande *et al.* 1986, 1987, Delalande 1987, Livescu *et al.* 1988) and direct absorption measurements (Lee *et al.* 1987, Chemla *et al.* 1987a, 1988a, Bar-Joseph *et al.* 1987b, Livescu *et al.* 1988, Huang *et al.* 1988).

Figure 18 shows absorption spectra of an undoped and an n-type ($N = 4{\cdot}8 \times 10^{11}\,\mathrm{cm}^{-2}$) modulation-doped InGaAs/InAlAs multiple quantum well structure ($L_z = 100\,\text{Å}$), as a function of temperature (Livescu *et al.* 1988). The absorption of the undoped sample exhibits the characteristic step-like structure associated with the constant 2D density of states. Excitonic peaks at the onset of each step are clearly seen at all temperatures. The strong peaks seen in the low-temperature spectrum ($T = 12\,\mathrm{K}$) are easily identified as transitions between $n_z = 1$, 2 and 3 electron and heavy-hole states. The weaker peaks correspond to transitions between $n_z = 1$ and 2 electron and light-hole states. With increasing temperature, the entire absorption shifts to lower energies, due to the decrease of the band gap, E_g. Simultaneously, the excitonic peaks broaden, due to interaction with thermal LO phonons, as discussed in section 2.1.

The modulation-doped sample has nominally the same structure as the undoped one, but its absorption reveals striking differences. Although the $n_z = 2$ and 3 transitions can be clearly identified too, the sharp $n_z = 1$ peaks have disappeared even from the low-temperature spectrum, being replaced by a single broad feature, blue shifted by a significant amount (about 40 meV). This blue shift is maintained over the whole temperature range. As the temperature is raised, the absorption edge peak broadens and disappears rapidly. At $T = 150\,\mathrm{K}$, only a 'knee' is left, which barely changes its shape up to room temperature. The higher energy peaks ($n_z = 2$ and 3) are observed at energies very similar to the corresponding peaks in the undoped sample, but they exhibit a somewhat larger width even at low temperature. In addition, their broadening from $T = 16$ to 300 K takes place at a much slower pace than that of the absorption edge peak. It is quite clear from these spectra already that the absorption edge peak is different in nature from the excitonic peaks seen in the undoped sample.

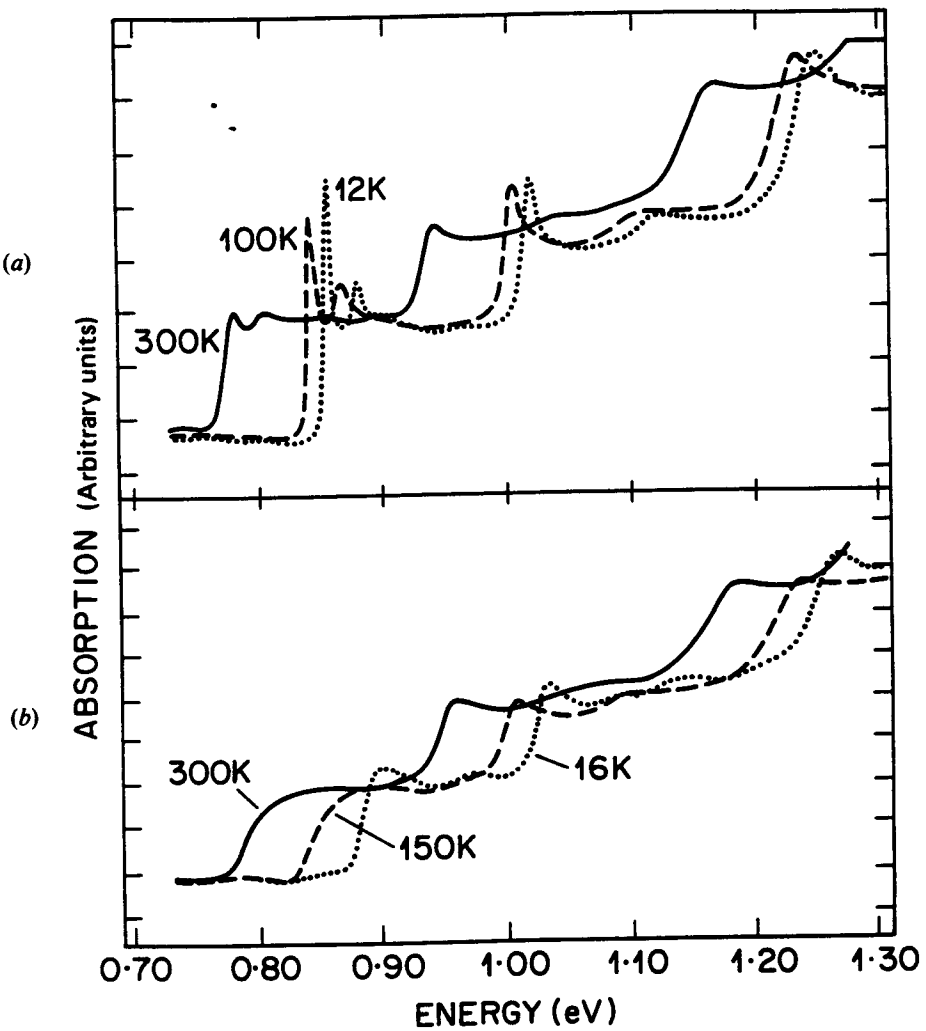

Figure 18. Absorption spectra of an undoped (*a*) and an n-type ($N = 4{\cdot}8 \times 10^{11}\,\mathrm{cm}^{-2}$) modulation-doped (*b*) InGaAs/InAlAs multiple quantum well structure ($L_z = 100\,\text{Å}$), as a function of temperature. (After Livescu *et al.* (1988).)

Similar measurements have been performed on n-type GaAs/AlGaAs multiple quantum well structures (Lee *et al.* 1987, Livescu *et al.* 1988, Huang *et al.* 1988). Figure 19 shows absorption (dashed line) and luminescence (full line) spectra of a sample with $N = 2{\cdot}6 \times 10^{11}\,\mathrm{cm}^{-2}$ and $L_z = 120\,\text{Å}$, as a function of temperature (Livescu *et al.* 1988). Similarly to the InGaAs/InAlAs system, the low-temperature absorption spectrum ($T = 10\,\mathrm{K}$) shows $n_z = 2$ and 3 transitions, while the sharp $n_z = 1$ exciton resonances, characteristic for the spectra of undoped samples, are replaced by a single peak. A blue shift of this peak with respect to the luminescence line is also observed. With increasing temperature, the absorption edge peak decreases and broadens, as in the previous sample. Simultaneously, the Stokes shift between luminescence and absorption diminishes. The changes are more spectacular here,

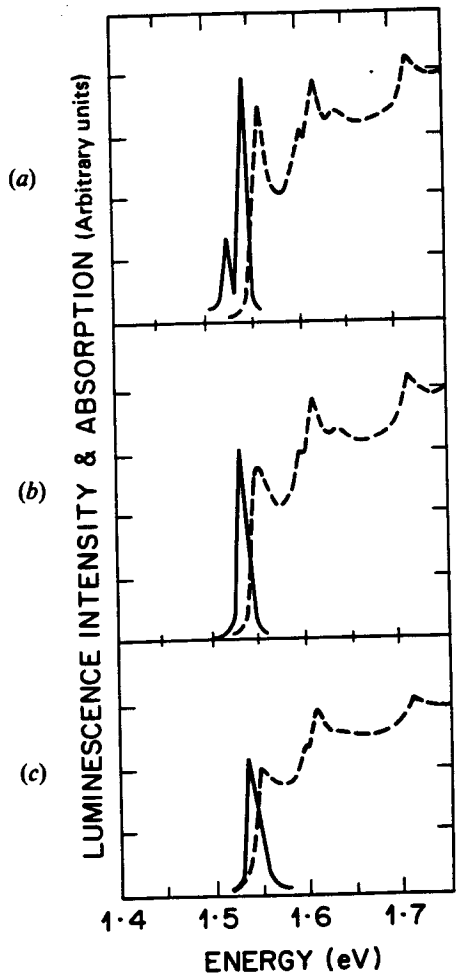

Figure 19. Absorption (dashed line) and luminescence (full line) spectra of an n-type ($N = 2{\cdot}6 \times 10^{11}\,\mathrm{cm}^{-2}$) modulation-doped GaAs/AlGaAs multiple quantum well structure ($L_z = 120\,\text{Å}$), as a function of temperature: (*a*), 10 K; (*b*), 50 K; (*c*), 100 K. (After Livescu *et al.* (1988).)

since the peak is much sharper to begin with. An increase in temperature of 50 K is enough to nearly double its linewidth. This should be compared with the situation in similar, undoped samples, where a temperature of 300 K is necessary to broaden the $n_z = 1$ heavy-hole exciton line by the same amount.

Figure 20 shows luminescence spectra of an n-type modulation-doped ($N = 9{\cdot}1 \times 10^{11}\,\mathrm{cm}^{-2}$) InGaAs/InP quantum well structure ($L_z = 100\,\text{Å}$), as a function of temperature (Skolnick *et al.* 1987). The low-temperature spectra reveal a clear asymmetry, with a strong enhancement towards high energies. Again, as the temperature is raised, this structure diminishes.

We shall discuss these and other results in the following paragraphs. The main features to be explained are:

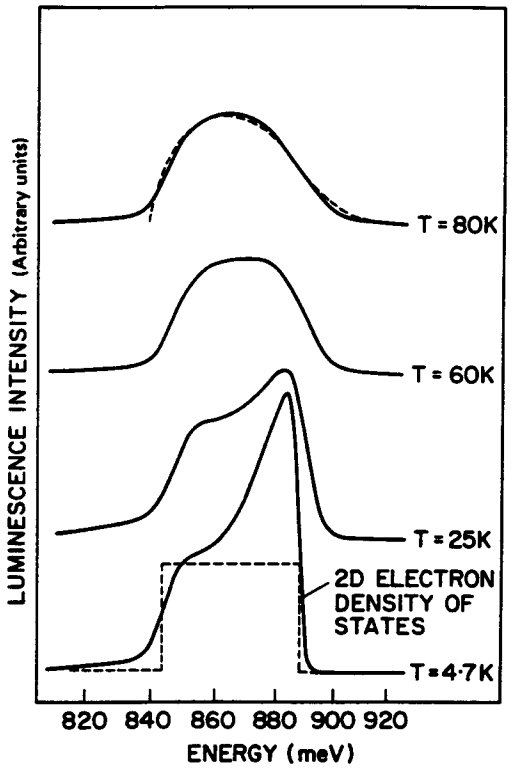

Figure 20. Luminescence spectra of an n-type ($N = 9{\cdot}1 \times 10^{11}\,\mathrm{cm}^{-2}$) modulation-doped InGaAs/InP quantum well structure ($L_z = 100\,\text{Å}$), as a function of temperature. Dashed lines: theoretical spectra from one-electron theory. (After Skolnick *et al.* (1987).)

(1) There is a Stokes shift between luminescence and absorption, which decreases with increasing temperature or decreasing doping.
(2) The absorption edge and—in alloy wells—the luminescence spectrum exhibit a peak which is strongly temperature dependent. Its behaviour is not consistent with that of a conventional exciton in an undoped quantum well structure.
(3) Except for small shifts and an increase in width, the higher energy absorption peaks are similar to those in undoped samples with identical structure. Temperature effects on these peaks are by far weaker than in the case of the edge peak.

We shall answer these and other questions by following the discussion of Ruckenstein *et al.* (1986) and Ruckenstein and Schmitt-Rink (1987).

We begin by considering the simple static picture corresponding to equations (2.3.18) and (2.3.21), in which the Fermi sea does not respond dynamically to the appearance or disappearance of a hole in the course of an optical transition. (For sake of clarity, we limit ourselves to n-type, homogeneous 2D systems, unless specified otherwise.) Although this simple picture is quite incomplete (see below), it yields already the right answers to most of the questions raised above. The model was originally introduced by Mahan (1967a) and applied to MDQWs by Kleinman (1985) and, more recently, by Rorison (1987) and Livescu *et al.* (1988), following some

related work by Schmitt-Rink and Ell (1985) and Schmitt-Rink *et al.* (1986) on photoexcited 2D systems. We shall discuss it in great detail, because it will also form the basis for our discussion of nonlinear optical effects in section 3.1.

According to section 2.1, the linear optical susceptibility, χ, of a homogeneous 2D semiconductor is given by the extension (Shinada and Sugano 1966) of Elliott's (1957) formula

$$\chi = \frac{2e^2|r_{vc}|^2}{L_z} \sum_n \frac{|\phi_n^0(r = 0)|^2}{E_n^0 - \omega - i\delta}, \tag{2.3.22}$$

where ϕ_n^0 and E_n^0 are respectively the unperturbed excitonic e–h relative motion wavefunctions and energies. (In the following, to distinguish the excitonic parameters in the presence of a perturbation from the unperturbed ones, we will label the latter with a superscript '0'). In linear response theory, the product of χ and the applied optical field, E, is identical to the polarization, P, induced by E. On the other hand, P will in general be given by the sum over its individual momentum space components, $er_{vc}P(k)$, corresponding to vertical optical transitions at points $\mathbf{k}$ in the Brillouin zone,

$$\begin{aligned} P &= \chi E \\ &= \frac{2er_{vc}}{L_z} \sum_k P(k). \end{aligned} \tag{2.3.23}$$

By using the k-space representation of the Wannier equation and identifying χE from equations (2.3.22) and (2.3.23), one readily finds that $P(k)$ obeys a Wannier equation off the energy shell, driven by the optical field, E.

$$\sum_{k'} [H^0_{k,k'} - (\omega + i\delta)\delta_{k,k'}]P(k') = er_{cv}E, \tag{2.3.24}$$

where

$$H^0_{k,k'} = (\epsilon_{ek} + \epsilon_{hk})\delta_{k,k'} - I(\mathbf{k} - \mathbf{k}') \tag{2.3.25}$$

is the unperturbed e–h relative motion Hamiltonian introduced in section 2.1, where the homogeneous Wannier equation (equation (2.1.11 *a*,*b*)) was discussed. The question is then simply how equation (2.3.24) and thus χ are modified by the presence of a Fermi sea.

Obviously, there are only two quantities which can change, namely the e–h relative motion Hamiltonian and the driving term, $er_{cv}E$. Because of the Pauli exclusion principle, optical transitions can only take place into unoccupied states. Therefore, in the presence of a conduction electron Fermi sea, we have to project out those final states that are already occupied, by multiplying $er_{cv}E$ in equation (2.3.24) by $1 - f_e(k)$,

$$er_{cv}E \rightarrow [1 - f_e(k)]er_{cv}E. \tag{2.3.26}$$

We shall call this effect the phase space filling (PSF) effect. In one-electron theory, it gives rise to the well known Burstein (1954) blue shift of the absorption edge, which accounts in part for point (1) above, namely the temperature- and density-dependent Stokes shift between absorption and emission: for a dilute finite-mass hole gas with a Maxwell–Boltzmann distribution f_h around $k = 0$ and a degenerate conduction electron Fermi sea, optical emission $\sim f_e f_h$ will be mainly from the bottom of the conduction band to the top of the valence band, namely at $\epsilon_{e0} + \epsilon_{h0}$, while optical absorption $\sim(1 - f_e)$ will start at $\epsilon_{ek_F} + \epsilon_{hk_F}$.

The changes in the e–h relative motion Hamiltonian comprise two kinds of corrections, the self-energy corrections discussed above and the corresponding vertex

corrections. The former correspond to the changes of the individual e and h energies due to exchange and correlation effects,

$$\epsilon_{ek} + \epsilon_{hk} \rightarrow \epsilon_{ek} + \epsilon_{hk} + \Sigma_e(k) + \Sigma_h(k), \tag{2.3.27}$$

while the latter describe the associated changes of the e–h interaction,

$$I(\mathbf{k} - \mathbf{k}') \rightarrow I(\mathbf{k} - \mathbf{k}') + \{[1 - f_e(k)]I_s(\mathbf{k} - \mathbf{k}') - I(\mathbf{k} - \mathbf{k}')\}. \tag{2.3.28}$$

First, $I(q)$ is replaced by some effective, screened interaction, $I_s(q)$, assumed to be local and unretarded, as discussed above. Then $I_s(q)$ is in turn multiplied by the PSF factor, $1 - f_e(k)$, because Coulomb scattering is of course also limited to final states above k_F.

The corrections in equations (2.3.27) and (2.3.28) are actually not independent of each other, but related by the Ward identity (Zimmermann *et al.* 1978, Haug and Schmitt-Rink 1984)

$$\Sigma_e(k) + \Sigma_h(k) = \sum_{\mathbf{k}'} \{[1 - f_e(k')]I_s(\mathbf{k} - \mathbf{k}') - I(\mathbf{k} - \mathbf{k}')\}. \tag{2.3.29}$$

Equation (2.3.29) is obviously identical to the sum of e and h Coulomb hole and e screened exchange self-energies, showing that, under the assumption of a local and unretarded interaction $I_s(q)$, equation (2.3.18) and (2.3.21) follow inevitably.

Summarizing equations (2.3.24)–(2.3.29), we find that, in the presence of a static conduction electron Fermi sea, the polarization $P(k)$ satisfies the equation

$$\sum_{\mathbf{k}'} [H^0_{\mathbf{k},\mathbf{k}'} + \delta H_{\mathbf{k},\mathbf{k}'} - (\omega + i\delta)\delta_{\mathbf{k},\mathbf{k}'}]P(k') = [1 - f_e(k)]er_{cv}E, \tag{2.3.30}$$

where

$$\begin{aligned}\delta H_{\mathbf{k},\mathbf{k}'} = & -\delta_{\mathbf{k},\mathbf{k}'} \sum_{\mathbf{k}''} I_s(\mathbf{k} - \mathbf{k}'')f_e(k'') + I_s(\mathbf{k} - \mathbf{k}')f_e(k) \\ & - \delta_{\mathbf{k},\mathbf{k}'} \sum_{\mathbf{k}''} [I(\mathbf{k} - \mathbf{k}'') - I_s(\mathbf{k} - \mathbf{k}'')] + [I(\mathbf{k} - \mathbf{k}') - I_s(\mathbf{k} - \mathbf{k}')].\end{aligned} \tag{2.3.31}$$

Equation (2.3.31) shows nicely the one-to-one correspondence between self-energy and vertex corrections and the fact that they always appear with opposite signs, which has important consequences (see below).

For low doping concentrations, $Na_0^2 \ll 1$, one can solve equations (2.3.30) and (2.3.31) in perturbation theory, by expanding about unperturbed exciton states (Schmitt-Rink and Ell 1985, Schmitt-Rink *et al.* 1985). The resulting optical susceptibility, χ, is given by

$$\chi = \frac{2e^2|r_{vc}|^2}{L_z} \sum_n \frac{f_n}{E_n - \omega - i\delta}, \tag{2.3.32}$$

where

$$\begin{aligned}f_n = & \phi^{0*}_n(r = 0) \sum_k [1 - f_e(k)]\phi^0_n(k) \\ & + \sum_{m \neq n} \frac{\phi^{0*}_n(r = 0)\langle m|\delta H|n\rangle\phi^0_m(r = 0) + (n \leftrightarrow m)}{E^0_n - E^0_m}\end{aligned} \tag{2.3.33}$$

are the renormalized oscillator strengths and

$$E_n = E^0_n + \langle n|\delta H|n\rangle, \tag{2.3.34}$$

the renormalized transition energies. Here, it is understood that all quantities are expanded up to $O(Na_0^2)$. Three types of effects can be identified:

(i) a shift of the exciton energies as a result of exciton–electron collisions,
(ii) a corresponding exciton wavefunction renormalization (second term in equation (2.3.33)), and
(iii) a PSF correction to the oscillator strength (first term in equation (2.3.33)).

Both (ii) and (iii) give rise to a decrease of χ, that is a bleaching, because they both reduce the probability $|\phi_n(r = 0)|^2$ of finding the e and h in the same unit cell.

The detailed study of the shift equation (2.3.34) reveals that (i) for infinitely separated e and h, it reduces to the BGR, $E_k = E_k^0 + \Sigma_e(k) + \Sigma_h(k)$, while (ii) for bound states, a strong compensation between vertex and self-energy corrections takes place, that is, the decrease in binding energy partially cancels the decrease in band gap. This important phenomenon, the relative constancy of bound state energies, was first explained by Gay (1971, 1972) and put on firm grounds by Zimmerman *et al.* (1978). The point is very simple: when one brings e and h together to form a bound state, their opposite polarization clouds partially cancel each other. The smaller the bound state radius, the larger this cancellation. For infinitely separated e and h, on the other hand, no such cancellation exists and one recovers the usual BGR.

Alternatively, one can explain the relative constancy of bound state energies in terms of a partial cancellation of attractive and repulsive forces, by comparing the expectation values of the first and last two terms in equation (2.3.31). The first two terms describe the effects of the exclusion principle and—in a weakly non-ideal boson picture—are suitably reinterpreted as being due to hard core repulsion between excitons and electrons. The last two terms describe the effects of screening and are thus equivalent to a poor man's Van der Waals attraction. Hard core repulsion gives rise to a blue shift, Van der Waals attraction gives rise to a red shift; again, a partial cancellation can be expected (Nozieres and Comte 1982, Haug and Schmitt-Rink 1984).

The changes in exciton oscillator strength can similarly be interpreted in an intuitive fashion (Schmitt-Rink *et al.* 1985). For $Na_0^2 \ll 1$, one finds from equation (2.3.33)

$$\frac{\delta f_{1s}}{f_{1s}^0} = -\frac{N}{N_s}, \tag{2.3.35}$$

with a temperature dependent saturation parameter, N_s. For $I_s(q) = I(q)$, N_s was estimated by Schmitt-Rink *et al.* (1985) and evaluated exactly by Zimmermann (1988a). Here, we shall restrict ourselves to the discussion of its qualitative behaviour.

It is often thought that screening governs the behaviour of N_s and thus of the unbinding of excitons. While this is partly correct in 3D, this notion must be clearly rejected in 2D. If one models the screened Coulomb interaction, $I_s(q)$, by its long-wavelength RPA value, then it is well known that the unbinding of 3D excitons takes place for a screening length, κ^{-1}, of the order of the exciton Bohr radius. This is Mott's (1974) original criterion. The point is that in 3D one needs a critical coupling strength to form a bound state. In 2D and 1D, however, bound states occur for arbitrarily small attractive potentials, which leads an extension of the Mott criterion *ad absurdum*. (Similarly, all states are localized in 2D and 1D disordered systems.) Zero-temperature studies of screened Coulombic impurities in 2D by Stern and Howard (1967), Brum *et al.* (1984) and Bastard (1985) demonstrate this fact very

nicely: with increasing N, the binding energy decreases until it saturates at some substantial fraction of its unscreened value, due to the constant 2D screening length. Enhanced multilayer screening reduces the magnitude of this value, depending on the ratio of the screening length to the layer spacing (Visscher and Falicov 1971, Fetter 1973, 1974, Hawrylak and Quinn 1986).

The consequences of this characteristic property of 2D systems for optical effects were not considered until recently (Schmitt-Rink *et al.* 1985, Kleinman 1985). If the effects of screening are weak, then the bleaching of exciton resonances will be mainly related to the blocking of the phase space that participates in the exciton wavefunction. A good measure of this effect, correct within a factor of two or three, is the relative change in oscillator strength due to PSF.

$$\frac{N}{N_S^{PSF}} = \lim_{N\to 0} \sum_k f_e(k)\phi_{1s}^0(k)/\phi_{1s}^0(r=0). \tag{2.3.36}$$

The evaluation of equation (2.3.36) is straightforward and yields (Schmitt-Rink *et al.* 1985)

$$\frac{1}{N_S^{PSF}} = \begin{cases} \pi a_0^2, & T \ll E_0, \qquad (2.3.37a) \\ 2\pi a_0^2 \dfrac{m}{m_e}\dfrac{E_0}{T}, & T \gg E_0. \qquad (2.3.37b) \end{cases}$$

This result has the following intuitive interpretation: when an exciton is created optically, the area occupied by it cannot sustain more carriers, that is, an exciton and an electron cannot occupy the same space (equation (2.3.37*a*)). Consequently, when $k_F a_0 \sim O(1)$, the excitonic optical absorption diminishes. Even in the case of hot free electrons (equation (2.3.37*b*)), the same notion can be retained, only now we must note that only a fraction of the electrons of order $(\lambda_e/a_0)^2 \sim E_0/T$ occupy the phase space sampled by an exciton (λ_e is the thermal de Broglie wavelength); thus electrons with thermal wavelength much smaller than the Bohr radius can occupy the same space as an exciton without violating Pauli exclusion.

This extremely simple concept explains a series of experimental observations on doped and photoexcited (see section 3.1) QWs remarkably well. We are referring to the facts that (i) in n-type MDQWs the $n_z = 1$ heavy- and light-hole excitons disappear approximately at the same density, while in p-type samples the $n_z = 1$ heavy-hole exciton disappears first (Miller and Kleinman 1985); and (ii) $n_z \geqslant 2$ excitons, for which PSF is ineffective, show up as in undoped samples, except for small red shifts and broadenings, which are obviously due to residual screening effects (point 3 above). (There is obviously some resemblance to the observation that in bulk semiconductors the states far above the fundamental absorption edge are hardly influenced by many-body effects because of their large kinetic energy.) An estimate of the exciton broadening was given by Feng and Spector (1987).

Recent low-temperature transmission experiments on single MDQW ($L_z = 100$ Å) InGaAs/InAlAs field-effect transmitter (FET) structures showed these different renormalizations once more and very clearly (Chemla *et al.* 1987a, 1988a, Bar Joseph *et al.* 1987b). Figure 21 shows the structure and its differential transmission $\Delta T/T$ (minus the change in absorption), as the electron concentration is varied continuously from $N \sim 0$ to $N \sim 8 \times 10^{11}$ cm^{-2} by increasing the gate-to-source voltage. At the $n_z = 1$ transitions, $\Delta T/T$ is positive and increases with N until the heavy- and light-hole exciton

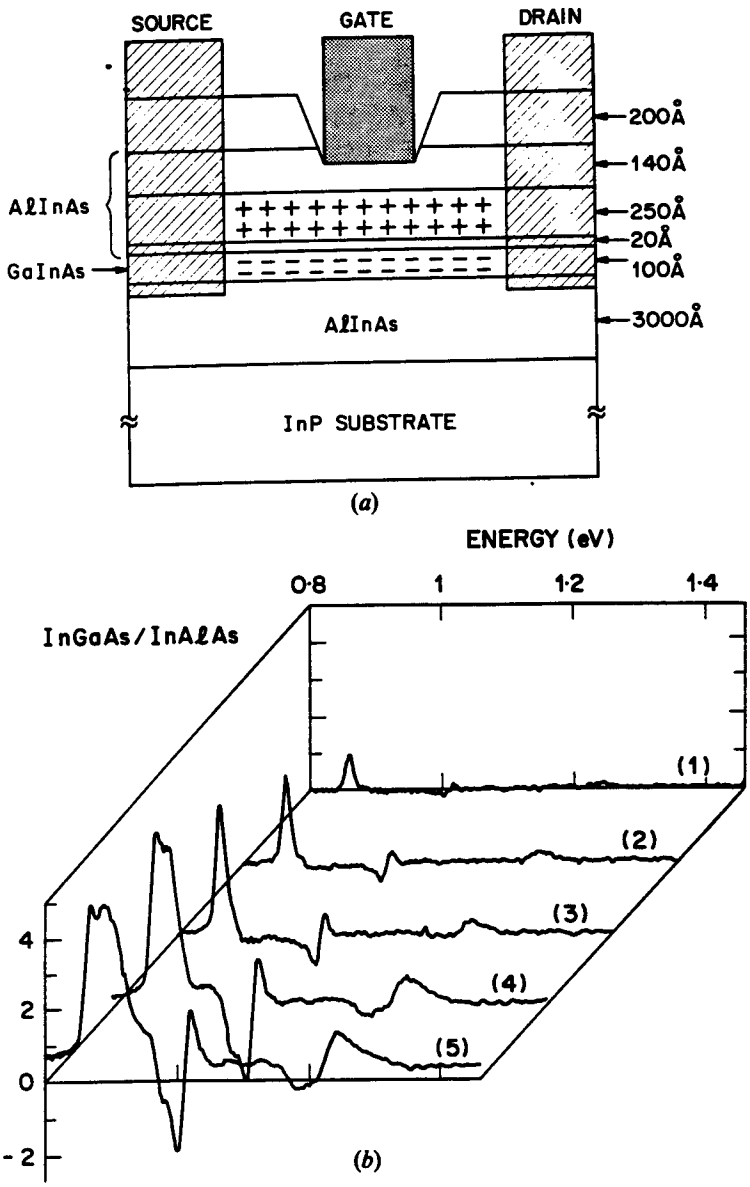

Figure 21. (*a*) Structure of field effect transistor. The L_z = 110 Å InGaAs layer is undoped, the central L_z = 250 Å InAlAs layer is doped with Si ($N = 1{\cdot}2 \times 10^{18}\,\mathrm{cm}^{-3}$). (*b*) Differential transmission spectra at T = 10 K. Spectra 1 to 5 correspond to increasing gate-to-source voltage. (After Bar-Joseph *et al.* (1987).)

resonances appear clearly. This behaviour corresponds to the progressive phase space quenching of the absorption as the electrons fill up the $n_z = 1$ conduction band. At the $n_z = 2$ and 3 transitions, the signal is smaller, with a differential lineshape showing positive and negative parts indicative of red shift and broadening (note that electrostatic effects contribute to $\Delta T/T$ as well). The detailed analysis also reveals the qualitative $N^{1/3}$ behaviour of the BGR, as did luminescence and luminescence excitation

experiments on similar one-sided (L_z = 150 Å) GaAs/AlGaAs MDQW (Delalande *et al.* 1986, 1987, Delalande 1987).

What remains to be discussed is point (2) above, namely the nature of the edge peak at high doping concentrations, N. We first note that even in this limit the generic structure equation (2.3.22) of Elliott's formula can actually be retained. By using a unitary transformation, similar to the one which relates the Dyson and Holstein–Primakoff transformations, the exact solution of the non-Hermitian problem equations (2.3.30) and (2.3.31) can be written as (Stolz 1974, Haug and Schmitt-Rink 1985, Schmitt-Rink *et al.* 1986)

$$\chi = \frac{2e^2|r_{vc}|^2}{L_z} \sum_n \frac{\left|\sum_{\mathbf{k}} [1 - f_e(k)]^{1/2} \phi_n(k)\right|^2}{E_n - \omega - i\delta}, \tag{2.3.38}$$

where ϕ_n and E_n are now eigenfunctions and energies of the Hermitian e–h relative motion Hamiltonian

$$H_{\mathbf{k},\mathbf{k}'} = (E_{ek} + E_{hk})\delta_{\mathbf{k},\mathbf{k}'} - [1 - f_e(k)]^{1/2} I_s(\mathbf{k} - \mathbf{k}')[1 - f_e(k')]^{1/2}. \tag{2.3.39}$$

For large N, excitons no longer exist, so that the e–h wavefunctions, $\phi_n(\mathbf{k})$, are scattering states, $\phi_{\mathbf{p}}(\mathbf{k})$, classified according to the e–h relative momentum, $\mathbf{p}$. The e–h energies are $E_p = E_{ep} + E_{hp}$ and are given by equations (2.3.27) and (2.3.29).

By analogy with standard definitions, $\phi_{\mathbf{p}}(\mathbf{k})$ can be written in the form

$$\phi_{\mathbf{p}}(\mathbf{k}) = \delta_{\mathbf{k},\mathbf{p}} + \frac{[1 - f_e(k)]^{1/2} \mathbf{T}(\mathbf{k}, \mathbf{p})[1 - f_e(p)]^{1/2}}{E_p - E_k + i\delta}, \tag{2.3.40}$$

where $\mathbf{T}(\mathbf{k}, \mathbf{p})$ is the on-shell T matrix defined through

$$\mathbf{T}(\mathbf{k}, \mathbf{p})[1 - f_e(p)]^{1/2} = -\sum_{\mathbf{k}'} I_s(\mathbf{k} - \mathbf{k}')[1 - f_e(k')]^{1/2} \phi_{\mathbf{p}}(\mathbf{k}'). \tag{2.3.41}$$

Equation (2.3.40) corresponds to outgoing wave boundary conditions. Substituting equation (2.3.41) into equation (2.3.40), we obtain the Bethe–Salpeter Equation (BSE) for the on-shell T matrix

$$\mathbf{T}(\mathbf{k}, \mathbf{p}) = -I_s(\mathbf{k} - \mathbf{p}) - \sum_{\mathbf{k}'} I_s(\mathbf{k} - \mathbf{k}') \frac{1 - f_e(k')}{E_p - E_k' + i\delta} \mathbf{T}(\mathbf{k}', \mathbf{p}). \tag{2.3.42}$$

Since only s-wave scattering contributes to χ, we can replace the interaction, I_s, by its angle-averaged value,

$$I_s(k, k') = \frac{1}{2\pi} \int_0^{2\pi} d\varrho\, I_s(\mathbf{k} - \mathbf{k}'), \tag{2.3.43}$$

where ϱ is the angle between $\mathbf{k}$ and $\mathbf{k}'$.

With use of a method developed by Noyes (1965), the BSE equation (2.3.42) can be transformed into a non-singular integral equation. Multiplying equation (2.3.42) by $I_s(k, p)/I_s(p, p)$ and subtracting the result from equation (2.3.42), one finds

$$\mathbf{T}(k, p) = \frac{I_s(k, p)}{I_s(p, p)} \mathbf{T}(p, p) - \sum_{k'} \left[I_s(k, k') - \frac{I_s(k, p) I_s(p, k')}{I_s(p, p)} \right] \times \frac{1 - f_e(k')}{E_p - E_{k'} + i\delta} \mathbf{T}(k', p). \tag{2.3.44}$$

The solution of this equation can be expressed as

$$\mathbf{T}(k, p) = \mathbf{T}(p, p) f(k, p), \tag{2.3.45}$$

where

$$f(k, p) = \frac{I_s(k, p)}{I_s(p, p)} - \sum_{k'} \left[I_s(k, k') - \frac{I_s(k, p) I_s(p, k')}{I_s(p, p)} \right] \times \frac{1 - f_e(k')}{E_p - E'_k} f(k', p), \tag{2.3.46}$$

$$\mathbf{T}(p, p) = \frac{-I_s(p, p)}{1 + \Lambda_1(p)}, \tag{2.3.47}$$

with

$$\Lambda_1(p) = \sum_k I_s(p, k) f(k, p) \frac{1 - f_e(k)}{E_p - E_k + i\delta}. \tag{2.3.48}$$

Obviously, the kernel of equation (2.3.46) is now finite for $k' = p$, and $f(p, p) = 1$.

The oscillator strength for transitions into scattering states is, according to equation (2.3.38), determined by

$$\sum_k [1 - f_e(k)]^{1/2} \phi_p(k) = [1 - f_e(p)]^{1/2} \left[1 - \frac{\Lambda_2(p)}{1 + \Lambda_1(p)} \right], \tag{2.3.49}$$

where

$$\Lambda_2(p) = \sum_k I_s(p, p) f(k, p) \frac{1 - f_e(k)}{E_p - E_k + i\delta}. \tag{2.3.50}$$

Substituting this expression into equation (2.3.38), we finally obtain for the absorption coefficient

$$\operatorname{Im} \chi = \lambda \operatorname{Im} \chi_0, \tag{2.3.51}$$

where

$$\operatorname{Im} \chi_0 = \frac{2\pi e^2 |r_{vc}|^2}{L_z} \sum_p [1 - f_e(p)] \delta(\omega - E_p) \tag{2.3.52}$$

is the one-electron result (including the BGR) and

$$\lambda = \left| 1 - \frac{\Lambda_2(p)}{1 + \Lambda_1(p)} \right|^2_{E_p = \omega} \tag{2.3.53}$$

is an enhancement factor that describes the residual e–h correlation.

Exact numerical solutions of the BSE were performed for the related problems of direct optical transitions in photoexcited indirect Ge (Zimmermann *et al.* 1981, Schweizer *et al.* 1983) and for photoexcited QWs (Schmitt-Rink *et al.* 1986). For small electron densities, N, equation (2.3.53) reduces to the results of Elliott (1957) and Shinada and Sugano (1966). For large N, it is sufficient to keep only the leading term in equation (2.3.46), in which case a closed analytical solution is obtained. At zero temperature, λ is found to exhibit a pole, situated above the renormalized band gap $E'_g = E_0$, close to the one-electron absorption threshold E_{k_F}. The existence (in the static Fermi sea picture) of such a bound state with respect to the Fermi level was first discussed by Mahan (1967a) and we shall therefore refer to it as the 'Mahan exciton'. It is due to the residual e–h correlation in combination with the sharpness of the Fermi surface and formally equivalent to loosely bound Cooper pairs in superconductors.

As already noted by Mahan, such a bound state in the continuum must eventually shift and broaden, as a result of interactions with particle–hole excitations of the Fermi sea. However, to accomplish this 'unbinding of the Mahan exciton' theoretically, one must allow for the dynamical response of the Fermi sea to the appearance (or disappearance) of the hole in the course of optical transitions (see below). The less ambitious approach simply consists of broadening the Mahan exciton by hand (Mahan 1967a, Rorison 1987, Skolnick *et al.* 1987, Livescu *et al.* 1988), which yields already a reasonable description of many experimental data.

As the temperature is raised, the Fermi surface is smeared, and the Mahan exciton disappears. This can be viewed as thermal ionization, just like in the case of loosely bound Cooper pairs. The static Fermi sea picture reduces then more or less to one-electron theory (including the BGR), until, for temperatures much larger than the Fermi energy ϵ_F, real excitons, that is bound states in the gap, reappear. (Clearly, this latter point must be discarded, because in reality the increasing broadening due to phonons will always suppress the effect.)

While this simple picture—the existence at low temperatures of a bound state below the Burstein edge—explains the qualitative behaviour of the experimental data and point (2) above, the actual physics and correct theory are much more complicated. Including the full dynamical response of the Fermi sea in a detailed calculation of optical spectra represents a highly non-trivial task, outside the scope of conventional perturbation theory, as discussed qualitatively by Gavoret *et al.* (1969) and Ruckenstein and Schmitt-Rink (1987). The easiest way to understand the origin of this difficulty is to consider the absorption process in the idealized limit of an infinite hole mass, by analogy with the discussion of the soft X-ray spectra of metals.

There are two effects one must consider: the first was discussed by Mahan (1967b), who showed that by considering all processes which involve repeated scattering of an electron and a hole, including the dynamical vertex corrections ignored within the static Fermi sea picture, the sharp bound state at the Fermi level changes into a power-law singularity. The second effect is related to the 'orthogonality catastrophe' discussed by Anderson (1967) and Hopfield (1969). Anderson proved that the overlap between the electron ground state wavefunction in the absence of the hole and that with the hole present vanishes in the limit of a large system. As a result of this effect alone, the zero-temperature absorption spectrum would be non-vanishing only away from the edge, since in that case, due to the creation of particle–hole pairs, the final state would be an excited state, not affected by Anderson's theorem. Formally, this orthogonality theorem is contained in the (dynamical) hole self-energy. The singularity due to the 'final state interactions' discussed by Mahan usually dominates, and thus the zero-temperature absorption spectrum at high densities displays a power-law singularity at the Fermi level.

The physics underlying this singularity is the sudden appearance of the hole in the course of the absorption process. It leads to a readjustment of all the electrons into a new (scattering) state, which shows up as an infinite number of low-lying particle–hole excitations of the Fermi sea.

In a series of papers (Roulet *et al.* 1969, Nozieres *et al.* 1969, Nozieres and de Dominicis 1969, Combescot and Nozieres 1971), Nozieres and co-workers developed a rigorous theory of these effects, which had also great impact on related problems, such as the Kondo effect. In particular, Combescot and Nozieres (1971) showed that the power-law behaviour persists even in the low-density excitonic limit, with a threshold energy and an exponent always parameterized in terms of the s-wave e–h

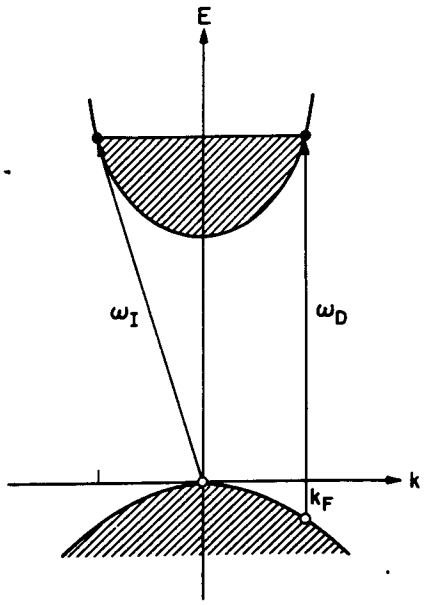

Figure 22. Direct (with threshold ω_D) and indirect (with threshold ω_I) absorption processes for a finite hole mass. Energy and momentum conservation is guaranteed by collective excitations of the Fermi sea.

scattering phase shift. The threshold energy is obtained from a generalization of Fumi's (1955) theorem, while the exponent, in agreement with Hopfield's (1969) rule of thumb, is related to the number of electrons required to screen the hole, as determined by the Friedel (1952) sum rule.

Thus, for an infinite hole mass, the low-temperature optical spectra always display a power-law singularity, the nature of which changes continuously from excitons dressed with collective excitations of the Fermi sea in the low-doping limit to a Fermi level singularity in the high-doping limit. The experiments on InGaAs/InP MDQW shown in figure 20 are completely accounted for by this picture, because the holes are localized by alloy disorder and hence infinitely heavy (Skolnick *et al.* 1987). As the temperature is raised, the edge singularity is smeared until finally ($T = 80\,\mathrm{K}$) one-electron behaviour is recovered.

In the case of a finite hole mass, the recoil of the hole will smear the edge singularity over a frequency range $(m_e/m_h)\epsilon_F$, the effective 'bandwidth' of the hole. As shown in figure 22 for the case of absorption, optical processes can now be separated into two categories, direct and indirect (Auger-like) transitions. In the high-doping limit, direct (vertical) transitions require a minimum energy $\omega_D = E_g' + (1 + m_e/m_h)\epsilon_F$. In indirect transitions, electrons are excited above the Fermi level under the simultaneous excitation of particle–hole pairs or plasmons, which ensure energy and momentum conservation. As can be seen from figure 22, the indirect threshold (i.e. the minimum energy required for such a process) is given by $\omega_I = E_g' + \epsilon_F$. When the recoil energy $\omega_D - \omega_I$ is much larger than the residual Coulomb interaction, as measured by the binding energy of the Mahan exciton, the edge singularity disappears completely. Otherwise, a broadened resonance survives between the two thresholds.

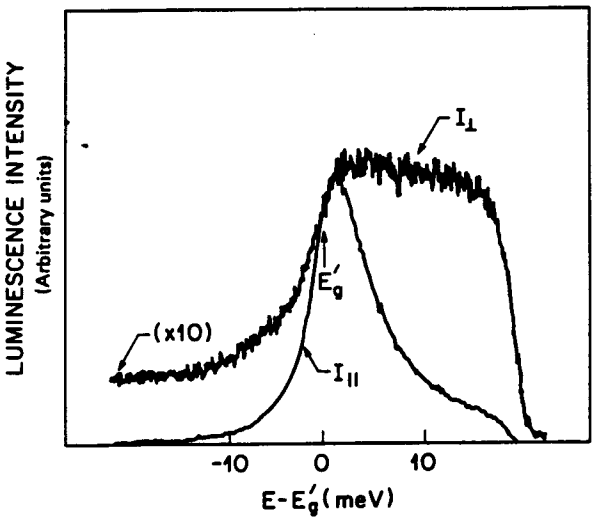

Figure 23. Luminescence spectra of an n-type modulation-doped ($N = 6 \times 10^{11}\,\mathrm{cm}^{-2}$) GaAs/AlGaAs multiple quantum well structure ($L_z = 226\,\text{Å}$) at $T = 4\,\mathrm{K}$. $I_\parallel$: polarization parallel to the layers; $I_\perp$: polarization perpendicular to the layers. E_g' denotes the renormalized band gap. (After Sooryakumar *et al.* (1985).)

This is, for example, the situation in the experimental data on the GaAs/AlGaAs MDQW shown in figure 19.

Unfortunately, very little can be easily calculated in the case of a finite hole mass, except for the behaviour of the absorption coefficient near the indirect threshold, which can be obtained from second-order perturbation theory. As shown by Ruckenstein *et al.* (1986) and Ruckenstein and Schmitt-Rink (1987), MDQW exhibit a low-energy absorption tail varying like $(\omega - \omega_i)^3$. At the direct threshold, perturbation theory diverges. As discussed qualitatively by Gavoret *et al.* (1969), the cure of this divergence requires a non-trivial self-consistent renormalization of both self-energy and vertex corrections. A 'minimal' calculational scheme, based on Fadeev-like equations (which describe exactly correlations up to three particles (Fadeev 1965, Gloeckle 1983)), was suggested by Ruckenstein and Schmitt-Rink (1987). A nice treatment of a closely related problem, namely 'shake-up' in the gain spectrum of photoexcited semiconductors, was given by Müller and Haug (1987).

The dynamical response of the Fermi sea to the appearance or disappearance of the hole in the course of optical transitions must also be invoked to explain other experiments: Ruckenstein *et al.* (1986) demonstrated circular polarization anomalies in luminescence from n-type GaAs/AlGaAs MDQWs which were tentatively attributed to a large e–h exchange in combination with a collective screening of the hole spin, just like in the Kondo effect (between successive impurity spin flips). Independent evidence for a large e–h exchange was recently reported by Bauer *et al.* (1987). In GaAs/AlGaAs MDQW waveguide structures, Sooryakumar *et al.* (1985, 1987) observed an unexpectedly strong emission $I_\perp$ with polarization perpendicular to the layers, shown in figure 23 together with $I_\parallel$. As can be seen, the spectra for the two polarizations also exhibit drastic differences in lineshapes. If the $n_z = 1$ heavy-hole band (the final state in emission) had only $J_z = \pm\frac{3}{2}$ character, the ratio $I_\perp/I_\parallel$ should

vanish, as discussed in section 2.1. Therefore, the data in figure 23 indicate a surprisingly large mixing of $J_z = \pm\frac{1}{2}$ light-hole and $J_z = \pm\frac{3}{2}$ heavy-hole character, especially near $k = 0$, where it is unexpected. Again, collective excitations of the Fermi sea were invoked to account for this behaviour. A first principles calculation of the effect was attempted by Chang and Sanders (1985), while Sham put forward a purely phenomenological model that accounts surprisingly well for the observations (Sooryakumar *et al.* 1987).

We conclude this section by merely noting that most of the fascinating observations discussed above could never be made in doped bulk semiconductors, because of the strong ionized impurity scattering. MDQWs are thus unique, by providing ideal environments for studying many-body physics. Modulation-doped spherical heterostructures, consisting for example of a small Si-doped AlGaAs core in a GaAs matrix, would be the ultimate thing, a man-made 'superatom' (Inoshita *et al.* 1986).

3. Nonlinear optical properties

The nature of the nonlinear optical response of semiconductors is different depending on whether virtual or real e–h populations are generated. Correspondingly, excitation below and above the absorption edge have to be clearly distinguished. Before presenting particular results, it is useful to discuss these two cases in very broad terms.

In the case of photoexcitation of virtual e and h well below the absorption edge, the coherent laser field, E, induces a coherent polarization, P, of the valence electrons that persists essentially only as long as the laser is applied. The nonlinear polarization can couple various optical fields, which exchange photons via the material, but no net power is deposited in the latter. During application of the laser field, the state of the semiconductor is a coherent superposition of all excited (e–h pair) states. The individual components have exactly the same interactions as if they were actually populated, but they do not participate in any real relaxation process. If they did relax by real collisions, their quantum-mechanical phase would be disturbed and, as far as the driving field is concerned, photons would be absorbed in real transitions. By a simple application of the uncertainty principle, the amount of time the photons spend in an excited state is $\tau \sim \Delta E^{-1}$, where ΔE is the difference between the photon energy and the excited state energy, for example, $\Delta E = E_g - \omega$ in the case of band-to-band transitions. As long as this time is short compared with the characteristic dephasing time of the excited state, the transitions will be predominantly virtual. Virtual transitions are therefore only favoured under off-resonant excitation. The corresponding coherent optical nonlinearities are small, because of the large differences ΔE between the photon energies and the absorption edge; however, they are extremely fast, limited only by the uncertainty principle.

Photoexcitation above the absorption edge generates predominantly real e–h pairs with no particular quantum-mechanical phase coherence, except for the initial time regime before the first collision. Owing to the strong absorption, however, such resonant excitation produces a large number of e and h for a given laser intensity, and hence large changes in the optical properties of the material. Real e and h, once generated, undergo a number of relaxation processes; the changes they induce in the optical spectra persist of course as long as the e and h themselves, that is for the lifetime. For the specific case of semiconductors, the excited e and h can form bound (excitons, trions, biexcitons) or unbound (e–h plasma) states, which produce different effects (Haug and Schmitt-Rink 1984, Chemla 1985, Henneberger 1986, Haug 1988).

Furthermore, ultrafast photogeneration can produce non-equilibrium distributions of these states. Two relaxation times should be distinguished. The first is the time it takes the photoexcited e and h to reach a thermodynamic equilibrium among themselves (usually a fraction of a picosecond), and the second one the time it takes them to equilibrate with the lattice (in the picosecond range). Optical transients can occur, for example, if excited species transform into one another during thermalization. Excitons that are generated by resonant excitation within the absorption peak are only stable at low temperatures where they can last as long as several ns. As discussed in section 2.1, in the case of III–V QWs at room temperature, they are thermally unstable and very quickly transform into free e–h pairs. Since the two species have different effects on the optical spectra, it is necessary to distinguish among them experimentally and theoretically.

In this section, we will review the experimental and theoretical investigations of excitonic optical nonlinearities in semiconductor microstructures. Following the above discussion and section 2, we will distinguish between e–h plasma, exciton and virtual e–h pair induced effects in undoped and in biased microstructures. Experimentally, virtual e–h pair effects are produced by excitation well below the absorption edge and e–h plasma effects by excitation above it. At room temperature, and in III–V compounds, exciton effects are more difficult to select; not only resonant excitation must be used, but they must be observed in times short compared with the exciton ionization time. This requires femtosecond spectroscopic techniques.

The experimental method most widely used (and most informative) is the 'pump and probe' technique, which is quite similar in spirit to the 'dope and probe' technique discussed in section 2.3: a strong pump beam is used to excite a large number of e–h pairs (virtual or real) the excitation spectrum of which is then probed by a weak test beam. Measuring the transmitted test intensity provides information on the absorption and gain of the sample. It is also possible to measure the photons diffracted by interference between pump and test beam in directions different from those of the incident beams. The corresponding diffraction efficiency provides information both on the change of refractive index and absorption. These techniques have been extensively discussed in the literature, for instance by Chemla *et al.* (1984).

3.1. *Effects of real electron–hole populations*

We begin by considering the experiments in which an optically created real and thermalized e–h phasma is responsible for the changes in optical properties, similar to the situation in MDQWs discussed in section 2.3. The e–h plasma can be generated either directly above the gap (Shank *et al.* 1983, Chemla *et al.* 1984, 1988b, Park *et al.* 1988) or indirectly following exciton creation by resonant absorption (Miller *et al.* 1982b, Weiner *et al.* 1986, Tai *et al.* 1987b) or LO phonon-assisted absorption (Von Lehmen *et al.* 1986a, 1987). For thermalization to be completed, observation must take place a few picoseconds after excitation.

It is found experimentally that the changes in the absorption spectrum do not depend on the excitation wavelength or on its duration. They depend only on the density, N, and temperature, T, of excited e–h pairs. A typical example of the modification of the room-temperature absorption spectrum as a function of N is presented in figure 24 for a GaAs/AlGaAs multiple quantum well structure ($L_z = 96$ Å) and N between ~ 0 and $\sim 2 \times 10^{12}\,\mathrm{cm}^{-2}$ (Chemla *et al.* 1988b). In the particular case of this set of spectra, the sample was excited with a 100 fs pump pulse about 60 meV above the $n_z = 1$ heavy-hole resonance and was probed several picoseconds

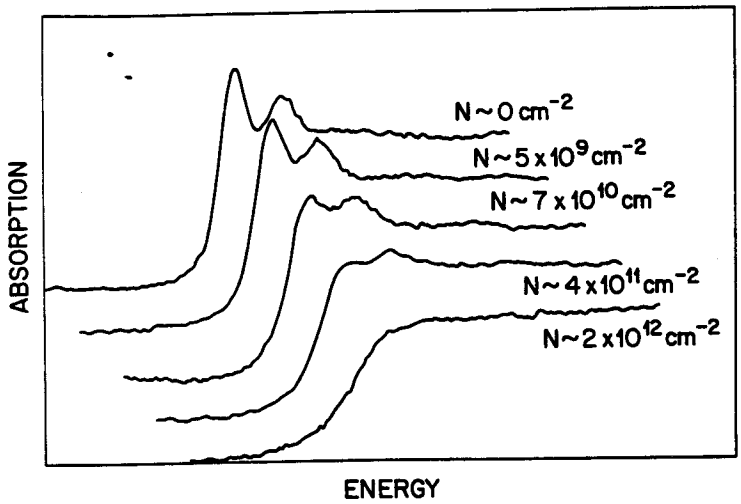

Figure 24. Room temperature absorption spectra of a GaAs/AlGaAs multiple quantum well structure (L_z = 96 Å) for free e–h pair densities between $N \sim 0$ and $N \sim 2 \times 10^{12}\,\mathrm{cm}^{-2}$, measured after thermalization. (After Chemla *et al.* (1988b).)

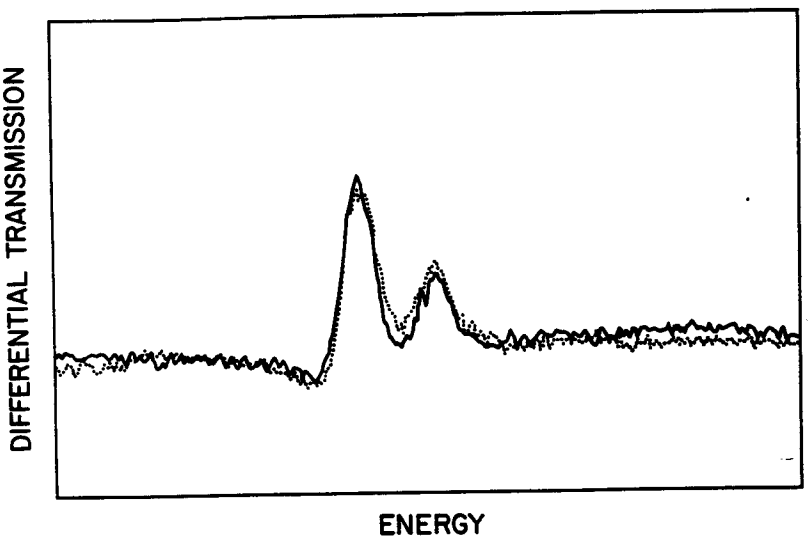

Figure 25. Room-temperature differential transmission spectra of a GaAs/AlGaAs multiple quantum well structure (L_z = 96 Å) for selective generation of $n_z = 1$ heavy-hole excitons (full line) and free e–h pairs (dotted line), measured after exciton ionization and thermalization. (After Chemla *et al.* (1988b).)

later by a broadband test continuum. A very smooth evolution is seen, the $n_z = 1$ heavy- and light-hole resonances weaken and are progressively replaced by a smooth absorption edge. The independence of the nonlinear absorption on the excitation wavelength and thus on the way the e–h plasma is created is clearly demonstrated in figure 25. Here, two typical differential transmission spectra (unperturbed absorption minus absorption in the presence of the pump beam) are compared (Chemla *et al.* 1988b). They were measured about 2 ps after selective generation of $n_z = 1$

heavy-hole excitons (full line) and free e–h pairs (dotted line). The pump intensities were adjusted to produce the same density of pairs. Within the experimental accuracy, the two curves are not distinguishable.

The global changes of the optical spectra near the absorption edge are interpreted just like in MDQWs (section 2.3) and photoexcited bulk semiconductors. As the e–h plasma density increases, the energy of free e–h pairs becomes renormalized (BGR), whereas that of the bound states hardly changes. The binding energy of the bound states measured from the renormalized scattering continuum decreases. The resonances lose oscillator strength, both because of the occupation of states out of which the excitons are constructed (PSF) and because of the loss of e–h correlation (i.e. the excitons are becoming larger). The width of the peaks increases because of collisional broadening. At low e–h pair densities, when the continuum is still far from the resonances, only the loss of oscillator strength and the broadening are apparent. However, if the density continues to increase, the resonances merge in the continuum, and eventually the continuum edge is the only remaining spectral feature. Finally, at still higher densities (not shown in figure 24), when the e–h plasma becomes degenerate,

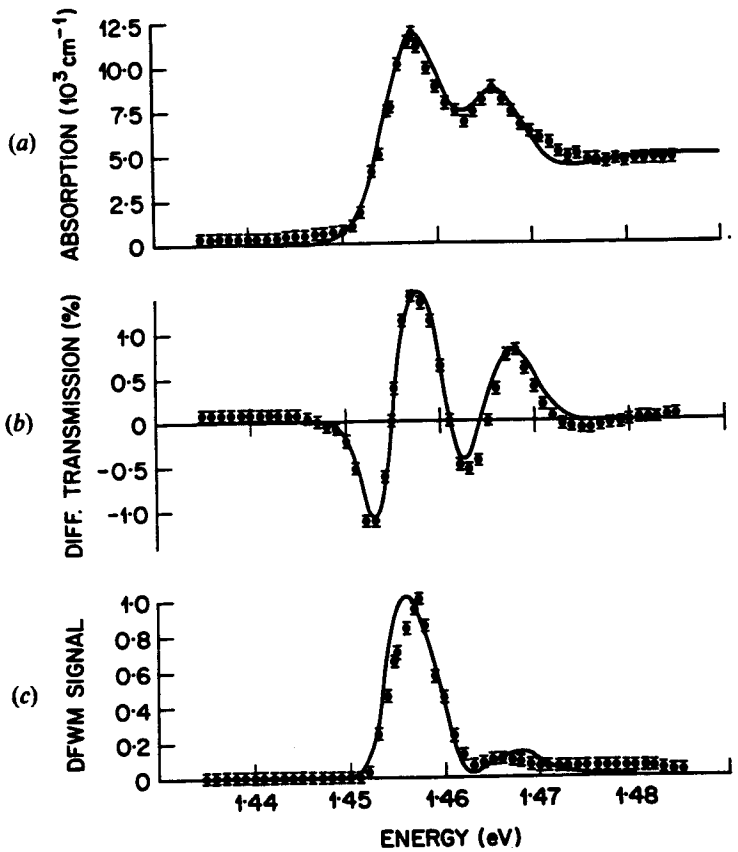

Figure 26. Semi-empirical fits of room temperature absorption (*a*) and differential transmission (*b*) of a GaAs/AlGaAs multiple quantum well structure (L_z = 96 Å). The theoretical DFWM spectrum (full line in (*c*)) is obtained from the nonlinear cross section σ and η shown in figure 27. (After Miller *et al.* (1983a), Chemla *et al.* (1984).)

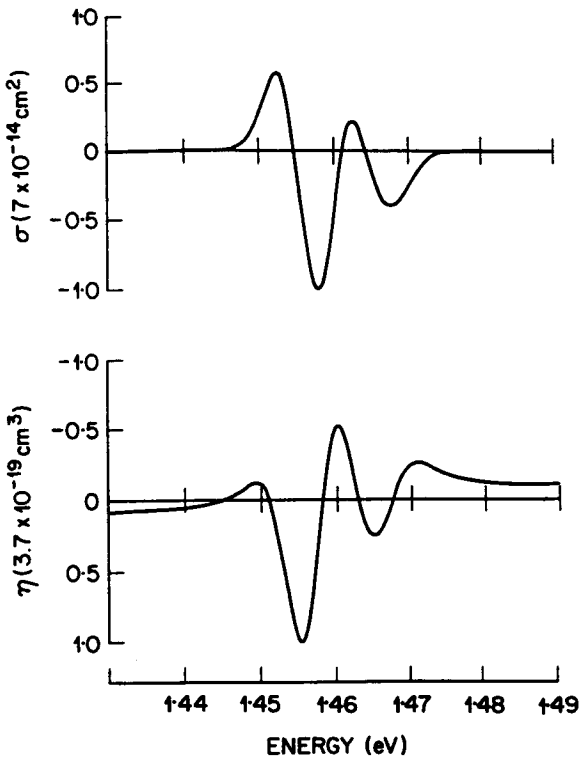

Figure 27. Room-temperature nonlinear absorption and refraction spectra of a GaAs/AlGaAs multiple quantum well structure (L_z = 96 Å). σ and η describe respectively the change of absorption and refractive index induced by one e–h pair and are obtained from the fits shown in figures 26(*a*) and (*b*). (After Miller *et al.* (1983a), Chemla *et al.* (1984).)

optical gain develops between the renormalized band gap, E_g', and the chemical potential, $\mu = \mu_e + \mu_h$, due to the population inversion (Shank *et al.* 1983, Weber *et al.* 1988).

Additional information on the refractive index changes has been obtained from degenerate four-wave mixing (DFWM) experiments using tunable picosecond pump and probe lasers (Miller *et al.* 1983a, Chemla *et al.* 1984, Tai *et al.* 1987b). For low e–h pair densities, N, the bleaching of excitons can be characterized by a nonlinear absorption cross section σ and a nonlinear refractive index η, which measure respectively the change of the absorption coefficient and refractive index induced by one e–h pair,

$$\alpha = \alpha_0 - \sigma\bar{N}, \tag{3.1.1 a}$$

$$n = n_0 - \eta\bar{N}. \tag{3.1.1 b}$$

Here, to be consistent with the usual definitions, $\bar{N}$ is the e–h pair density per unit volume. σ and η are related by Kramers–Krönig relations; together they determine the DFWM diffraction efficiency. Figure 27 shows typical spectra of σ and η, as obtained from a semi-empirical fit of measured changes in transmission (and subsequent Kramers–Krönig transformation) shown in figure 26(*b*) (Miller *et al.* 1983a, Chemla

et al. 1984). The nonlinearities are extremely large and in this particular sample (a GaAs/AlGaAs multiple quantum well structure with $L_z = 96\,\text{Å}$) peak at $\sigma \sim 7 \times 10^{-14}\,\text{cm}^2$ and $\eta \sim 3{\cdot}7 \times 10^{-19}\,\text{cm}^3$. Figure 26(*c*) shows a comparison of the measured diffraction efficiency with the theoretical prediction based on the spectra of σ and η. The agreement is excellent. Similar results ($\sigma \sim 2{\cdot}8 \times 10^{-14}\,\text{cm}^2$ and $\eta \sim 3 \times 10^{-19}\,\text{cm}^3$) have been reported for room temperature InGaAs/Inp multiple quantum well structures with $L_z = 100\,\text{Å}$ (Tai *et al.* 1987 b). Using the solution of the rate equation for the carrier density,

$$\frac{d\bar{N}}{dt} = 2|E_p|^2 \operatorname{Im}\chi - \frac{\bar{N}}{\tau}, \tag{3.1.2}$$

where E_p is the pump field and τ the lifetime, these numbers can be translated into peak values $n_2 \sim 2 \times 10^{-1}\,\text{cm}^2\,\text{kW}^{-1}$ and $|\chi^{(3)}| \sim 6 \times 10^{-2}$ e.s.u. for the GaAs/AlGaAs sample and $n_2 \sim 3{\cdot}5 \times 10^{-1}\,\text{cm}^2\,\text{kW}^{-1}$ and $|\chi^{(3)}| \sim 8 \times 10^{-2}$ e.s.u. for the InGaAs/InP one. Within the experimental uncertainties, there is no difference. These values are very large in absolute terms (see below).

The impressive magnitude of room temperature nonlinear optical effects in high-quality GaAs/AlGaAs QWs was demonstrated by degenerate four-wave mixing using the output of a commercial c.w. laser diode as the sole light source. A diffraction efficiency of $\sim 5 \times 10^{-5}$ was observed in a $1{\cdot}25\,\mu\text{m}$ thick sample, using only a $\sim 17\,\text{W}\,\text{cm}^{-2}$ pump intensity (Miller *et al.* 1983b). Optical (bistable) devices using GaAs/AlGaAs and InGaAs/InP QWs as the active medium in nonlinear Fabry–Pérot etalons have been operated and raised much interest for applications in all-optical logic (Peyghambarian and Gibbs 1985, Gibbs 1985, Tai *et al.* 1987a). These devices exceed the e–h pair densities at which excitons cease to exist, and rely on interband saturation to complete the switching (see below). GaAs/AlGaAs QWs have also been used as saturable absorbers to mode-lock semiconductor laser diodes. Stable operation producing pulses as short as $1{\cdot}6\,\text{ps}$ has been demonstrated (Smith *et al.* 1985).

The extreme sensitivity of GaAs/AlGaAs QW excitons to the presence of e–h pairs has been exploited to study the exponential absorption tail and LO phonon sidebands at photon energies below the absorption edge (Von Lehmen *et al.* 1986a, 1987). The cross-sections for these processes are very small and they had previously only been observed in bulk GaAs (Sturge 1962). It is extremely difficult to measure by classical methods (i.e. plain transmission) such a small absorption in a micrometre thickness multiple quantum well structure, and new nonlinear methods have to be devised to perform these investigations. Since the final result of absorption is the generation of real e–h pairs, a weak test beam can be used to probe the transmission of a sample at the peak of the $n_z = 1$ heavy-hole exciton resonance, as an intense pump beam excites the QE structure below the absorption edge. For moderate pump intensities, according to equation (3.1.1), the test beam measures the e–h pair density and hence it maps out the pump beam absorption. At high temperatures, when the phonon population is large, the absorption tail is found to follow Urbach's rule (1953), while at low temperatures, a kink appears approximately one LO phonon energy below the exciton resonance, as shown by the experimental data (open circles) in figure 28 for a GaAs/AlGaAs multiple quantum well structure ($L_z = 96\,\text{Å}$) at $T = 75\,\text{K}$ (Von Lehmen *et al.* 1986a, 1987). This expected feature (Liebler *et al.* 1985) corresponds to the threshold for one-LO-phonon-assisted transitions. The step-like edge and the subsequent resonance enhancement are in remarkable agreement with an extension of the 3D second-order perturbation theory (Segall 1966) to the 2D case, retaining as

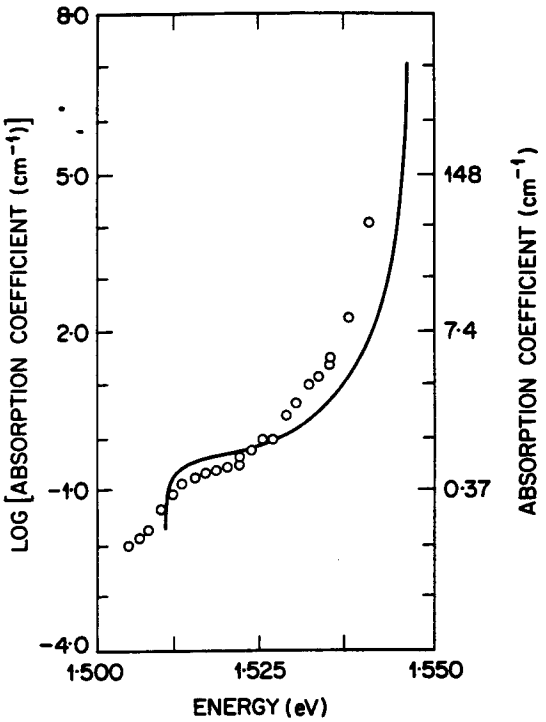

Figure 28. Absorption of a GaAs/AlGaAs multiple quantum well structure (L_z = 96 Å) at T = 75 K in the energy range of the exponential absorption tail below the n_z = 1 heavy-hole exciton. The open circles are experimental data based on a new nonlinear technique, the full line shows the contribution of one-LO-phonon-assisted transitions calculated in perturbation theory. (After Von Lehmen *et al.* (1986a, 1987).)

intermediate and final states the n_z = 1 heavy-hole exciton only. The theoretical lineshape (full line) calculated without adjustable parameters agrees very well with the data. The agreement can be improved further if the zero-LO phonon process on the high-energy side and multi-LO phonon processes on the low-energy side are accounted for. Below the one-LO phonon edge, the absorption, although non-zero, is extremely small ($\sim 10^{-1}\,\mathrm{cm}^{-1}$).

In addition to pump and probe experiments, room-temperature saturation measurements have been performed under c.w. resonant pumping of n_z = 1 heavy-hole excitons in GaAs/AlGaAs (Miller *et al.* 1982b), InGaAs/InAlAs (Weiner *et al.* 1986) and InGaAs/InP (Tai *et al.* 1987b) QW structures. Like in low-temperature GaAs (Gibbs *et al.* 1979), the experimental data can be very well fitted assuming the simple saturation form

$$\alpha = \frac{\alpha_0}{1 + |E_p|^2/|E_s|^2}, \tag{3.1.3}$$

which results from equation (3.1.1 *a*) and the steady state solution of equation (3.1.2). The saturation intensities, $I_s = (nc|E_s|^2)/(2\pi)$, for saturation of the n_z = 1 heavy-hole exciton are found to be very small; less than 1 kW cm^{-2} in the GaAs/AlGaAs ($\tau \sim 20$ ns) and InGaAs/InP ($\tau \sim 30$ ns) samples and about 3 kW cm^{-2} in the InGaAs/InAlAs one ($\tau \sim 1{\cdot}5$ ns).

Does one have to conclude that QWs and still lower dimensional structures are better nonlinear optical materials? At low temperatures in one sense confinement does not buy anything except a larger *linear* susceptibility to start with (and, of course, tunability of the absorption edge). As pointed out by Schmitt-Rink *et al.* (1987), the nonlinear changes per photoexcited e–h pair at low temperatures are independent of dimensionality (apart from geometrical and lifetime factors) and similar to those of the underlying atomic transition. This is most easily demonstrated by considering the form in equation (2.3.35) of the nonlinear optical susceptibility, χ,

$$\chi = \chi_0\left(1 - \frac{N}{N_s}\right), \tag{3.1.4}$$

which becomes exact in the limit of quantum dots, where PSF is the only surviving saturation mechanism (Schmitt-Rink *et al.* 1987). Substituting equation (3.1.4) into equation (3.1.2) one finds in the steady state

$$\chi = \frac{\chi_0}{1 + |E|^2/|E_s|^2}, \tag{3.1.5}$$

with

$$|E_s|^2 = \frac{\bar{N}_s}{2\tau \operatorname{Im} \chi_0}. \tag{3.1.6}$$

As discussed in section 2, χ_0 scales like the inverse confinement volume, no matter whether this confinement is externally imposed or due to e–h Coulomb interaction (i.e. excitonic), and so does N_s: the two effects exactly cancel each other. Thus, the available absolute changes in optical properties increase as one goes to lower dimensions (which may be very important for devices, which are frequently limited by our inability to make a sufficiently large change in optical properties efficiently, especially refractive index), but the energy density required to achieve a given change stays the same.

Unlike in bulk semiconductors (Zimmermann *et al.* 1981, Loewenau *et al.* 1982, Schweizer *et al.* 1983, Haug and Schmitt-Rink 1984, 1985, Schaefer *et al.* 1988a), good microscopic calculations of nonlinear QW absorption and refraction spectra unfortunately do not exist. First attempts have been made only recently (Schaefer *et al.* 1987). Besides the various difficulties also encountered in bulk materials (see below), two additional problems are faced in low-dimensional systems; namely (i) the pronounced effects of Coulomb repulsion between like particles, discussed in section 2.3, and (ii) fluctuation effects. Neither of them has been elaborated, and just like in the case of MDQWs one can only conjecture what the important physics is. Various clues are provided by experiments and, so far, this has been quite a fruitful approach. Most of the experimental observations can be qualitatively understood; often, even the numbers work out surprisingly well.

Starting with Kuramoto and Kamimura (1974), the BGR in a 2D e–h plasma has been calculated by a number of people (Andryushin and Silin 1976a,b, Chakroborty and Campbell 1984, Schmitt-Rink *et al.* 1984, Schmitt-Rink and Ell 1985, Kleinman 1986, Bauer and Ando 1986b). RPA-type calculations along the lines discussed in section 2.3 all yield zero-temperature results close to the simple interpolation formula of Schmitt-Rink *et al.* (1984) and Schmitt-Rink and Ell (1985),

$$E_g' - E_g = -3{\cdot}1(Na_0^2)^{1/3}E_0, \tag{3.1.7}$$

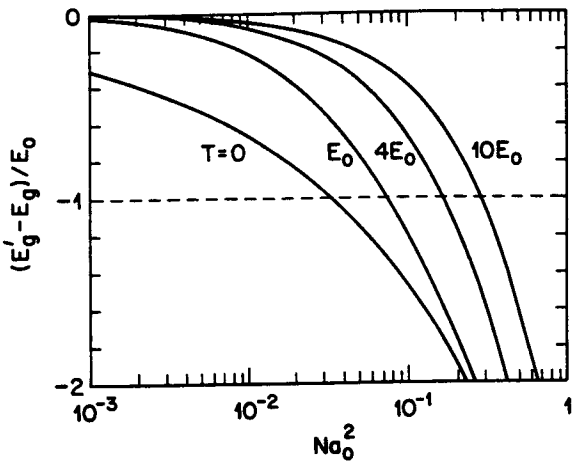

Figure 29. Renormalized band gap, E_g', of a 2D homogeneous semiconductor, calculated in RPA as function of free e–h pair density, N, for various temperatures, T. (After Schmitt-Rink *et al.* (1984), Schmitt-Rink and Ell (1985).)

which exhibits the characteristic $N^{1/3}$ behaviour discussed in section 2.3. Figure 29 shows $E_g' = E_e(0) + E_h(0)$ for various temperatures T. The minimum of the ground state energy per e–h pair is found to be $\sim -0{\cdot}87\,E_0$ at $r_s \sim 1{\cdot}4$, where $r_s = (\pi N a_0^2)^{-1/2}$ is the 2D density parameter (Kuramoto and Kamimura 1974, Schmitt-Rink and Ell 1985). Somewhat lower values have been obtained by Andryushin and Silin (1976a,b), while a Jastrow function calculation of Chakraborty and Campbell (1984) yields a value closer to the Hartree–Fock (HF) result (as expected). Just like in the bulk, there will be no e–h liquid condensation in direct gap materials, because of the short radiative lifetimes τ. Short-range correlations will be most significant in the non-degenerate, classical limit, because at low temperatures, T, the e–h attraction dominates (see below). One way or the other, RPA-type calculations are not to be trusted at low e–h pair densities, N, and values for $E_g - E_g'$ smaller than those shown in figure 29 are expected. As discussed in section 2.3, finite-layer-size effects partially restore the validity of the RPA, but at the same time also reduce the absolute value of the BGR. For finite L_z, $T = 0$, and large e–h pair densities, N, one might be tempted to use equation (3.1.7) with actual exciton parameters or construct a Padé approximation which connects equation (3.1.7) to the 3D HF result, which also varies like $N^{1/3}$ (see the discussion in section 2.3). The $N^{1/3}$ behaviour of the BGR has been observed in GaAs/AlGaAs QW lasers by Tarucha *et al.* (1984) and, more recently, in a series of QW structures by Traenkle *et al.* (1987a,b). The latter authors deduced from a lineshape analysis of the photoluminescence under high excitation absolute values in almost exact agreement with equation (3.1.7), which is at best surprising. Recently, the density dependence of the BGR has been determined more accurately by Weber *et al.* (1988). These authors have directly measured the chemical potential in 100 Å GaAs QWs under nanosecond excitation, from the gain-absorption cross-over.

This measurement does not depend on a lineshape analysis and its accuracy is only determined by the error in N. It was found that

$$(E_g' - E_g)\,(\text{meV}) \sim -3{\cdot}6 \times 10^{-3}\,[N\,(\text{cm}^{-2})]^{1/3}.$$

This is substantially smaller than the pure 2D result. However, it is more realistic to account for the finite well width and to use effective values for the binding energy and Bohr radius in equation (3.1.7) instead of the pure 2D parameters $E_0 = 4R$ and $a_0 = a_B/2$. For the case of 100 Å GaAs QWs variational calculations (see section 2.1) give $E_0 \sim 8{\cdot}7$ meV which corresponds to $a_0 \sim 126$ Å. With these values, the BGR predicted by equation (3.1.7) is

$$(E_g' - E_g)\,(\text{meV}) \sim -3{\cdot}1 \times 10^{-3}[N\,(\text{cm}^{-2})]^{1/3},$$

in reasonable agreement with the experiments. Weber *et al.* have also estimated the intersubband BGR from the shift of the $n_z = 2$ and 3 excitons. It was found to be much less ($\sim 15\%$) than that of the $n_z = 1$ edge. As mentioned in section 2.3, this is due to (i) the cancellation of self-energy and vertex corrections for bound states and (ii) the large perpendicular wave-vector mismatch which reduces correlations.

The substantial effects of 2D fluctuations can be most easily demonstrated by considering the optical spectra in the limit of high e–h pair densities, N, such that bound states are no longer stable. This limit, which is relevant to QW lasers (Holonyak 1985), has been investigated in detail by Schmitt-Rink *et al.* (1986), using a static Fermi sea picture similar to that described in section 2.3 (equations (2.3.38)–(2.3.53), but with a PSF factor $1 - f_e(k) - f_h(k)$). Just like in MDQWs, it is found that the e–h correlation is concentrated near the chemical potential, μ, namely in the cross-over region from gain to absorption, as shown in figure 30. The full and dashed lines give respectively the theoretical absorption with and without static e–h correlation.

The strong excitonic enhancement near the chemical potential, μ, reflects the tendency of the system to form e–h Cooper pairs, that is, to undergo a transition to the excitonic insulator state (Keldysh and Kopaev 1965). It is found that within the static Fermi sea picture, the excitonic enhancement factor, λ, equation (2.3.53), diverges at some finite critical temperature, T_c. This latter result is clearly an artefact. As shown by Hohenberg (1967), in 2D systems and at finite temperatures, T, long-range order is always destroyed by fluctuations, thus $T_c = 0$. Just like in MDQWs, the notion of a static Fermi sea leads thus to spurious results, the cure of which requires again a self-consistent renormalization of both (dynamical) self-energy and

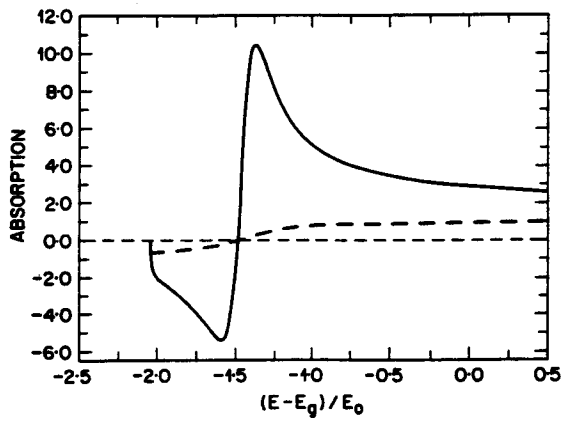

Figure 30. Theoretical absorption and gain spectra of a 2D homogeneous semiconductor with (full line) and without (dashed line) static e–h correlation, $T/E_0 = 0{\cdot}1$ and $Na_0^2 = 0{\cdot}1$. (After Schmitt-Rink *et al.* (1986).)

(dynamical) vertex corrections. First attempts in this direction have been reported by Schaefer *et al.* (1988 a).

The saturation of the excitonic optical absorption due to an e–h plasma has been studied theoretically by Schmitt-Rink and Ell (1985), using various static and dynamic RPA-type models for the effective interaction, $I_s(q)$, and by Schmitt-Rink *et al.* (1985). The main points can be discussed following section 2.3 and figure 29. Assuming that the absolute exciton energy stays constant, as observed, the criterion for the unbinding of excitons is $E_g' = E_{1s}^0$, which yields Mott densities, N_c, an order of magnitude higher than in 3D (in excitonic units). The physical reason underlying this result is the reduced screening efficiency in 2D already discussed. Andryushin and Silin (1979) give a low-temperature value $N_c a_0^2 \sim 0{\cdot}06$, corresponding to $r_s \sim 2{\cdot}3$.

The effects of multi-layer screening have been studied by Dahl (1988), assuming RPA-type static screening and neglecting everything else (in particular PSF). As expected (Visscher and Falicov 1971, Fetter 1973, 1974), it is found that local field effects are pronounced for screening lengths much larger than the layer spacing, as realized in the non-degenerate, classical limit. On the other hand, experiments have been performed at room temperature on GaAs/AlGaAs single QW ($L_z = 107$ Å) waveguide structures to investigate this effect (Weiner *et al.* 1985b). Within the experimental uncertainties, no difference in saturation behaviour compared to the multiple quantum well case is found, which provides yet another clue for the reduced efficiency of screening in 2D.

Following section 2.3, it is then quite natural to attribute the saturation of the excitonic absorption mainly to overlap effects, the filling of the states out of which the excitons are constructed (Schmitt-Rink *et al.* 1985). In 3D and at high temperatures, T, larger than the exciton binding energy, such a criterion would be rather meaningless: excitons would unbind because of screening long before such overlap effects become important. On the other hand, in room-temperature III–V bulk materials, excitons play relatively little role anyway, so that there is actually not much of a difference in the dominant saturation mechanism; as pointed out first by Loewenau *et al.* (1982) and studied systematically by Lee *et al.* (1986), the main nonlinearity in the case of an exciton linewidth larger than the binding energy is plain bandfilling. This explains then why the saturation density $\tilde{N}_s$ hardly changes as one goes from room temperature GaAs to GaAs/AlGaAs QWs (Park *et al.* 1988): the dominant mechanism is the same, though exciton saturation in one case and interband saturation in the other. At room temperature, an improvement of III–V QWs over the corresponding bulk materials does therefore indeed arise, because full advantage can be taken of the increase in linear susceptibility. Together with the long lifetime τ in high-quality material, this accounts for the low saturation intensities and large nonlinearities observed.

Neglecting exciton broadening, as investigated by Feng and Spector (1987), and the reduction of the exciton binding energy, the saturation density, N_s, is estimated from the extension of equation (2.3.36) to the two-component case,

$$\frac{N}{N_s^{\mathrm{PSF}}} = \lim_{N\to 0} \sum_k [f_e(k) + f_h(k)]\phi_{1s}^0(k)/\phi_{1s}^0(r=0), \tag{3.1.8}$$

which yields

$$\frac{1}{N_s^{\mathrm{PSF}}} = 2\pi a_0^2, \qquad T \ll E_0, \tag{3.1.9a}$$

$$= 2\pi a_0^2 \frac{E_0}{T}, \quad T \gg E_0. \tag{3.1.9b}$$

Improved estimates along the lines discussed in section 2.3 (equations (2.3.32)–(2.3.34)), including the PSF effect on the e–h interaction as well as the corresponding e and h exchange self-energies, have been given by Schmitt-Rink *et al.* (1985) and Zimmermann (1988a). Schmitt-Rink and Ell (1985) estimated N_s, using variational exciton wavefunctions and, in addition, various RPA-type screening models. In view of the large uncertainties in the treatment of correlations, equation (3.1.8) is as good as any of the other models, and presumably correct within a factor of two or three. For the pure 2D case and using the material parameters of GaAs ($E_0 \sim 16{\cdot}8$ meV, $a_0 \sim 70$ Å), equation (3.1.9*b*) yields a room-temperature saturation density $N_s^{PSF} \sim 5 \times 10^{11}\,\mathrm{cm}^{-2}$, which compares reasonably well with the experimental values of Miller *et al.* (1982b), Chemla *et al.* (1984) and Park *et al.* (1988).

To test the conjecture that in 2D the effects of screening are weak compared with the effects of the exclusion principle, a direct experimental comparison of both effects at room temperature has been performed (Knox *et al.* 1986a). The principle of these investigations is the following. Using femtosecond laser pulses it is possible to generate non-equilibrium carrier distributions in the continuum between the $n_z = 1$ and 2 exciton resonances and to observe their effects on the absorption spectrum before and during their relaxation. If the e and h excess energies are less than the LO phonon energy, exchange of energy with the lattice will take a rather long time and the carriers will first thermalize among themselves before reaching an equilibrium with the lattice. Immediately after excitation, the carriers do not occupy states out of which the $n_z = 1$ and 2 excitons are constructed and thus the Pauli principle effects are not effective, whereas screening sets in right away. As the carriers equilibrate among themselves, their distribution evolves toward a thermal one and they start to fill up the states at the bottom of the $n_z = 1$ subbands. Therefore they produce PSF on the corresponding excitons. Only the high-energy tails of the thermalized distributions will extend up to the bottom of the $n_z = 2$ subbands, so that for these PSF remains basically ineffective. Therefore the evolution of the absorption at the $n_z = 1$ excitons during thermalization will first show the effects of screening and then how PSF is turned on, whereas at the $n_z = 2$ heavy-hole exciton resonance there should be little (if any) change during thermalization. Then, on a much longer time scale, the carriers will equilibrate with the lattice and eventually recombine.

This process is shown in figure 31, where room-temperature differential transmission spectra of a GaAs/AlGaAs multiple quantum well structure ($L = 96$ Å) are presented. The spectra were measured with broad-band 50 fs probe pulses in 50 fs intervals from 100 fs before to 200 fs after arrival of a narrow-band 100 fs pump pulse. The spectral distribution of the pump photons is shown at the bottom of the figure; the pump pulse produces approximately $N \sim 2 \times 10^{10}\,\mathrm{cm}^{-2}$ e–h pairs. Immediately upon its arrival, one sees absorption changes at the $n_z = 1$ and 2 excitons as well as spectral hole burning in the continuum, corresponding to state filling by the non-equilibrium carrier distributions. The $n_z = 1$ excitons lose some oscillator strength and broaden slightly, whereas the $n_z = 2$ heavy-hole exciton experiences also a very small red shift due to the weak intersubband BGR. These changes are consistent with those due to screening by free carriers, discussed above and in section 2.3 for MDQWs. Note that such small changes can only be seen because of the enormous improvements of femtosecond spectroscopic techniques (Fork *et al.* 1981, Knox *et al.* 1984). As the carriers thermalize, the spectral hole in the continuum changes shape and shifts to lower energies. Accompanying this relaxation, the bleaching of the $n_z = 1$ resonances increases and finally settles after 200 fs at the same level as in the case of thermalized

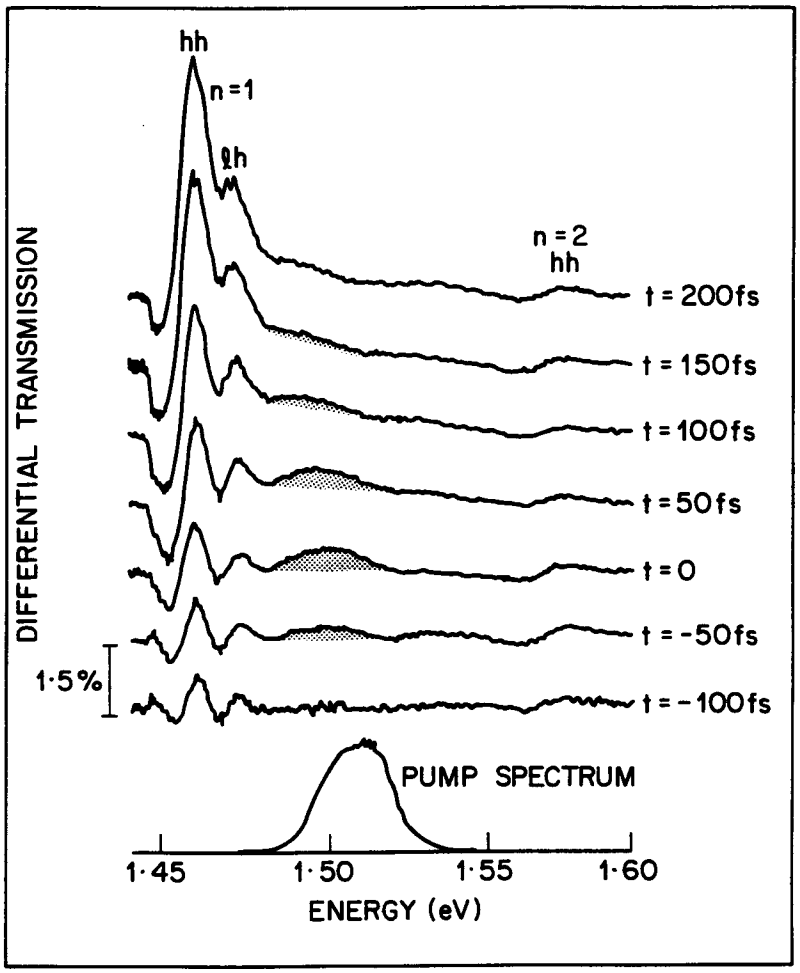

Figure 31. Room-temperature differential transmission spectra of a GaAs/AlGaAs multiple quantum well structure (L_z = 96 Å), measured with broad-band 50 fs probe pulses in 50 fs intervals before and after excitation of non-equilibrium e and h distributions by a narrow-band 100 fs pump pulse. Initially, the pump burns a spectral hole in the absorption spectrum, which then thermalizes within ~ 200 fs. During thermalization, the effects of the exclusion principle on the n_z = 1 exciton resonances are 'turned on'. (After Knox *et al.* (1986a).)

e–h plasma generation discussed previously. The changes at the n_z = 2 heavy-hole exciton resonance remain essentially the same, showing that the screening has not changed significantly. The comparison of the n_z = 1 heavy-hole exciton bleaching at t = 0 and after t = 200 fs shows that the effects of the exclusion principle are several times larger than those of screening, confirming the reduced efficiency of screening in 2D. In addition, the data also contain a wealth of information about carrier relaxation in microstructures that is not directly relevant to our discussion.

All the experimental results and interpretations discussed so far pertain to a single exciton embedded in a gas of free electrons and holes, namely an e–h plasma.

However, even if the photoexcited e–h pairs exist in the form of excitons, one can still use the same (phenomenological) language to describe the saturation of the excitonic optical absorption (apart from some subtleties, see below). An exciton gas can be generated selectively by resonant excitation. At low temperatures, that is, temperatures smaller than the binding energy, excitons are thermally stable and only disappear by recombination, whereas at high temperatures, that is, temperatures larger than the binding energy, they are unstable against thermal ionization. In the dilute limit, as discussed in section 2.1. the latter process is due to collisions with thermal LO phonons, and the corresponding ionization time can be readily estimated from the homogeneous absorption linewidth. In typical III–V QWs and at room temperature, it is found to be a fraction of a picosecond. Femtosecond spectroscopic techniques are thus necessary to resolve exciton-induced nonlinear optical effects at high temperatures (Peyghambarian *et al.* 1984, Knox *et al.* 1985). These experiments have for the first time resolved the dynamics of thermal exciton ionization. In addition, they have also shown some unexpected results that we now discuss.

Figure 32 shows room temperature differential transmission spectra of a GaAs/AlGaAs multiple quantum well structure (L_z = 96 Å), measured with broad-band 50 fs probe pulses in 50 fs intervals before and after resonant n_z = 1 heavy-hole exciton excitation by a narrow-band 100 fs pump pulse (Knox *et al.* 1985). Initially, a strong bleaching of the n_z = 1 heavy-hole exciton absorption lasting less than 1 ps occurs, then the absorption recovers partly and settles at the same value as it would

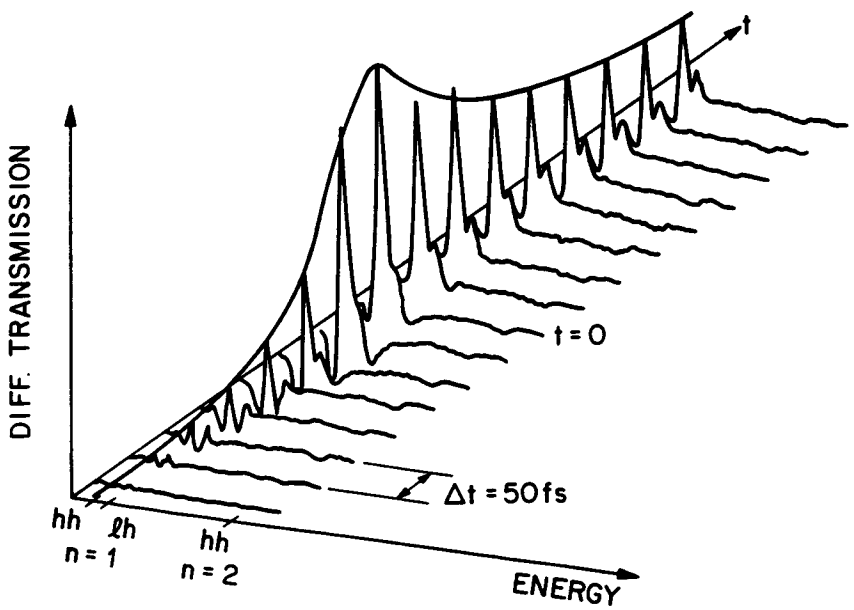

Figure 32. Room-temperature differential transmission spectra of a GaAs/AlGaAs multiple quantum well structure (L_z = 96 Å), measured with broad-band 50 fs probe pulses in 50 fs intervals before and after resonant n_z = 1 heavy-hole exciton excitation by a narrow-band 100 fs pump pulse. Initially, the absorption is reduced efficiently as excitons are created in the sample. It then recovers partly in ~ 300 fs as the excitons are thermally ionized by collisions with LO phonons. The absorption then settles at the same value as it would under cw excitation. (After Knox *et al.* (1985).)

under c.w. excitation. The dynamics of the $n_z = 1$ heavy-hole exciton bleaching can be described assuming the instantaneous generation of $n_z = 1$ heavy-hole excitons (the number of excitons following the integral of the pump pulse, see equation (3.1.2)), which transform with a ~ 300 fs time constant into free $n_z = 1$ e and h, which then live for long times. The excitons ionize because of the large temperature, and, as discussed above, this thermal ionization is due to collisions with LO phonons. The measured ionization time of ~ 300 fs is in remarkable agreement with the value obtained from the homogeneous absorption linewidth (see section 2.1).

The transient excitons produce, before they ionize, a strong bleaching of the $n_z = 1$ heavy-hole exciton resonance about twice as large as that due to the free e and h at long times, while the changes at the $n_z = 2$ heavy-hole exciton resonance are again small. In addition, the lineshape of the differential spectra at short and long times is different (Chemla and Miller 1985). This result is in seeming contradiction to commonly accepted ideas and deserves some discussion.

In earlier experiments on low-temperature bulk GaAs, it was found that excitons produce much smaller nonlinear optical effects than an e–h plasma (Fehrenbach *et al.* 1982). Guided by the (incomplete) notion that the saturation of 3D excitons, even at low temperatures, is due to screening, this was attributed to the fact that screening in a dielectric exciton gas is much weaker than in a metallic e–h plasma. The above QW experiment presents two novel aspects, namely (i) reduced dimensionality and (ii) ultrashort optical pulse excitation at room temperature, both of which are important in the interpretation (Schmitt-Rink *et al.* 1985).

First, as already discussed several times, the efficiency of free-carrier screening is reduced in 2D, which is consequently even more true in the case of excitons. As a result, the effects of the exclusion principle are strongly enhanced. Following our simplistic discussion of e–h plasma effects, the initial saturation of the excitonic optical absorption would then be mainly related to excitonic PSF, that is, the fact that the area already occupied by an exciton cannot sustain more excitons. This explains then in a simple fashion why the bleaching due to the resonantly excited $n_z = 1$ heavy-hole excitons is larger than that due to the free e and h released via thermal exciton ionization. Between the absorption event and the first collision with a LO phonon, the resonantly excited excitons have not yet had time to thermalize and therefore, for this very short time of ~ 300 fs, they are essentially at zero temperature (they are created with only a small amount of kinetic energy). Then, because the LO phonon energy is much larger than the exciton binding energy, the first collision with a LO phonon ionizes the excitons and produces free e and h of rather large thermal energy. At long times, these thermally activated free e and h are essentially at room temperature and hence the experiment compares the effects of 'cold' excitons (at short times) to those of a 'hot' room-temperature e–h plasma of the same density (at long times). The exclusion principle effects due to the 'hot' e–h plasma are smaller than those due to the 'cold' excitons, because they decrease with decreasing thermal wavelength to Bohr radius ratio, as discussed above (equation (3.1.9)). This accounts then for the different bleaching of the $n_z = 1$ heavy-hole exciton resonance at short and long times and explains also the smaller changes of the absorption at the $n_z = 1$ light-hole exciton resonance, only the electron component of which is subject to PSF (Schmitt-Rink *et al.* 1985).

The magnitude of excitonic exclusion principle effects can again be estimated from equation (3.1.8). It is only necessary to note that the resonant creation of one 1s

exciton at the bottom of its band corresponds to an occupation probability $|\phi^0_{1s}(k)|^2$ in fermion space, which is equally shared between spin up and down particles, so that

$$f_e(k) = f_h(k) = (N|\phi^0_{1s}(k)|^2)/2, \tag{3.1.10}$$

where N in this case is the exciton density. This very intuitive result is, of course, theoretically substantiated (Haug and Schmitt-Rink 1984). Substituting equation (3.1.10) into equation (3.1.8), one finds (Schmitt-Rink *et al.* 1985)

$$\frac{1}{N_s^{PSF}} = \tfrac{8}{7}\pi a_0^2, \tag{3.1.11}$$

that is, the bleaching efficiency of 'cold' excitons is smaller (by a factor of about two) than that of a 'cold' e–h plasma, equation (3.1.9*a*), because plane wave states have a larger overlap with a given exciton than other excitons. Using the actual Bohr radius, $a_0 \sim 126$ Å, of the $L_z = 96$ Å sample, equation (3.1.11) yields a saturation density due to 'cold' excitons $N_s^{PSF} \sim 2 \times 10^{11}\,\mathrm{cm}^{-2}$, which agrees almost exactly with the experimental one. Together with equation (3.1.9*b*), $N_s^{PSF} \sim 5 \times 10^{11}\,\mathrm{cm}^{-2}$, a ratio at room temperature of 'cold' exciton to 'hot' e–h plasma induced bleaching of about three is found, again in good agreement with the data.

Yet another confirmation of this simple physical picture was obtained from the observation of an exciton blue shift in narrow GaAs/AlGaAs QWs (Peyghambarian *et al.* 1984, Hulin *et al.* 1986a, Masumoto *et al.* 1986, Weinert *et al.* 1987). As discussed previously, 3D exciton resonances hardly change their position as the density of excitons increases, which can be explained in terms of an almost exact cancellation of a blue shift due to Pauli exclusion (short-range hard core repulsion) and a red shift due to screening (long-range Van der Waals attraction). In 2D QWs, because of the quenching of the effects of screening, the blue shift due to Pauli exclusion is no longer balanced and thus should be measurable (Schmitt-Rink *et al.* 1985). Luminescence (Weinert *et al.* 1987) and absorption (Peyghambarian *et al.* 1984, Hulin *et al.* 1986a, Masumoto *et al.* 1986) measurements performed on QWs of various thicknesses have shown this blue shift when excitons are selectively generated or, at low temperatures, when they are formed after a few picoseconds from photoexcited free e and h. The shift is rather difficult to observe in thick layers, but is large enough to be observed in the narrowest QWs (< 100 Å), where the dimensionality approaches the pure 2D limit. A typical example is presented in figure 33, which shows transmission spectra of a GaAs/AlGaAs multiple quantum well structure ($L_z = 50$ Å) at $T = 15$ K, measured with broad-band 120 fs probe pulses before and after resonant $n_z = 1$ heavy-hole exciton excitation by a narrow-band 120 fs pump pulse (Peyghambarian *et al.* 1984). At low temperatures, an exciton blue shift has also been observed in the layered semiconductor BiI_3 (Watanabe *et al.* 1986), while for bulk GaAs only a very small shift (Schultheis *et al.* 1986a) or no shift at all (Fehrenbach *et al.* 1982, 1985) have been reported. This implies that the compressibility of a weakly non-ideal 2D exciton gas is positive, thus a weakly non-ideal 2D exciton is thermodynamically stable (apart from possible collapse into biexcitons, see below), in disagreement with some earlier theoretical results by Klyuchnik and Lozovik (1978).

Beyond the simple PSF picture described above, the distinction has to be made between the susceptibility, χ_p, experienced by the pump beam and that experienced by the test beam, χ_t (Haug and Schmitt-Rink 1984, Schmitt-Rink and Chemla 1986). The point is that the excitons created by the pump beam and those created by the test beam can exchange (boson exchange), which gives rise to *additional terms* in the effective e–h

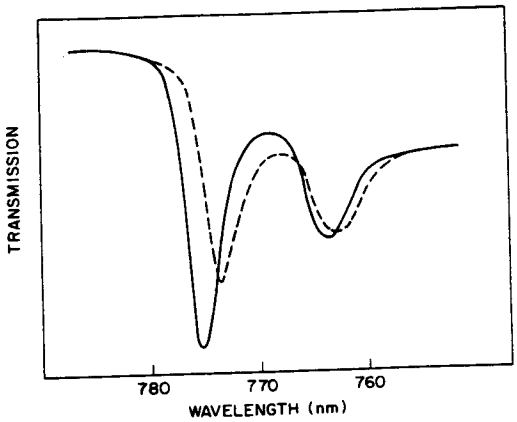

Figure 33. Transmission of a GaAs/AlGaAs multiple quantum well structure (L_z = 50 Å) at T = 15 K, measured with broad-band 120 fs probe pulses before and after resonant n_z = 1 heavy-hole excitation by a narrow-band 120 fs pump pulse; (——), −5 ps and (– – –), +1 ps. (After Peyghambarian *et al.* (1984).)

relative motion Hamiltonian underlying χ_t. This subtlety is less relevant in the case of thermalized e–h plasma-induced exciton bleaching, where the e–h pairs generated at some point by the pump beam (the e–h plasma) and those probed by the test beam (the excitons) are distinct.

Similar to equations (2.3.30) and (2.3.31), the polarization, $P_p(k)$, induced by the pump beam, E_p, satisfies the inhomogeneous Wannier equation

$$\sum_{k'} [H^0_{k,k'} + \delta H_{k,k'} - (\omega_p + i\delta)\delta_{k,k'}]P_p(k') = [1 - f_e(k) - f_h(k)]er_{cv}E_p, \qquad (3.1.12)$$

where the change in the e–h relative motion Hamiltonian, δH, consists in general of a part due to fermion exchange,

$$\delta H^H_{k,k'} = -\delta_{k,k'} \sum_{k''} I(\mathbf{k} - \mathbf{k}'')[f_e(k'') + f_h(k'')] + I(\mathbf{k} - \mathbf{k}')[f_e(k) + f_h(k)], \qquad (3.1.13)$$

and a part that describes the effects of correlations ('screening'). While the former is exact and always derivable from a variational principle, the latter is usually the subject of rather uncontrolled approximations. The superscript H in equation (3.1.13) stands for Hartree, because, in a weakly non-ideal Bose gas picture, equation (3.1.13) is equivalent to the functional derivative of the exciton Hartree self-energy (Schmitt-Rink and Haug 1984).

Through the second term in equation (2.3.33), equation (3.1.13) yields a contribution to the saturation density, N_s, of the same size as N_s^{PSF}. Estimates of this contribution have been given by Schmitt-Rink *et al.* (1985), both for exciton and e–h plasma induced exciton bleaching, while an exact numerical evaluation of this term has been performed by Zimmerman (1988a). Using equation (3.1.10), one finds in the case of selective exciton generation, for $Na_0^2 \ll 1$,

$$\delta H^H_{k,k'} = -\delta_{k,k'} N \sum_{k''} I(\mathbf{k} - \mathbf{k}'')|\phi^0_{1s}(k'')|^2 + N|\phi^0_{1s}(k)|^2 I(\mathbf{k} - \mathbf{k}'). \qquad (3.1.14)$$

Substituting this expression into equation (2.3.34), one obtains a Hartree blue shift of the 1s exciton resonance due to exciton–exciton collisions and as experienced by the

pump beam (Bobrysheva *et al.* 1980a, Schmitt-Rink *et al.* 1985)

$$\delta E_{1s}^{H} = N \sum_{k,k'} [\phi_{1s}^{0}(k') - \phi_{1s}^{0}(k)]\phi_{1s}^{0}{}^{*}(k)|\phi_{1s}^{0}(k')|^2 I(\mathbf{k} - \mathbf{k}')$$

$$= 4\pi N a_0^2 \left(1 - \frac{315\pi^2}{4096}\right) E_0. \tag{3.1.15}$$

The corresponding result in 3D is $(13\pi N a_B^3 R)/3$ (Keldysh and Kozlov 1968). Equation (3.1.15) is of course nothing but the Heitler–London exchange integral.

The polarization, $P_t(k)$, induced by the test beam, E_t, satisfies also an inhomogeneous Wannier equation of the form equation (3.1.12), but with additional contributions to δH. For $Na_0^2 \ll 1$, exciton exchange between pump and test beam yields a Fock (F) term (Schmitt-Rink and Haug 1984, Schmitt-Rink and Chemla 1986)

$$\delta H_{k,k'}^{F} = \delta_{k,k'} N\phi_{1s}^{0}{}^{*}(k) \sum_{k''} I(\mathbf{k} - \mathbf{k}'')\phi_{1s}^{0}(k'') - N\phi_{1s}^{0}(k) I(\mathbf{k} - \mathbf{k}')\phi_{1s}^{0}{}^{*}(k'), \tag{3.1.16}$$

the expectation value of which in the 1s state is identical to equation (3.1.15). The blue shift of the 1s exciton resonance as seen by the test beam is thus

$$\delta E_{1s}^{HF} = 8\pi N a_0^2 \left(1 - \frac{315\pi^2}{4096}\right) E_0. \tag{3.1.17}$$

The corresponding result in 3D is $(26\pi N a_B^3 R)/3$ (Keldysh and Kozlov 1968). Corrections to equations (3.1.17) have been calculated by Manzke *et al.* (1987). From second-order perturbation theory in the effective exciton–exciton interaction, they find a negative correlation ('screening') contribution about one-quarter the magnitude of equation (3.1.17), showing once more the reduced efficiency of 'screening' in 2D and confirming the conjecture of Schmitt-Rink *et al.* (1985).

While the inclusion of δH leads to a smaller saturation density for the pump beam (compared to N_s^{PSF}), this is not necessarily true for the test beam. In fact, within the HF approximation outlined above, the opposite behaviour is found. This has been recognized only recently, in studies of the optical Stark effect (see section 3.2). The point is rather simple. From equations (3.1.14) and (3.1.16), one obtains a blue shift of the band gap under selective exciton generation and as seen by the test beam only,

$$\delta E_g^{HF} = N \sum_{k''} [\phi_{1s}^{0}{}^{*}(k = 0) - \phi_{1s}^{0}{}^{*}(k'')]\phi_{1s}^{0}(k'') I(k'')$$

$$= 8\pi N a_0^2 \left(1 - \frac{3\pi}{16}\right) E_0, \tag{3.1.18}$$

which is *larger* than that of the exciton, equation (3.1.17). The corresponding result in 3D is $24\pi N a_B^3 R$ (Haug 1976). This implies an *increased* exciton binding energy, and, through the second term in equation (2.3.33), a *negative* contribution to the saturation density, N_s, again of the same magnitude as N_s^{PSF}.

This result deserves some comments. First of all, it is not an artefact of uncontrolled approximations, but a genuine variational bound. The underlying physics is the same as the one stressed in the context of PSF. Equations (3.1.18) and (3.1.17) simply state that at low temperatures exciton–exciton interactions are smaller than exciton–carrier interactions, which is well established experimentally (Fehrenbach *et al.* 1982, 1985, Schultheis *et al.* 1986a). The important question is how much of this HF behaviour

survives a more complete treatment. In the absence of any rigorous calculations (first attempts have been made only recently (Schaefer *et al.* 1988b)) one can only speculate. (In bulk GaAs, Fehrenbach *et al.* (1985) actually claimed a blue shift of the band gap, but none of the 1s exciton.) What one can definitely conclude is that saturation of the pump beam susceptibility occurs for smaller exciton densities than that of the test beam.

The above discussion explains also why, at least in the case of selective exciton generation, the theoretical test beam saturation density based on PSF alone agrees almost exactly with the experimental one. One way or the other, there is less reduction of the band gap and decrease of the exciton binding energy than in the case of e–h plasma generation, so that it is not too bad an approximation to neglect these effects completely. The same is true in 3D. In fact, the early measurements on low-temperature bulk GaAs by Gibbs *et al.* (1979) are well accounted for by PSF. The concept has in the meantime been extended to 1D excitons in polydiacetylene-PTS (Greene *et al.* 1987, 1988, Kajzar *et al.* 1988), where it works even better. This should not be too surprising, because the more excitons are confined the less polarizable they are and the more the effects of Pauli exclusion dominate. In the limit of Frenkel excitons (with internal Coulomb confinement) or quantum dots (with external confinement), PSF is the one and only saturation mechanism (Schmitt-Rink *et al.* 1987).

Excitonic optical nonlinearities have also been investigated in II–VI ZnSe/MnZnSe QWs (Andersen *et al.* 1986), which are believed to be intermediate between 2D and 3D, with a large offset in the conduction band but only a small one in the valence band. A new luminescence line in these structures was tentatively assigned to quantum-confined biexctions (Fu *et al.* 1988), as was done before in the case of GaAs/AlGaAs QWs (Miller *et al.* 1982c). As shown first by Bobrysheva *et al.* (1980b) and later by Kleinman (1983), the biexciton binding energy increases indeed as one proceeds from 3D to 2D, making them more resolved. These considerations have recently been extended to quantum wires (Banyai *et al.* 1987). They suggest the possibility of biexcitonic nonlinearities, for eample, due to two-photon absorption (Hanamura 1973, Haug and Schmitt-Rink 1984, Abram 1985, Henneberger 1986). One might have some doubts, however, whether improvements over CuCl, the 'classic' biexciton material, are possible. Just like in the case of low-temperature excitons, confinement does not buy anything as far as the nonlinear cross-section per photoexcited e–h pair is concerned. The point is again very simple. In the two-photon process, biexcitons are created via an exciton in the intermediate state. Any valence electron within a molecular radius of this virtual exciton can complete the transition, so that the optical matrix element for transitions from the exciton to the biexciton state scales like the ratio of the biexciton volume to that of the exciton (Hanamura 1973). Apart from geometrical factors, this ratio does not depend dramatically on dimensionality. (In quantum dots, 'biexcitons' correspond to transitions between upper Hubbard levels and are not bound.)

3.2. *Effects of virtual electron–hole populations*

Coherent nonlinear optical processes are produced by the excitation of semiconductors in the transparency region well below the absorption edge. They are often referred to as 'non-resonant' (Bloembergen 1965), in the sense that the excitation does not coincide with an absorption line; they do have resonant enhancements however, as such absorption lines are approached. Such nonlinearities have been widely investigated in the near and medium infrared (Chemla 1980). The underlying physics

can be described as follows. The valence electrons are held in equilibrium by the large atomic fields, E_{atom}; the application of optical fields, E, not negligible compared with E_{atom}, induces anharmonic charge density fluctuations that in turn can interact with other optical fields. The mutual coupling of the optical fields (E) via the anharmonic charge density fluctuations causes exchange of photons among the optical fields; in the process, however, no net power is deposited in the medium. Coherent nonlinear optical processes are characterized by the fact that non-resonant optical fields induce only virtual e–h populations, which last essentially only as long as the fields are applied.

In the standard textbook description of these processes, the 'ground state' of the semiconductor in the presence of the optical fields is represented by a coherent superposition of all excited (e–h pair) states. The expectation value of the polarization is calculated formally using the density matrix formalism. Spatial dispersion is often negligible and only dipolar effects are retained. They are described by an interaction Hamiltonian of the form $-PE$, where P is the polarization of the medium. In the usual discussion of nonlinear optics, the expectation value of P is expanded in a power series of the E values, the coefficients being the non-resonant nonlinear susceptibilities, $\chi^{(3)}$, $\chi^{(5)}$ and so on. Finally, the field propagation and the interaction among fields are analysed by solving the corresponding Maxwell equations coupled by the nonlinear polarization (Shen 1984).

The non-resonant nonlinear susceptibilities, $\chi^{(n)}$, are global parameters and their formal expressions involve infinite sums over complete sets of states, in which the behaviour of particular states is difficult to isolate. Until recently, specific experimental investigations of excitonic effects had been rather scarce and theoretical models had been limited to semi-empirical descriptions, where the exciton levels were characterized by *ad hoc* matrix elements and spectroscopically determined energies. This concept was applied (with some success) to virtual biexciton formation in wide-gap semiconductors, such as CuCl (Chemla and Maruani 1982, Haug and Schmitt-Rink 1984, Abram 1985, Henneberger 1986).

Clearly, the most natural way to probe excitonic effects in non-resonant nonlinear optical processes is to measure the exciton absorption while the sample is excited well below the absorption edge by a strong essentially monochromatic pump beam and to look for transient changes that persist only as long as the excitation. It is fair to say that in QWs these effects (coherent excitonic optical nonlinearities due to virtual e–h pairs) were first observed accidentally (Mysyrowicz *et al.* 1986, Von Lehmen *et al.* 1986b).

In time-resolved studies of the exponential absorption tail and phonon sidebands (see section 3.1) in GaAs/AlGaAs multiple quantum well structures ($L_z = 96$ Å) at $T = 70$ K, using 6 ps pump and probe pulses, strong and transient changes of the probe beam transmission, as shown in figure 34, have been observed (Von Lehmen *et al.* 1986b). These changes can be positive or negative depending on the spectral position of the probe beam with respect to the $n_z = 1$ heavy-hole exciton resonance. *They last only as long as the pump pulse.* In addition, if the pump detuning from the absorption edge is not too large, as in figure 34, much weaker effects due to real e–h pairs generated through phonon-assisted transitions are also seen. This process is easily distinguished from the fast effects. It persists for the carrier lifetime and completely disappears for large detunings of the pump beam. The fast component of the change in probe beam transmission was studied as a function of the pump parameters. It was found that it is linear in the inverse pump detuning from the $n_z = 1$ heavy-hole exciton resonance, $(E^0_{1s} - \omega_p)^{-1}$, for fixed pump intensity (figure 35 (*a*)), and linear in the pump intensity, $|E_p|^2$, for fixed pump detuning (figure 35 (*b*)). Moreover, a lineshape

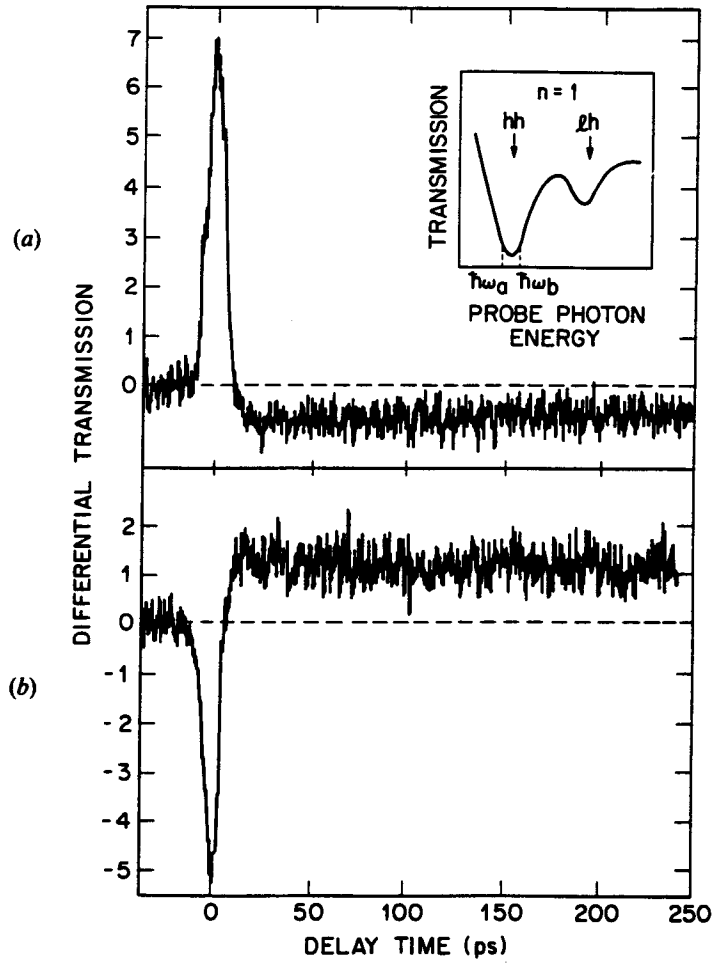

Figure 34. Differential transmission of a GaAs/AlGaAs multiple quantum well structure (L_z = 96 Å) at T = 70 K, as a function of pump-probe delay. The pump pulse has a duration of 6 ps and is tuned 25 meV below the n_z = 1 heavy-hole exciton resonance. The probe pulses have a duration of 6 ps and are tuned ~ 1 meV below the n_z = 1 heavy-hole exciton resonance in (*a*) and ~ 1 meV above the n_z = 1 heavy-hole exciton resonance in (*b*). (After Von Lehmen *et al.* (1986b).)

analysis of the fast and slow components as a function of the probe frequency around the n_z = 1 exciton resonances revealed their very different spectral profiles (Von Lehmen *et al.* 1986b). The slow component has all the characteristics of e–h plasma induced exciton bleaching and broadening discussed in section 3.1. The fast component is much larger and its differential transmission spectrum varies like the derivative of the linear absorption; it corresponds to a transient blue shift of the exciton resonances. For a pump detuning ~ 30 meV and a pump intensity ~ 8 MW cm^{-2}, the magnitude of the shift is ~ 0·2 meV for the n = 1 heavy-hole exciton peak and ~ 0·05 meV for the n = 1 light-hole exciton peak. Similar numbers were found in InGaAs/InP QWs under similar excitation conditions (Tai *et al.* 1987c).

The same effects have also been observed using femtosecond pump and probe pulses, although at much higher intensities (Mysyrowicz *et al.* 1986, Joffre *et al.*

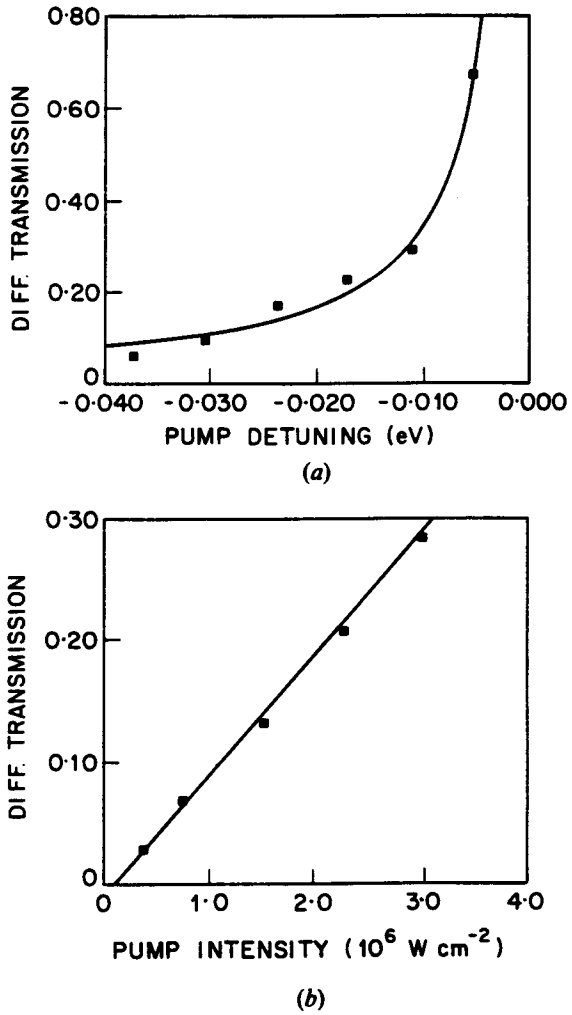

Figure 35. Differential transmission at zero pump-probe delay, as a function of pump detuning from the $n_z = 1$ heavy-hole exciton resonance for fixed pump intensity (*a*) and pump intensity for fixed pump detuning (*b*). (After Von Lehmen *et al.* (1986b).)

1987). Again, they were found accidentally in studies of the exciton blue shift due to exciton–exciton interactions in narrow QWs discussed in section 3.1. Figure 36 shows absorption spectra of a GaAs/AlGaAs multiple quantum well structure ($L_z = 100$ Å) at $T = 15$ K, measured with broad-band 100 fs probe pulses during excitation of virtual e–h pairs 46 meV below the $n_z = 1$ heavy-hole exciton resonance by narrow-band 400 fs pump pulses of various intensities (Joffre *et al.* 1987). In addition, in these high-intensity data, there is clear evidence of a decrease in exciton absorption (see below). Hulin *et al.* (1986b) exploited the effects to operate a GaAs/AlGaAs optical gate with subpicosecond switch on and off times.

In conclusion, strong photoexcitation of a semiconductor in the transparency region well below the absorption edge gives rise to a transient exciton blue shift at low

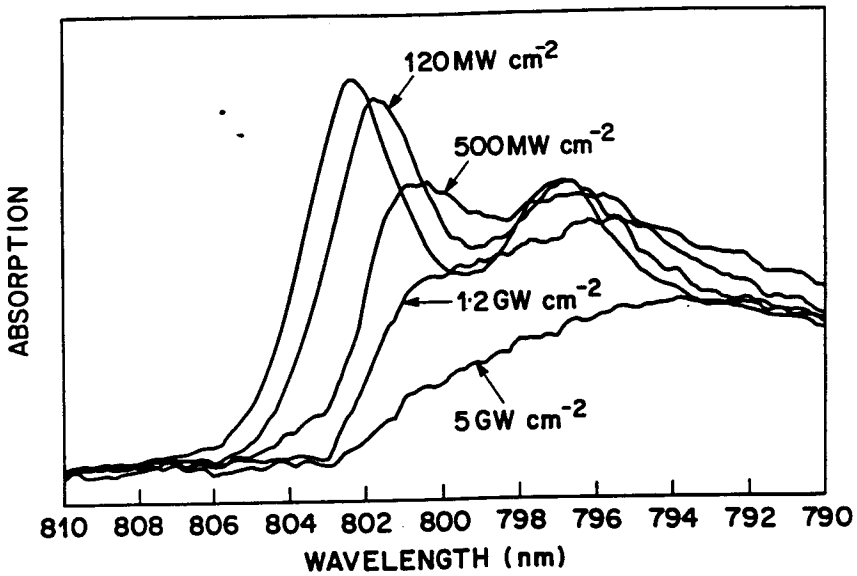

Figure 36. Absorption spectra of a GaAs/AlGaAs multiple quantum well structure (L_z = 100 Å) at T = 15 K, measured with broad-band 100 fs probe pulses during excitation of virtual e–h pairs 46 meV below the n_z = 1 heavy-hole exciton resonance by narrow-band 400 fs pump pulses of various intensities. (After Joffre *et al.* (1987).)

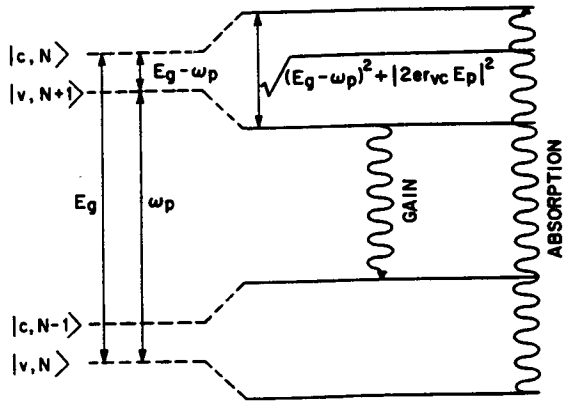

Figure 37. Unperturbed (dashed lines) and perturbed (full lines) energy levels of a two-level system in the presence of a nonresonant pump beam with frequency ω_p and amplitude E_p.

intensities and, in addition, a transient decrease in exciton absorption at high intensities, which last exactly as long as the pump pulse.

Exactly the same phenomena, a shift and bleaching of spectral lines in a strong non-resonant laser field, have been extensively studied in the 1970s in atomic vapours, such as Na, by Liao and Bjorkholm (1976). In atomic physics, the analogy to effects previously considered has often been emphasized by using similar terminology. For example, to emphasize the analogy to the renormalizations in the photon vacuum, known as the Lamb shift, the blue shift itself is sometimes referred to as 'lamp shift'.

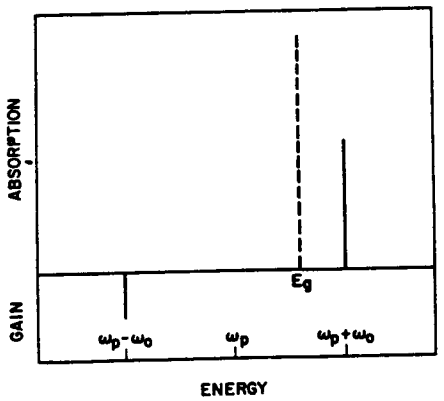

Figure 38. Optical excitation spectrum of the two-level system shown in figure 37. The dashed line gives the unperturbed absorption at E_g, the full lines the absorption (at $\omega_p + \omega_0$) and gain (at $\omega_p - \omega_0$) in the presence of a non-resonant pump beam at ω_p. ω_0 is the Rabi frequency, given in equation (3.2.1).

Similarly, the analogy to d.c. field induced effects is reflected by such terms as 'optical', 'dynamical', or 'a.c. Stark effect'. We note that this effect is one of the most fundamental phenomena in light–matter interactions. Before turning to the above experiments on Wannier excitons, we will review its explanation for a single atom, where the problem can be readily understood; see for example Feneuille (1977).

We consider a simple two-level atom or, for that matter, a Frenkel exciton or an individual band-to-band transition in the presence of a non-resonant monochromatic laser field with frequency ω_p and amplitude E_p, as shown in figure 37. Following our previous notation, we denote the ground state by v, the excited state by c, and the energy gap by E_g. The unperturbed eigenstates of the system are product states of the electron states and the photon states. As shown by the dashed lines in figure 37, there is a series of states $|v, N\rangle$, $|v, N+1\rangle$ and so on, with $N, N+1, \ldots$ photons and the electron in the ground state v, and a series of states $|c, N-1\rangle$, $|c, N\rangle$ and so on, with $N-1, N, \ldots$ photons and the electron in the excited state c. If the pump detuning, $E_g - \omega_p$, is not too large, the states $|c, N\rangle$ and $|v, N+1\rangle$ are almost degenerate. The dipole interaction mixes these states, leading to new, 'dressed atom' eigenstates, shown by the full lines in figure 37. The energy difference between the centres of two such neighbouring doublets is ω_p, and in the classical limit the doublet splitting itself is given by the famous Rabi (1937) frequency,

$$\omega_0 = [(E_g - \omega_p)^2 + 4|er_{vc}E_p|^2]^{1/2}, \qquad (3.2.1)$$

which measures the amount of time the electron spends in the excited state.

A test beam induces optical transitions between these dressed atom states. In the steady state, its absorption is proportional to both the transition rate and the population difference between states in neighbouring doublets. Under non-resonant excitation, there is much more population in the lower v-like state of each doublet than in the upper c-like one. Furthermore, the transition rate for transitions that conserve N is the largest. Consequently, the optical excitation spectrum shown in figure 38 consists of a blue-shifted absorption at $\omega_p + \omega_0$ and stimulated emission at $\omega_p - \omega_0$, with much lower intensity. In the latter process, two pump photons are

destroyed and a test photon and blue-shifted transition are created. Such gain in an uninverted system was first observed by Wu *et al.* (1977). When ω_p equals E_g, all dressed atom states have the same transition rates and populations, and no excitations are possible. In reality, because of dissipation, this limit is usually not realized. Dephasing leads to a rather complicated absorption and to the famous three-peaked resonance fluorescence spectrum (Mollow 1969, 1970), measured first by Schuda *et al.* (1974).

The dressed atom picture, which predicts an a.c. Stark shift, $\omega_0 - E_g + \omega_p$, of the absorption edge and a corresponding bleaching, was invoked by Mysyrowicz *et al.* (1986) to explain their experimental data. Using equation (3.2.1), which becomes exact for pump detunings much larger than the exciton binding energy (see below), and expanding the square root, one finds indeed that the order of magnitude of the observed shifts and their dependence on pump parameters are accounted for quite well. In general, however, this picture is only valid for Frenkel excitons, namely isolated atoms, and there is no reason why it should apply to Wannier excitons as well. As we shall see, it does not account for various subtleties, in particular the fact that there is essentially no loss of exciton oscillator strength (the observed decrease in exciton absorption at high intensities is rather due to a broadening, see below).

The first (and so far only) *consistent* theory of the a.c. Stark effect in semiconductors has been given by Schmitt-Rink and Chemla (1986) and Schmitt-Rink *et al.* (1988), using an extension of the HF theory outlined in section 3.1. to coherently driven virtual e–h pairs and arbitrary pump intensities. In its present form, this approach does not account for (i) correlations ('screening'), (ii) virtual formation of *bound* biexcitons (Haug and Schmitt-Rink 1984, Abram 1985, Henneberger 1986) and (iii) interactions other than the Coulomb interaction, such as phonon-mediated ones (Greene *et al.* 1988). The latter two effects can in principle by readily included (see below); they are however not important for the experiments discussed above. As for (i), the validity of the HF theory obviously increases with detuning.

With the general theoretical description requires the use of Kadanoff and Baym (1962) and Keldysh (1965) non-equilibrium Green's function techniques (Schaefer and Treusch 1986, Müller *et al.* 1987, Haug *et al.* 1987, Haug 1988, Schmitt-Rink *et al.* 1988, Hartmann *et al.* 1988, Schaefer 1988, Schaeffer 1988, private communication), the HF theory of the a.c. Stark effect can as well be derived from simple, Bloch-type equations of motion for the reduced density matrix, neglecting the collision term (Schmitt-Rink and Chemla 1986, Schmitt-Rink *et al.* 1988).

Consider first a two-band semiconductor in the absence of Coulomb interactions (and thus of excitons), as done by Poluektov *et al.* (1975) and Wautelet and Laude (1978). Interband transitions with different e–h relative momenta, $\mathbf{k}$, do then decouple, and each individual transition behaves in much the same fashion as the two-level system discussed previously, with a Rabi frequency

$$\omega_k = [(\epsilon_{ek} + \epsilon_{hk} - \omega_p)^2 + 4|er_{vc}E_p|^2]^{1/2}. \tag{3.2.2}$$

Figure 39 shows a sketch of the resulting renormalized conduction and valence band energies for $m_e = m_h$, corresponding to the $|c, N\rangle$ and $|v, N\rangle$-like dressed atom states in figure 37 (Schmitt-Rink *et al.* 1988). For non-resonant excitation, $\omega_p < E_g$, the conduction and valence band energies are blue shifted, the Stark shift decreasing with increasing detuning from the pump frequency, $\epsilon_{ek} + \epsilon_{hk} - \omega_p$ (figure 39 (*a*)). For resonant excitation, $\omega_p > E_g$, gaps of magnitude $2|er_{vc}E_p|$ open at ω_p. As before,

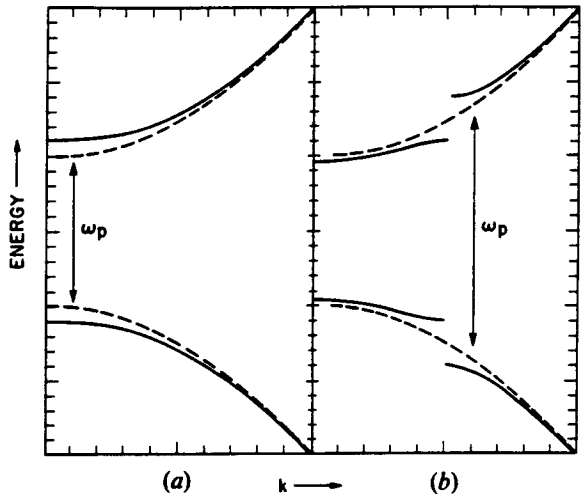

Figure 39. Sketch of the renormalized conduction and valence band energies as a function of momentum, k, for $m_e = m_h$ and (a) non-resonant excitation, $\omega_p < E_g$, (b) resonant excitation, $\omega_p > E_g$, of free e–h pairs. The dashed lines show the unperturbed energies. (After Schmitt-Rink *et al.* (1988).)

for $\epsilon_{ek} + \epsilon_{hk} = \omega_p$, the state with N photons and an electron in the valence band is degenerate with the state with $N - 1$ photons and the electron in the conduction band. The degeneracy is removed by the dipole interaction, which leads to the Stark splitting of the bands at ω_p. Furthermore, the states with e–h pair energies larger than $\omega_p + 2|er_{vc}E_p|$ are blue shifted, while those with e–h pair energies smaller than $\omega_p - 2|er_{vc}E_p|$ are red shifted (figure 39 (b)).

The latter case (figure 39 (b)) is relevant to the initial coherent transient that occurs in spectral hole burning experiments before the first collision (Oudar *et al.* 1985, Knox *et al.* 1986a, Fluegel *et al.* 1987). This initial time regime, depending on the excitation density and excess energy above the gap, can be as short as a few femtoseconds. Another situation in which figure 39 (b) becomes relevant is the saturated state of a semiconductor, in which the conduction and valence bands are filled up to the pump frequency, $\mu = \omega_p$. Starting with Galitskii *et al.* (1970), this state has been studied by a number of authors, assuming that carrier–carrier and carrier–phonon collisions quickly drive the e and h towards thermal equilibrium (Elesin 1971, Aleksandrov and Elesin 1971, Harbich and Mahler 1981, Haug 1985, Comte and Mahler 1986, Hartmann *et al.* 1988).

The non-equilibrium distributions, $f_e(k) = f_h(k)$, corresponding to figure 39 (a) and (b) are sketched in figure 40 (a) and (b) respectively (Schmitt-Rink *et al.* 1988). For non-resonant excitation, $\omega_p < E_g$, the distribution function is maximum at the gap and decreases smoothly with increasing detuning from the pump frequency, because the electrons spend less and less time in the excited state (figure 40 (a)). For resonant excitation, $\omega_p > E_g$, it peaks at the pump frequency, and again decreases smoothly with increasing detuning (figure 40 (b)). In the absence of relaxation, this is as expected. The maximum value of $\frac{1}{2}$ at ω_p corresponds to a perfect mixing of conduction and valence band states and to a complete bleaching of the pump beam absorption. Self-induced transparency along these lines has been suggested by Poluektov *et al.* (1975).

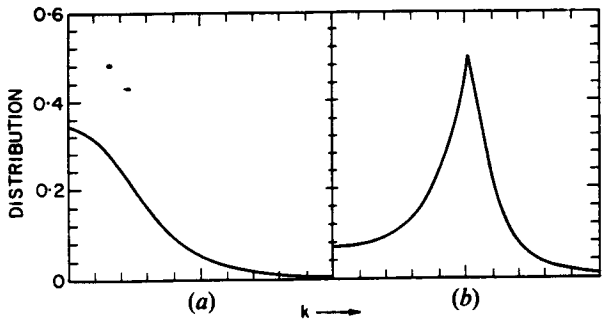

Figure 40. Sketch of the non-equilibrium distribution as a function of momentum, k, for (a) non-resonant excitation, $\omega_p < E_g$, (b) resonant excitation, $\omega_p > E_g$, of free e–h pairs. (After Schmitt-Rink *et al.* (1988).)

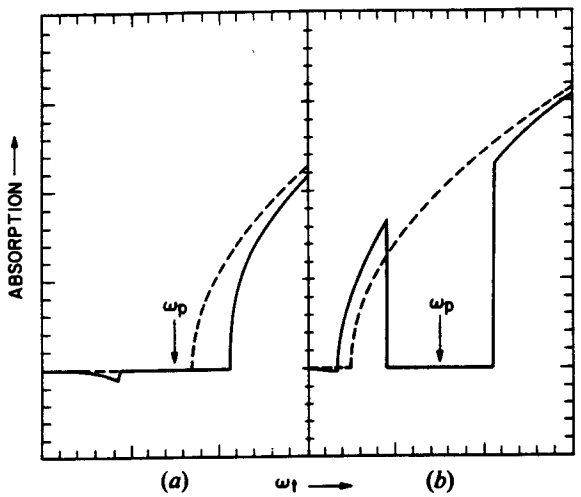

Figure 41. Sketch of the test beam absorption as a function of frequency, ω_t, for (a) non-resonant excitation, $\omega_p < E_g$, (b) resonant excitation, $\omega_p > E_g$, of free e–h pairs. The dashed lines show the unperturbed absorption. (After Schmitt-Rink *et al.* (1988).)

The optical excitation spectrum is similar to that of an inhomogeneously broadened two-level system and sketched in figure 41 (Schmitt-Rink *et al.* 1988). As discussed above, optical transitions occur for test frequencies $\omega_t = \omega_p \pm \omega_k$. For non-resonant excitation, $\omega_p < E_g$, the absorption edge exhibits the a.c. Stark shift, and optical gain starts at a photon frequency symmetric about ω_p (figure 41 (a)). For resonant excitation, $\omega_p > E_g$, and according to the renormalized band structure sketched in figure 39 (b), the interband absorption shows a spectral hole of width $4|er_{vc}E_p|$ about ω_p, in which the semiconductor is transparent (figure 41 (b)). Any relaxation process and the finite spectral width of realistic laser pulses will round this feature as well as the non-equilibrium distribution figure 40 (b) (see for example figure 31).

Excitons are composite particles made from such free e and h states, usually with many atoms participating. As discussed in the previous section, their nonlinear optical properties are exclusively due to their mutual interaction, which has its roots in the internal and fermionic degrees of freedom. Non-interacting excitons are ideal bosons and the Hamiltonian describing their coupling to the light field is that of two coupled

harmonic oscillators, with polaritons being the dressed particles (Hopfield 1958). The obvious question is then how this notion of a weakly non-ideal exciton gas can be reconciled with the picture given above.

To answer this question, we shall follow our previous discussion in section 3.1 and address the issue starting from the momentum space picture, in which, as discussed above, electrons pulsate with the Rabi frequency between valence and conduction band. By noting that *during the time the electrons spend in the excited state* (i.e. the conduction band) *they behave in exactly the same fashion as real ones*, we can simply take over equations (3.1.12) and (3.1.13) for the coherent polarization, $P_p(k)$, induced by the pump beam, E_p,

$$(E_{ek} + E_{hk} - \omega_p)P_p(k) = [1 - f_e(k) - f_h(k)]\Delta_k, \tag{3.2.3}$$

where

$$E_{ik} = \epsilon_{ik} - \sum_{k'} I(\mathbf{k} - \mathbf{k}')f_i(k'), \quad i = e, h, \tag{3.2.4}$$

$$\Delta_k = er_{cv}E_p + \sum_{k'} I(\mathbf{k} - \mathbf{k}')P_p(k'). \tag{3.2.5}$$

The steady state distribution functions, $f_e(k)$ and $f_h(k)$, which enter these equations, are obtained from the solution of the collisionless kinetic equation. One finds (Schmitt-Rink and Chemla 1986, Schmitt-Rink *et al.* 1988)

$$f_e(k) = f_h(k) = \tfrac{1}{2}(1 - (1 - 4|P_p(k)|^2)^{1/2}]. \tag{3.2.6}$$

For non-interacting e–h pairs, $I = 0$, the solution of equations (3.2.3)–(3.2.6) yields the non-equilibrium distributions sketched in figure 40. The Coulomb interaction modifies this free e–h pair result in two ways: (i) the e–e and h–h Coulomb repulsion renormalize the individual e and h energies (second term in equation (3.2.4)) and (ii) the e–h Coulomb attraction renormalizes the Rabi frequency at resonance (second term in equation (3.2.5)). Both changes express the fact that in the presence of Coulomb interactions an e–h pair with a given $\mathbf{k}$ does not only experience the external field, E_p, but also a significant internal one, the 'molecular field' associated with virtual e–h pairs created at $\mathbf{k}'$. At each $\mathbf{k}$, external and Coulomb fields combine to give an effective self-consistent coherent 'local field', to which the system responds. The problem is thus similar to that of a paramagnet in an external magnetic field.

In the case of real and thermalized e–h pairs at low temperatures, it is possible for a coherent molecular field to be created spontaneously, without external field, just like in a magnet. Starting with the pioneering work of Keldysh and coworkers (Keldysh and Kopaev 1965, Keldysh and Kozlov 1968), this instability towards Bose condensation of real e–h pairs (the excitonic insulator transition) has received considerable theoretical attention in the past (Zimmermann 1976, Silin 1977, Hanamura and Haug 1977, Comte and Nozières 1982, Nozières and Comte 1982, Haug and Schmitt-Rink 1984, Cote and Griffin 1988). The present 'Bose condensation of virtual e–h pairs' is closely related, except that it is externally enforced by the 'symmetry breaking' pump field, E_p, rather than being spontaneous. This is reflected by the 'chemical potential' and the phase of the virtual e–h pairs. The chemical potential, μ, which is nothing but the minimum energy required to create an additional virtual e–h pair, is identical to the pump frequency, ω_p, and thus below the bottom of the lowest exciton band, E_{1s}^0; the phase of the virtual e–h pairs is pinned, it is the same as that of the pump field,

E_p. (Here and in the following, we consider nonresonant excitation only, $\omega_p < E_{1s}^0$). Apart from these differences (which have important consequences), a close analogy exists to the renormalizations encountered in excitonic insulators, antiferromagnets, superconductors and superfluids, which will form the basis of our following discussion.

For small Rabi frequencies, the local fields or 'local field corrections' dominate and transform the virtual e–h pairs into excitons. For large Rabi frequencies, much larger than the exciton binding energy, the external field dominates and the problem is best thought of in terms of individual band-to-band transitions, with only minor changes due to the Coulomb interaction. Thus, we recover the transition from real space pairing (tightly bound excitons) to momentum space pairing (weakly correlated, overlapping e–h 'Cooper pairs') discussed earlier in the context of spontaneous e–h pair condensation and superconductivity (Nozières and Schmitt-Rink 1985), and corresponding to the transition from local moment to itinerant magnetic behaviour.

In general, the set of nonlinear equations (3.2.3)–(3.2.6) can only be solved numerically, and corresponding results will be discussed below. We will only discuss its solution for non-resonant excitation with small pump intensities. In this limit, excitons are still well defined and the nonlinear corrections can be treated in perturbation theory, just like in sections 2.3 and 3.1.

For small pump intensities and $\omega_p < E_{1s}^0$, eq. (3.2.6) reduces to

$$f_e(k) = f_h(k) = |P_p(k)|^2. \tag{3.2.7}$$

Substituting this expression into equations (3.2.3)–(3.2.5), we obtain the perturbed inhomogeneous Wannier equation

$$\sum_{k'} (H^0_{k,k'} + \delta H^H_{k,k'} - \omega_p \delta_{k,k'}) P_p(k') = (1 - 2|P_p(k)|^2) e r_{cv} E_p, \tag{3.2.8}$$

where

$$\delta H^H_{k,k'} = -2\delta_{k,k'} \sum_{k''} I(\mathbf{k} - \mathbf{k}'')|P_p(k'')|^2 + 2|P_p(k)|^2 I(\mathbf{k} - \mathbf{k}'). \tag{3.2.9}$$

These equations are exactly of the form of the Gross–Pitaevskii equation (Gross 1961, Pitaevskii 1959, 1961) for the order parameter of a weakly non-ideal Bose gas, including a driving term and specialized to a spatially uniform situation. The order parameter is the coherent polarization, $P_p(k)$, induced by the pump beam, and *condensation occurs in all exciton states simultaneously*, due to the non-resonant excitation.

Substituting the linear response result

$$P_p(k) = \sum_n \frac{\phi_n^0(k)\phi_n^{0*}(r = 0)}{E_n^0 - \omega_p} e r_{cv} E_p \tag{3.2.10}$$

into equation (3.2.7), we find for the density of virtual e–h pairs

$$\begin{aligned} N &= 2 \sum_k |P_p(k)|^2 \\ &= 2 \sum_n \frac{|e r_{vc} E_p|^2 |\phi_n^0(r = 0)|^2}{(E_n^0 - \omega_p)^2}. \end{aligned} \tag{3.2.11}$$

If the pump detuning from the absorption edge is small, most of the virtual e–h pairs occupy the 1s exciton state and

$$|P_p(k)|^2 = \tfrac{1}{2} N |\phi_{1s}^0(k)|^2, \tag{3.2.12}$$

that is, we recover equation (3.1.10). Substituting this result back into equations (3.2.8) and (3.2.9), we see that we can carry over all our previous results, such as equations (3.1.11) and (3.1.15); the interaction of virtual 1s excitons among themselves and with the light field is exactly the same as that of real ones.

In the opposite limit of very large detunings from the absorption edge, the electrons spend less time in the excited state than it takes to form a bound state, that is, $(E_g - \omega_p)^{-1} \ll E_0^{-1}$, so that the polarization, equation (3.2.10), reduces to the free e–h pair value

$$P_p(k) = \frac{er_{cv}E_p}{E_g - \omega_p}. \tag{3.2.13}$$

Using an elegant representation in terms of the Coulomb Green function, Zimmermann (1988 b,c, private communication) was able to evaluate equations (3.2.10) and (3.2.11) for arbitrary detunings.

Equation (3.2.13) demonstrates a very fundamental point, already mentioned above: whenever the detuning is the largest energy in the problem (i.e. much larger than the confinement energy), neither Coulomb nor external confinement enhance non-resonant optical susceptibilities, because they involve sums over complete sets of states, which are of course independent of the basis set (Chemla *et al.* 1987 b). The situation is thus different from resonant excitation, where at least the linear susceptibility is enhanced.

Equations (3.2.8) and (3.2.9) can as well be derived from an effective exciton Hamiltonian with two basic ingredients: (i) an anharmonic exciton–photon interaction and (ii) an anharmonic exciton–exciton interaction (Schmitt-Rink 1988). The former is obtained from the linear exciton–photon interaction by projecting out the states that are already occupied, by preventing 'double occupancy'; it gives rise to the PSF correction to the oscillator strengths. The latter is the usual exciton–exciton interaction (Hanamura and Haug 1977, Haug and Schmitt-Rink 1984) and gives rise to the Hartree correction to the effective e–h relative motion Hamiltonian, δH^H. In general, this correction would be rigorously determined by the exciton T matrix, rather than by the first-order Heitler–London term, as in our approach. Besides the hard core repulsion of excitons, the T matrix would also describe their Van der Waals attraction, namely mutual exciton polarization, formally determined by 'intermediate state interactions'. The problem with these as well as 'final state interactions' is that the T matrix in the singlet channel diverges, signalling the instability of the system towards bound biexciton formation. This divergence can be removed, however, by allowing for coexistence of virtual particle (excitons) and molecule (biexcitons) condensates. Starting with Valatin and Butler (1958), such a pair condensation of bosons has been extensively studied in the past (Evans and Imry 1969, Doerre *et al.* 1979, Nozières and Saint-James 1982, Bobrysheva and Moskalenko 1983, Haug and Schmitt-Rink 1984). This would then also allow for a rigorous description of coherent two-photon generation of biexcitons, which so far has been treated rather naively. Again, when the pump detuning from the absorption edge is much larger than the biexciton binding energy, the process becomes irrelevant. It can always be circumvented by choosing appropriate laser polarizations: a circularly polarized pump beam cannot create biexcitons, nor can two different beams with identical circular polarization (in both cases, spin-aligned e–h pairs are produced).

The coherent 'ground state' of a semiconductor in the presence of the pump beam (i.e. the virtual condensate) is, of course, not what is being measured by a test beam.

A weak test beam, E_t, induces a polarization which has to be clearly distinguished from that induced by the pump beam. It measures the 'excitation spectrum', the linear fluctuations about the condensate. Unlike in real condensates, the excitation spectrum has a gap. In zero-order in the pump intensity, this gap is the difference between the 1s exciton energy and the pump frequency, $E_{1s}^0 - \omega_p$, namely the minimum energy required to create a real e–h pair out of the condensate. Owing to the anharmonic interactions, this gap will be renormalized and the condensate depleted, which then shows up as the a.c. Stark effect.

By linearizing equations (3.2.3)–(3.2.6) in the perturbation, E_t, Schmitt-Rink and Chemla (1986) and Schmitt-Rink *et al.* (1988) derived the perturbed inhomogeneous Wannier equation underlying the susceptibility, χ_t, experienced by the test beam. Their treatment follows the kinetic theory of superconductors (Bardeen *et al.* 1957, Anderson 1958, Bogolubov *et al.* 1958, Betbeder-Matibet and Nozières 1969) and generalizes earlier calculations by Keldysh and Kozlov (1968). Similar results for a real condensate have been obtained recently by Cote and Griffin (1988).

For small pump intensities and $\omega_p < E_{1s}^0$, one finds for the polarization induced by the test beam

$$\sum_{k'} [H^0_{k,k'} + \delta H^{HF}_{k,k'} - (\omega_t + i\delta)\delta_{k,k'}]P_t(k') = (1 - 2|P_p(k)|^2)er_{cv}E_t - \sum_{k'} \delta H^B_{k,k'}\bar{P}_t(k'), \tag{3.2.14a}$$

$$\sum_{k'} [H^0_{k,k'} + (\delta H^{HF}_{k,k'})^* + (\omega_t - 2\omega_p + i\delta)\delta_{k,k'}]\bar{P}_t(k') = -\sum_{k'} (\delta H^B_{k,k'})^* P_t(k'), \tag{3.2.14b}$$

where the Hartree correction, δH^H, is defined in eq. (3.2.9). δH^F and δH^B are Fock and Bogolubov corrections, which read respectively

$$\delta H^F_{k,k'} = 2\delta_{k,k'}P_p^*(k)\sum_{k''} I(\mathbf{k} - \mathbf{k}'')P_p(k'') - 2P_p(k)I(\mathbf{k} - \mathbf{k}')P_p^*(k') + 2er_{cv}E_pP_p^*(k)\delta_{k,k'}, \tag{3.2.15}$$

$$\delta H^B_{k,k'} = 2\delta_{k,k'}P_p(k)\sum_{k''} I(\mathbf{k} - \mathbf{k}'')P_p(k'') - 2P_p(k)I(\mathbf{k} - \mathbf{k}')P_p(k') + 2er_{cv}E_pP_p(k)\delta_{k,k'}. \tag{3.2.16}$$

These equations are exactly of the form of the Bogolubov–Beliaev equations (Bogolubov 1947, Beliaev 1958a,b) for the excitation spectrum of a weakly non-ideal Bose gas. Beside the PSF modification of the driving term, there are two elementary nonlinear processes, which determine the linear response to a weak test beam, E_t: (i) renormalization of e–h pairs (described by the H and F terms) and (ii) creation and annihilation of pairs of e–h pairs (described by the B term). The former process, renormalization of real e–h pairs excited out of the condensate, should not be confused with the renormalization of the virtual e–h pairs in the condensate, equation (3.2.9). It is due both to anharmonic interactions with the latter (first and second term in equation (3.2.15), equation (3.2.9)) and with pump photons (third term in equation (3.2.15)). In the latter process, two pump photons and thus two virtual e–h pairs out of the condensate are destroyed and two renormalized real e–h pairs are created, one of which eventually transforms into a test photon, and *vice versa*. Again, as evident from equation (3.2.16), both anharmonic interactions contribute to this nonlinear process, the 'depletion of the condensate' stimulated by the test beam, which

necessarily leads to optical gain, even though there is no population inversion. We thus recover the two basic renormalizations of the dressed atom picture discussed above.

If the pump detuning from the absorption edge is small, the polarization induced by the pump beam is given by equation (3.2.12). Substituting this result into equation (3.2.15), we recover equations (3.1.16)–(3.1.17), the HF shift of the 1s exciton resonance due to the anharmonic exciton–exciton interaction. An additional Stark contribution to this shift arises now from the anharmonic exciton–photon interaction, the third term in equation (3.2.15), the expectation value of which in the 1s state is

$$\begin{aligned}\delta E_{1s}^{F} &= 2er_{cv}E_{p}\sum_{k}P_{p}^{*}(k)|\phi_{1s}^{0}(k)|^{2} \\ &= \frac{2|er_{vc}E_{p}|^{2}}{E_{1s}^{0}-\omega_{p}}\frac{|\phi_{1s}^{0}(r=0)|^{2}}{N_{s}^{PSF}}.\end{aligned} \tag{3.2.17}$$

Here N_s^{PSF} is the saturation density due to excitonic PSF, defined in equations (3.1.8), (3.1.10) and (3.1.11). Similarly, we obtain for the Stark shift of the band gap

$$\begin{aligned}\delta E_{g}^{F} &= 2er_{cv}E_{p}P_{p}^{*}(k=0) \\ &= \frac{2|er_{cv}E_{p}|^{2}}{E_{1s}^{0}-\omega_{p}}\phi_{1s}^{0*}(k=0)\phi_{1s}^{0}(r=0).\end{aligned} \tag{3.2.18}$$

The first factor in equation (3.2.17) expresses the Stark shift of the atomic states that form the conduction and valence bands. The second factor describes the renormalization of this atomic shift due to excitonic effects. Its numerator reflects the fact that an exciton is built up from a linear combination of Bloch states that originate themselves from the atomic states. It expresses the enhancement of the oscillator strength due to the correlation in the excitonic state. The same factor appears in Elliott's formula for excitonic linear absorption. The denominator contains the saturation density, N_s^{PSF}, above which the concept of excitons becomes invalid. Note that the magnitude of this second factor is rather independent of dimension; $|\phi_{1s}^{0}(r=0)|^{2}/N_{s}^{PSF} = 7/2$ and 16/7 in 3D and 2D respectively. In the case of Frenkel excitons, we recover atomic behaviour.

In the $L_z = 96$ Å GaAs/AlGaAs multiple quantum well structure studied by Von Lehmen *et al.* (1986b), no shift of the 1s exciton resonances due to the anharmonic exciton–exciton interaction is seen under resonant excitation. Consequently, we consider only equation (3.2.17), the contribution of the anharmonic exciton–photon interaction. For a pump intensity of $I_p \sim 8\,\mathrm{MW\,cm^{-2}}$ and a pump detuning of $E_{1s}^{0} - \omega_p \sim 30$ meV, the magnitude of the theoretical shift is 0·15 meV for the heavy-hole exciton peak and a factor of four less for the light-hole exciton peak, in excellent agreement with the experimental data.

The general behaviour of the HF 1s exciton shift in 2D and 3D as a function of pump detuning from the absorption edge was evaluated by Zimmermann (1988b,c) and Ell *et al.* (1989), including both exciton–exciton (which dominate for very small detunings) and exciton–photon interactions. With increasing detuning, a slow decrease of the second factor in equation (3.2.17) to the free e–h pair value 1 is found, which can be easily seen by using equation (3.2.13).

As discussed above, for higher pump intensities, small optical gain is expected, just like in the case of atoms and free e–h pairs (figures 38 and 41 (*a*)). This gain is at least quadratic in the pump intensity and suitably reinterpreted in terms of the depletion of the condensate or simultaneous emission of a test photon and a collective excitation.

From equation (3.2.14), one obtains for the spectrum of collective excitations (Schmitt-Rink and Chemla 1986, Schmitt-Rink *et al.* 1988)

$$\omega_n = [(E_n^0 + \delta E_n^{HF} - \omega_p)^2 - |\delta E_n^B|^2]^{1/2}, \tag{3.2.19}$$

which is identical to the Bogolubov–Beliaev result, but has a gap. Again, ω_p can be thought of as the chemical potential. Optical absorption into renormalized exciton states occurs for $\omega_t = \omega_p + \omega_n$ and optical gain for

$$\omega_t = \omega_p - \omega_n = 2\omega_p - (\omega_p + \omega_n),$$

that is, at frequencies symmetric about ω_p.

For small pump detunings from the absorption edge, and if we neglect the contribution to equation (3.2.19) of the anharmonic exciton–exciton interaction, that is, if we keep only equation (3.2.17) and the corresponding δE_{1s}^B ($|\delta E_{1s}^B| = \delta E_{1s}^F$), equation (3.2.19) reduces to

$$\omega_{1s} = [(E_{1s}^0 - \omega_p)^2 + 4|er_{vc}E_p|^2|\phi_{1s}^0(r = 0)|^2/N_s^{PSF}]^{1/2}, \tag{3.2.20}$$

which is exactly the expression for the Rabi frequency of a two-level atom off resonance, equation (3.2.1), with suitable Wannier exciton modifications. For small pump intensities, this yields the Stark shift, equation (3.2.17), while for large pump intensities saturation sets in. In this context, it should be noted that for very high pump intensities it no longer makes sense to expand about unperturbed 1s exciton states, so that equation (3.2.20) *cannot* be expected to describe the saturation of the 1s exciton Stark shift correctly. For large detunings of the pump beam, much larger than the exciton binding energy, the free e–h pair result, equation (3.2.1), is recovered. Equation (3.2.20) also shows that, as far as the near-resonant Stark shift is concerned, one exciton behaves like N_s^{PSF} independent two-level atoms per unit volume (if exciton–exciton interactions can be neglected), that is, N_s^{PSF} states per unit volume are required to form an exciton, as is also implied by equation (3.1.4) for χ_p. Again, in the case of Frenkel excitons, the exact atomic behaviour is recovered.

The second factor in the band gap Stark shift, equation (3.2.18), is given by $\phi_{1s}^{0*}(k = 0)\phi_{1s}^0(r = 0) = 8$ and 4 in 3D and 2D respectively, while for large detunings δE_g^F reduces to its free e–h pair results and becomes equal to δE_{1s}^F (Ell *et al.* 1989). For small pump detunings from the absorption edge, the Stark shift of the band gap due to the anharmonic exciton–photon interaction is thus about a factor of two larger than that of the 1s exciton, thus the exciton binding energy as seen by the test beam increases. The same is true (in HF and for the same physical reasons) for the effects of the anharmonic exciton–exciton interaction, as discussed previously in section 3.1. The accompanying increase in exciton oscillator strength competes then with the decrease due to PSF. As a result, there is essentially no change in 1s exciton oscillator strength, which is consistent with the experimental observations of Von Lehmen *et al.* (1986 b). The integrated test beam absorption decreases of course, according to the PSF factor in equation (3.2.14), and just like in a two-level atom. Ell *et al.* (1989) and Schaefer (1988) solved the full HF equations of Schmitt-Rink and Chemla (1986) and Schmitt-Rink *et al.* (1988) numerically, and their results for the test beam absorption shown in figure 42 demonstrate the effect very nicely. The full line gives the unperturbed absorption in 2D, while the others correspond to increasing pump intensities for a detuning of $\omega_p = E_g - 2{\cdot}5E_0$. Basically, only a shift is seen up to the highest intensities considered. Recent experiments by Knox *et al.* (1989) confirmed the absence of bleaching at low pump intensities. At high intensities, a strong decrease in exciton absorption is seen, in agreement with the French measurements (Mysyrowicz

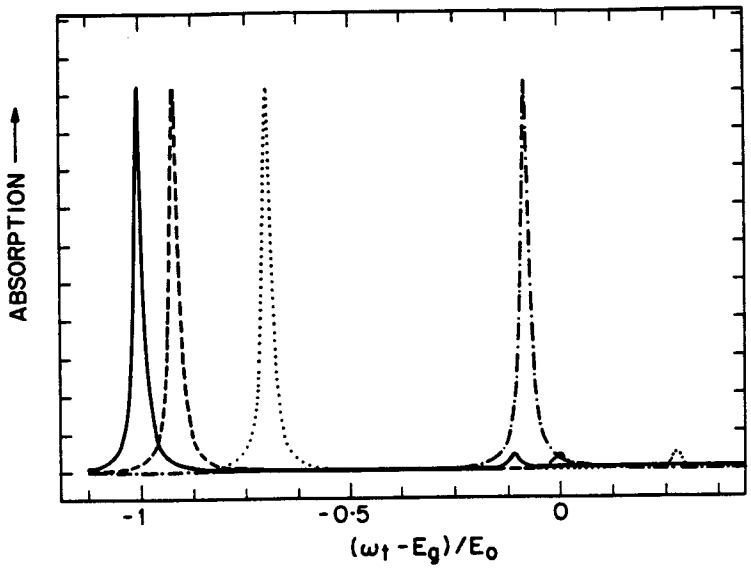

Figure 42. Excitonic test beam absorption spectra in 2D in the presence of a non-resonant pump beam with frequency $\omega_p = E_g - 2{\cdot}5E_0$. The full line shows the unperturbed absorption. (After Ell *et al.* (1989).)

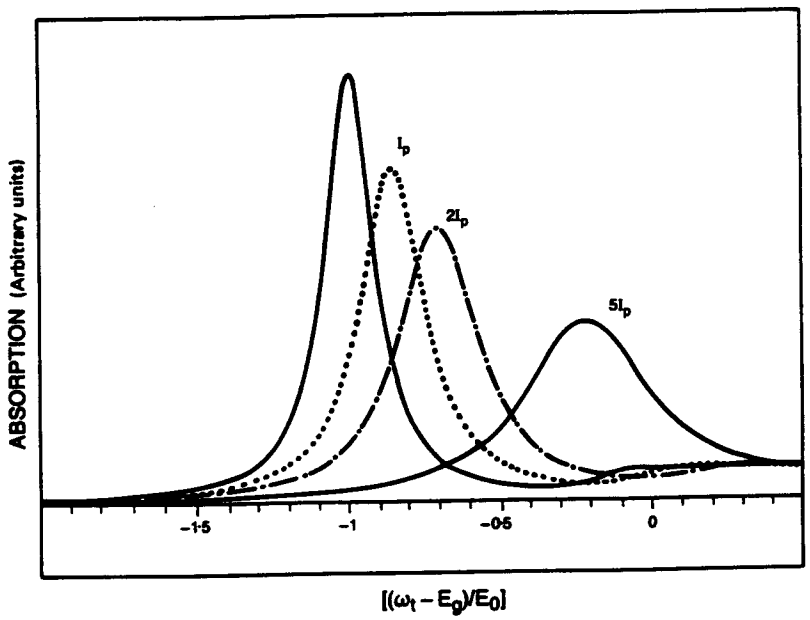

Figure 43. Excitonic test beam absorption spectra in 2D, including the effects of the finite pulse duration; $I_p = 0{\cdot}1\,\mathrm{GW\,cm^{-2}}$. (After Schaefer (1988).)

et al. 1986, Joffre *et al.* 1987). As shown by Schaefer (1988) and Balslev and Stahl (1988), this 'bleaching' is actually an 'inhomogeneous' broadening and can be traced back to the finite pulse duration. Figure 43 shows some of Schaefer's results, based on the numerical integration of the HF equations for a non-monochromatic pump beam. Clearly, these spectra reproduce the general features seen experimentally (e.g. figure 36).

Finally, it is worth noting that in none of the experiments discussed above was a pronounced dependence on polarization of the a.c. Stark effect observed. For excitons, according to the selection rules, for example for $\chi^{(3)}$, one would expect an effect for parallel polarizations of pump and probe beam only, as discussed by Froehlich *et al.* (1987). The latter authors suggested a *fast orientational relaxation* (of the real e–h pairs created by the test beam), which is not unrealistic (Schultheis *et al.* 1986a,b). The corresponding orientational dephasing time is expected to be of the order of the inverse homogeneous exciton linewidth, T_2. As discussed previously, in III–V QWs and at the centre of the $n_z = 1$ heavy-hole exciton peak exciton–phonon scattering alone yields already a T_2 of the order of one or several picoseconds, depending on the temperature. There is essentially no dephasing of the virtual e–h pairs created by the pump beam and, when the test beam is also tuned below the absorption edge, the symmetries of the $\chi^{(n)}$ should be restored, because the dephasing times increase exponentially according to Urbach's rule. For band-to-band transitions, no dramatic polarization dependence of the a.c. Stark effect is expected. This can be easily seen from the discussion of optical orientation (Miller and Kleinman 1985, Joffre *et al.* 1989).

3.3. *Effects of electric fields*

Thus far we have separately discussed the changes in optical properties induced by an electric field and the changes induced by carrier populations. In this section we will discuss some of the (nonlinear) optical consequences of creating carriers, either real or virtual, in the presence of a field.

The simplest effect is what can be called the 'self-electro-optic effect' (Miller *et al.* 1984b, 1985b, Miller 1985) (giving self-electro-optic effect devices (SEEDs)). The general principle here is that carriers created optically will change the field across the quantum wells, hence changing their optical properties through the QCSE. In a general sense, this is a nonlinear optical effect, because it is a change in optical properties caused by a light beam. We could implement this principle in many ways. We could create carriers in some separate photodiode or transistor to change a voltage across the quantum wells through some circuit; such devices are nonlinear optical devices in the general sense and are certainly SEEDs (Miller 1985c). One might debate whether such devices are optically nonlinear in some strict sense because electrical power is involved; it is worth noting that such devices can be made without any electrical power supply, deriving all their power from the incident light (Weiner *et al.* 1987b), in which case it is difficult not to class them as nonlinear optical devices. Such nonlinearities are certainly non-local (because a light beam at one place can influence the optical properties at another), and for this reason cannot strictly be described by the usual local nonlinear susceptibility formalism. They are similar to those involved in photorefractive materials where displacement of charges toward traps generates large electrical fields which in turn modify the optical properties through the normal electro-optic effect. Furthermore, the SEED nonlinearities belong to that class of nonlinearities in which the optical properties are dependent on the internal state of the material, not simply on the incident field, although the incident optical field can change the internal state. In the present case, the 'internal state' can be characterized by the voltage or field over the quantum wells, a 'state' that can certainly be changed by the incident light creating carriers. This is not merely a semantic distinction; this kind of nonlinearity can be intrinsically bistable in the incident light power (Miller 1984). Any response of the system that is multiple-valued

in the optical field obviously cannot be expanded in a power series in that field (power series are single-valued), and hence we cannot use normal nonlinear susceptibilities, which are power series coefficients. Another simple example of the same class of nonlinearity is thermal nonlinearities, in which changes in temperature change the optical properties (Miller 1984). The self-electro-optic effect can, however, be a very large and relatively fast nonlinearity; in terms of the energy required to induce a significant change in optical properties, it is actually one of the largest known optical nonlinearities, being larger by this measure even than the exciton bleaching effects in quantum wells discussed above, as we will explain below.

The simplest self-electro-optic effect implementation, and the only one we will consider explicitly here, is when the carriers are created in the biased quantum wells themselves, so as to screen the applied field because the electrons and holes are biased towards opposite sides of the wells. If they remain in the wells, there will be some reduction of the field in the wells and a resulting change in the absorption that can be calculated self-consistently (Brum *et al.* 1986). A rough estimate of the size of this effect can be obtained by considering the extreme case when the electron and hole populations are completely separated in the well by the field, giving two opposite sheets of charge within the wells. The resulting screening field F_S can be calculated as for a plane-parallel capacitor, giving $F_S = Ne/\epsilon$ where N is the areal carrier pair density. (Note, of course, that the field is independent of separation for a plane-parallel capacitor with a given charge density.) For $N \sim 3 \times 10^{11}\,\mathrm{cm}^{-2}$, $F_S \sim 4 \times 10^4\,\mathrm{V\,cm}^{-1}$. For a biased 100 Å quantum well, this will produce a fairly large change in absorption, but so also will the exciton saturation at this same density, and the order of magnitude of the change in absorption from both effects will be similar. To calculate this particular effect properly would therefore require a many-body calculation as discussed above, but with self-consistent solution for electric field changes also. A much larger optical nonlinearity can be obtained if we allow the carriers to transport out of the wells, say to the electrodes; in practice at room temperature this happens very efficiently (Miller *et al.* 1984 b). Now all the charge from all the wells is accumulated in one pair of sheets of charge, and consequently the resulting change in field is much larger. For example, to make the same field change of $4 \times 10^4\,\mathrm{V\,cm}^{-1}$ still requires a total areal density of $\sim 3 \times 10^{11}\,\mathrm{cm}^{-2}$. If, however, this charge comes from, say, 40 quantum wells, as might be typical for the $\sim 1\,\mu\mathrm{m}$ depletion region of a quantum well diode, we now only need to create $\sim 3 \times 10^{11}/40 \simeq 10^9\,\mathrm{cm}^{-2}$ in each layer initially. This gives us a much more efficient optical nonlinearity in terms of change in optical properties for a given absorbed optical energy. The absorbed optical energy, E_A, required per unit area is $E_A = (\omega/e)\epsilon F_S$, giving $E_A \sim 70\,\mathrm{nJ\,cm}^{-2} = 700\,\mathrm{aJ\,\mu m}^{-2}$ for our example parameters. To provide a similar change in optical absorption by exciton bleaching for a similar 1 μm of quantum wells would require absorbed optical energies per unit area approximately two orders of magnitude larger.

By incorporating such quantum well diodes in external circuits, we can control how fast the charge is removed from the electrodes and hence the operating speed and power of the nonlinearity (Miller *et al.* 1984b, 1985b), although the energy of operation can remain constant over many orders of magnitude. A variety of functions have been demonstrated (Miller 1987), including optical bistability. The bistability can be seen with only a series resistor and a voltage supply connected to a quantum well diode. Ultimate speeds of such devices will probably be limited by the transport time of the carriers out of the wells to the electrodes, perhaps to $\sim 100\,\mathrm{ps}$ timescales, although the dynamics of such processes is not currently fully understood.

Nonlinear optical effects with below-gap excitation in biased QWs present some specific aspects due both to the charge separation induced by the static electric field and the virtual nature of the photoexcited populations. Generation of ultrafast electrical transients (Chemla *et al.* 1987c) and enhanced cubic nonlinear effects for excitation close to the gap (Yamanishi 1987, Hiroshima *et al.* 1988, Shimizu 1988b) or close to mid-gap (Shimizu 1988b) have been predicted theoretically. By breaking the symmetry, the biasing field can also induce a quadratic response, such as second harmonic generation (Tsang *et al.* 1987, Shimizu 1988a). This effect is formally similar to the d.c. field induced second-harmonic generation used extensively to measure the nonlinearities of molecules in solution. Let us note that in heterostructures the symmetry breaking can also be introduced during the growth, for example by grading the composition of some alloy or using coupled asymmetric QWs (Khurgin 1987). So far, no experimental observation of these effects has been reported, most likely because of the complex structures of the samples required to observe them. They present nevertheless some novel and interesting features; in the following we will give a brief overview of the origin of these nonlinearities.

The most novel of these nonlinear effects is the production of ultrafast electrical transients, in that it is a completely different kind of nonlinear optical effect from the others discussed so far (Chemla *et al.* 1987). As shown in section 3.2, below-gap excitation generates virtual exciton populations in the QWs that last essentially only as long as the laser field is applied. Nevertheless the virtual excitons are polarized by the biasing electrostatic field. Their wavefunctions are approximately given by equation (2.2.5) with, according to equation (2.2.8), electron and hole distributions displaced towards opposite sides of the QW. Thus, during their transient presence in the QW, the virtual excitons generate a macroscopic polarization P_0, proportional to the e–h charge separation and density,

$$P_0 = -e \sum_{n_z} N_{n_z} \left[\int z_e |\psi^e_{n_z}(z_e)|^2 \, dz_e - \int z_h |\psi^h_{n_z}(z_h)|^2 \, dz_h \right], \tag{3.3.1}$$

where N_{n_z} is the virtual-pair density in the n_zth subband as given by equation (3.2.11). In the case of infinite barriers and if the e–h Coulomb attraction is neglected, it is possible to carry out the summation over the subbands exactly (Chemla *et al.* 1987, Yamanishi 1987). It is found that P_0 induces an electrostatic field $\delta F/F = -\delta\epsilon_0/\epsilon_0$, with

$$\frac{\delta\epsilon_0}{\epsilon_0} = \frac{|er_{vc}E_p|^2}{(2R)^2} \left(\frac{R}{W}\right)^{5/2} u(\Delta, \sigma) \tag{3.3.2}$$

where $W = \pi^2/(2mL_z^2) = E_1^e + E_1^h$ measures the confinement energy of the e–h pair and $u(\Delta, \sigma)$ is a universal function of the normalized pump detuning, $\Delta = (E_g + W - \omega_p)/W$, and the electron/hole mass ratio, $\sigma = m_e/m_h$. The plot of the function $u(\Delta, \sigma)$ is given in figure 44, showing two different regimes. For small detunings, $\Delta \ll 1$, the most resonant $n_z = 1$ ground state is dominant giving the intuitive result that the change of dielectric constant is proportional to the pair density in the $n_z = 1$ subband, N_1, and to the sum of the corresponding electron and hole polarizabilities,

$$\delta\epsilon_0 \sim 4\pi N_1(\alpha_{e1} + \alpha_{h1}), \tag{3.3.3}$$

where the polarizabilities α_{j1} (j = e, h) are given by

$$\alpha_{j1} = 2e^2 \sum_{n_z} \frac{[\langle n_z|z|1\rangle]^2}{(E^j_{n_z} - E^j_1)}. \tag{3.3.4}$$

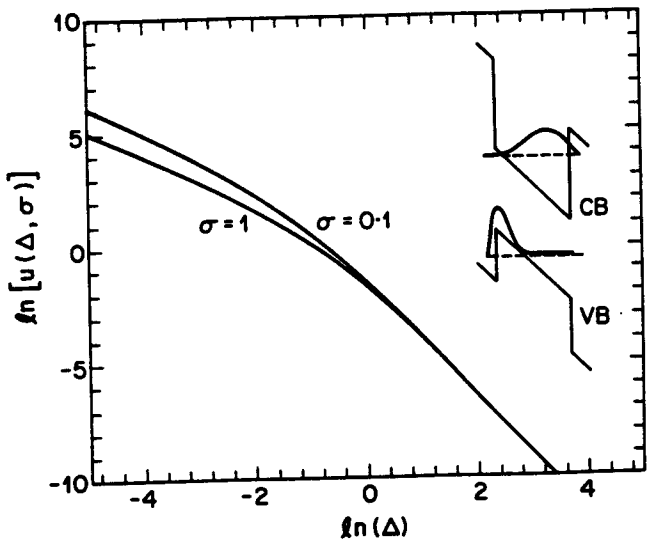

Figure 44. A plot of the universal function $u(\Delta, \sigma)$, which determines the change of dielectric constant, against the log of the normalized pump detuning, Δ. Two curves are shown for electron–hole mass ratio $\sigma = m_e/m_h = 0{\cdot}1$ and 1. The inset shows the $n_z = 1$ electron and hole wavefunctions in the direction normal to the layer for a biased quantum well. (After Chemla *et al.* (1987).)

In the other limit of large detuning ($\Delta \gg 1$), $\delta\epsilon_0/\epsilon_0$ becomes independent of the well thickness and tends toward the bulk value. It is interesting to note that the relative change in the applied field, $\delta F/F$, becomes larger as the QW thickness increases because of the larger charge separation. On the other hand, the magnitude of the field that can be applied before the excitons are field-ionized decreases very quickly with L_z, hence reducing the usefulness of the effect. Optimum QW thicknesses probably correspond to those showing well defined QCSE, $L_z \sim 100$ Å. We note that the effect also works for bias fields applied in the QW plane, with a magnitude close to the bulk value, except for very small detunings.

In first order in the virtual population density, this effect can also be viewed as a field-induced rectification (Bloembergen 1965). Using the language of nonlinear optics, it is possible to consider that the QCSE and QCFK discussed in section 2.2 arise from the imaginary part of the third-order susceptibility $\chi^{(3)}(-\omega,\omega,0,0)$ such that

$$P = \chi^{(3)}(-\omega, \omega, 0, 0)F^2E. \tag{3.3.5}$$

We can expect that corresponding to the real part of $\chi^{(3)}(-\omega,\omega,0,0)$ there is also a quadratic electrorefraction, namely a change of refractive index in the transparency region of the QW, proportional to the square of the applied field, F, as was discussed above in section 2.2.

By virtue of the general permutation symmetries of nonlinear optical susceptibilities (Bloembergen 1965) this implies that there must be another susceptibility $\chi^{(3)}(0, 0, -\omega, \omega)$ exactly equal to $\chi^{(3)}(-\omega,\omega,0,0)$ which describes the generation of a static polarization proportional to the biasing field and the intensity of the pump laser,

$$P_0 = \chi^{(3)}(0, 0, -\omega_p, \omega_p)FE_pE_p^*. \tag{3.3.6}$$

This, of course, is nothing more than the polarization, P_0, calculated from consideration of the microscopic processes in equation (3.3.1). The expression in equation (3.3.6) can be exploited to obtain from the experimental QCSE an estimate of the transient static field, δF, including excitonic corrections that are not contained in equation (3.3.1). For example, it is found that for a $10\,\mathrm{GW\,cm^{-2}}$ excitation (corresponding to 100 pJ, 100 fs optical pulses focussed to a $10\,\mu\mathrm{m}^2$ area), 42 meV below the gap of GaAs QWs and a $F \sim 10^5\,\mathrm{V\,cm^{-1}}$ applied field, a $\delta F \sim 2 \times 10^4\,\mathrm{V\,cm^{-1}}$, 100 fs transient pulse would be produced. The signature of such an effect would be to demonstrate the propagation of the transient pulse by observing its effects outside the region of the QW where it is produced, but at the time of writing this has not yet been achieved.

4. Conclusions

Despite the length of this article, and the many references contained therein to an impressive body of work, it represents only the start of the field of study of optics in semiconductor microstructures. At the time of writing, only work in GaAs quantum wells is in any sense mature. Consequently, this review covers primarily III–V semiconductors, with emphasis on quantum well structures, and deals primarily with direct gap type I systems. Work in other materials systems and in structures confined in more dimensions is much less advanced, and will doubtless be the subject of much future research.

The basic linear optical properties of these structures are now relatively well understood for undoped systems both with and without electric fields. Although good experimental data on the optical properties of doped quantum well structures are now available, the theory is still in a primitive state at least for quantitative predictions; some features are qualitatively understood.

As for the nonlinear optical effects, there is a large body of work especially on real populations close to the fundamental gap. The theory accounts rather well for the experiments in the low and medium density regime. At high density, for multiple subband occupation, much theoretical work remains to be done. The effects of virtual populations have just started to be investigated experimentally as well as theoretically. At this time, theory and experiments are in qualitative agreement in the regimes that have been explored. The nonlinear effects in the presence of electrical fields are understood in the quasi-steady state regime, although the dynamic behaviour is only now being explored. As for virtual transitions with electric fields, the many interesting proposals remain mere theoretical speculations at this time.

An obvious extension of these investigations would be toward lower dimensional structures such as quantum wires and boxes. Some phenomena have been theoretically explored, but much remains to be done experimentally because of the extreme difficulty in the fabrication of these structures.

Acknowledgements

We would like to take this opportunity to acknowledge the collaboration, stimulus and advice of many colleagues in our own work in the area of quantum wells. The list is so long that any attempt at a complete list here will only offend because of some accidental omission. Without all of these many people, both at AT&T Bell Laboratories and elsewhere, all of this work would have been impossible.

References

ABRAM, I., 1985, *J. phys. Soc. Am.* B, **2**, 1204.

AHN, D., and CHUANG, S. L., 1986a, *Phys. Rev.* B, **34**, 9084; 1986b, *Appl. Phys. Lett.*, **49**, 1450; 1987a, *Ibid.*, **35**, 4149; 1987b, *IEEE J. quant. Electron.*, **23**, 2196.

ALEKSANDROV, A. S., and ELESIN, V. F., 1971, *Soviet Phys. Semicond.*, **5**, 542.

ALIBERT, C., GAILLARD, S., BRUM, J. A., BASTARD, G., FRIJLINK, P., and ERMAN, M., 1985, *Solid St. Commun.*, **53**, 457.

ANDERSEN, D. R., KOLODZIEJSKI, L. A., GUNSHOR, R. L., DATTA, S., KAPLAN, A. E., and NURMIKKO, A. V., 1986, *Appl. Phys. Lett.*, **48**, 1559.

ANDERSON, P. W., 1958, *Phys. Rev.*, **112**, 1900; 1967, *Phys. Rev. Lett.*, **18**, 1049.

ANDO, T., FOWLER, A. B., and STERN, F., 1982, *Rev. mod. Phys.*, **54**, 437.

ANDO, T., and MORI, S., 1979, *J. phys. Soc. Japan*, **47**, 1518.

ANDRYUSHYN, E. A., and SILIN, A. P., 1976a, *Soviet Phys. Solid St.*, **18**, 1243; 1976b, *Solid St. Commun.*, **20**, 453;: 1979, *Soviet Phys. Solid St.*, **21**, 129.

AUSTIN, E. J., and JAROS, M., 1985a, *Appl. Phys. Lett.*, **47**, 274; 1985b, *Phys. Rev.* B, **31**, 5569; 1986, *J. Phys.* C, **19**, 533; 1987, *J. appl. Phys.*, **62**, 558.

BAJEMA, K., MERLIN, R., JUANG, F., HONG, S., SINGH, J., and BHATTACHARYA, P. K., 1987, *Phys. Rev.* B, **36**, 1300.

BALSLEV, I., and STAHL, A., 1988, *Solid St. Commun.*, **67**, 85.

BANYAI, L., GALBRAITH, I., ELL, C., and HAUG, H., 1987, *Phys. Rev.* B, **36**, 6099.

BAR-JOSEPH, I., KLINGSHIRN, C., MILLER, D. A. B., CHEMLA, D. S., KOREN, U., and MILLER, B. I., 1987a, *Appl. Phys. Lett.*, **59**, 1010.

BAR-JOSEPH, I., KUO, J. M., KLINGSHIRN, C., LIVESCU, G., CHANG, T. Y., MILLER, D. A. B., and CHEMLA, D. S., 1987b, *Phys. Rev. Lett.*, **59**, 1357.

BARDEEN, J., COOPER, L. N., and SCHRIEFFER, J. R., 1957, *Phys. Rev.*, **108**, 1175.

BASTARD, G., 1984, *Phys. Rev.* B, **30**, 3547; 1985, *J. Lumin.*, **30**, 488.

BASTARD, G., and BRUM, J. A., 1986, *IEEE J. Quant. Electron.*, **22**, 1625.

BASTARD, G., MENDEZ, E. E., CHANG, L. L., and ESAKI, L., 1982, *Phys. Rev.* B, **26**, 1974; 1983, *Ibid.*, **28**, 3241.

BAUER, G. E. W., and ANDO, T., 1985, *Phys. Rev.* B, **31**, 8321; 1986a, *J. Phys.* C, **19**, 1537; 1986b, *Phys. Rev.* B, **34**, 1300; 1987, *Proceedings of the 18th International Conference on the Physics of Semiconductors*, edited by O. Engström (Singapore: World Scientific), p. 537.

BAUER, R., BIMBERG, D., CHRISTEN, J., OERTEL, D., MARS, D., MILLER, J. N., FUKUNAGA, T., and NAKASHIMA, H., 1987, *Proceedings of the 18th International Conference on the Physics of Semiconductors*, edited by O. Engström (Singapore: World Scientific), p. 525.

BEHN, U., and GOBSCH, G., 1987, *Solid St. Commun.*, **64**, 1451.

BELIAEV, S. T., 1958a, *Soviet Phys. JETP*, **7**, 289; 1958b, *Ibid.*, **7**, 299.

BETBEDER-MATIBET, O., and NOZIÈRES, P., 1969, *Ann. Phys.*, **51**, 392.

BLEUSE, J., BASTARD, G., and VOISIN, P., 1988, *Phys. Rev. Lett.*, **60**, 220.

BLOEMBERGEN, N., 1965, *Nonlinear Optics* (New York: Benjamin).

BLOSSEY, D. F., 1970, *Phys. Rev.* B, **2**, 3976; 1971, *Phys. Rev.* B, **3**, 1382.

BOBRYSHEVA, A. I., BERYL, S. I., MOSKALENKO, S. A., and POKATYLOV, E. P., 1980b, *Phys. Stat. sol.* (b), **100**, 281.

BOBRYSHEVA, A. I., ZYUKOV, V. T., and BERYL, S. I., 1980a, *Phys. Stat. sol.* (b), **101**, 69.

BOBRYSHEVA, A. I., and MOSKALENKO, S. A., 1983, *Soviet Phys. Solid St.*, **25**, 1891.

BOGOLUBOV, N. N., 1947, *J. Phys. USSR*, **11**, 23.

BOGOLUBOV, N. N., TOLMACHEV, V. V., and SHIRKOV, D. V., 1958, *A New Method in the Theory of Superconductivity* (Moscow: Academy of Sciences of the U.S.S.R.).

BORONDO, F., and SANCHEZ-DEHESA, J., 1986, *Phys. Rev.* B, **33**, 8758.

BOTTCHER, C. J. F., 1973, *Theory of Electric Polarization* (Amsterdam: Elsevier).

BROIDO, D. A., KOTELES, E. S., JAGANNATH, C., and CHI, J. Y., 1988, *Phys. Rev.* B, **37**, 2725.

BROIDO, D. A., and SHAM, L. J., 1985, *Phys. Rev.* B, **31**, 888; 1986, *Ibid.*, **34**, 3917.

BRUM, J. A., and BASTARD, G., 1985, *Phys. Rev.* B, **31**, 3893.

BRUM, J. A., BASTARD, G., and GUILLEMONT, C., 1984, *Phys. Rev.* B, **30**, 905.

BRUM, J. A., VOISIN, P. and BASTARD, G., 1986, *Phys. Rev.* B, **33**, 1063.

BRUS, L. E., 1986, *IEEE J. quant. Electron.*, **22**, 1909.

BURSTEIN, E., 1954, *Phys. Rev.*, **93**, 632.
BRYANT, G. W., 1987, *Phys. Rev. Lett.*, **59**, 1140; 1988, *Phys. Rev.*, **37**, 8763.
CEPERLEY, D., 1978, *Phys. Rev.* B, **18**, 3126.
CHAKRABORTY, T., and CAMPBELL, C., 1984, *Phys. Rev.* B, **29**, 6640.
CHANG, Y. C., and SANDERS, G. D., 1985, *Phys. Rev.* B, **32**, 5521.
CHANG, Y. C., and SCHULMAN, J. N., 1983, *Appl. Phys. Lett.*, **43**, 536.
CHEMLA, D. S., 1980, *Rep. Prog. Phys.*, **43**, 1191; 1985, *J. opt. Soc. Am.* B, **2**, 1133.
CHEMLA, D. S., BAR-JOSEPH, I., KLINGSHIRN, C., MILLER, D. A. B., KUO, J. M., and CHANG, T. Y., 1987a, *Appl. Phys. Lett.*, **50**, 585.
CHEMLA, D. S., BAR-JOSEPH, I., KUO, J. M., CHANG, T. Y., KLINGSHIRN, C., LIVESCU, G., and MILLER, D. A. B., 1988a, *IEEE J. quant. Electron.*, **24**, 1664.
CHEMLA, D. S., and MARUANI, A., 1982, *Prog. quant. Electron.*, **8**, 1.
CHEMLA, D. S., and MILLER, D. A. B., 1985, *J. Opt. Soc. Am.* B, **2**, 1155.
CHEMLA, D. S., MILLER, D. A. B., and SCHMITT-RINK, S., 1987b, *Phys. Rev. Lett.*, **59**, 1018.
CHEMLA, D. S., MILLER, D. A. B., SMITH, P. W., GOSSARD, A. C., and WIEGMANN, W., 1984, *IEEE J. quant. Electron.*, **20**, 265.
CHEMLA, D. S., SCHMITT-RINK, S., and MILLER, D. A. B., 1988b, *Optical Nonlinearities and Instabilities in Semiconductors*, edited by H. Haug (New York: Academic), p. 83.
CHEN, Y. J., KOTELES, E. S., ELMAN, B. S., and ARMIENTO, C. A., 1987, *Phys. Rev.* B, **36**, 4562.
COLLINS, R. T., KLITZING, K., and PLOOG, K., 1986a, *Phys. Rev.* B, **33**, 4378; 1986b, *Appl. Phys. Lett.*, **49**, 406.
COLLINS, R. T., VINA, L., WANG, W. I., MAILHIOT, C., and SMITH, D. L., 1987, *Proc. SPIE*, **792**, 2.
COMBESCOT, M., and NOZIÈRES, P., 1971, *J. Phys.*, Paris, **32**, 913.
COMTE, C., and MAHLER, G., 1986, *Phys. Rev.* B, **34**, 7164.
COMTE, C., and NOZIÈRES, P., 1982, *J. Phys.*, Paris, **43**, 1069.
COTE, R., and GRIFFIN, A., 1988, *Phys. Rev.* B, **37**, 4539.
DAHL, D. A., 1988, *Phys. Rev.* B, **37**, 6882.
DANAN, G., LADAN, F. R., MOLLOT, F., and PLANEL, R., 1987, *Appl. Phys. Lett.*, **51**, 1605.
DELALANDE, C., 1987, *Physica Scripta* T, **19**, 129.
DELALANDE, C., BASTARD, G., ORGONASI, J., BRUM, J. A., LIU, H. W., VOOS, M., WEIMANN G., and SCHLAPP, W., 1987, *Phys. Rev. Lett.*, **59**, 2690.
DELALANDE, C., ORGONASI, J., MEYNARDIER, M. H., BRUM, J. A., and BASTARD, G., 1986, *Solid St. Commun.*, **59**, 613.
DIMMOCK, J. O., 1967, *Semiconductors and Semimetals*, Vol. 3, edited by R. K. Willardson and A. C. Beer (New York: Academic), p. 259.
DINGLE, R., STOERMER, H. L., GOSSARD, A. C., and WIEGMANN, W., 1978, *Appl. Phys. Lett.*, **33**, 665.
DINGLE, R., WIEGMANN, W., and HENRY, C. H., 1974, *Phys. Rev. Lett.*, **33**, 827.
DOERRE, P., HAUG, H., and TRAN THOAI, D. B., 1979, *J. low. temp. Phys.*, **35**, 465.
DOW, J. D., and REDFIELD, D., 1970, *Phys. Rev.* B, **1**, 3358.
DRESSELHAUS, G., KIP, A. F., and KITTEL, C., 1955, *Phys. Rev.*, **98**, 368.
EKENBERG, U., and ALTARELLI, M., 1984, *Phys. Rev.* B, **30**, 3569.
ELESIN, V. F., 1971, *Soviet Phys. JETP*, **32**, 328.
ELL, C., MÜLLER, J. F., EL SAYED, K., and HAUG, H., 1989, *Phys. Rev. Lett.*, **62**, 304.
ELLIOTT, R. J., 1957, *Phys. Rev.*, **108**, 1384.
EVANS, W. A. B., and IMRY, Y., 1969, *Nuovo Cim.* B, **63**, 155.
FADEEV, L. D., 1965, *Mathematical Aspects of the Three-Body Problem in Quantum Scattering Theory* (New York: Davey).
FEHRENBACH, G. W., SCHAEFER, W., TREUSCH, J., and ULBRICH, R. G., 1982, *Phys. Rev. Lett.*, **49**, 1281.
FEHRENBACH, G. W., SCHAEFER, W., and ULBRICH, R. G., 1985, *J. Lumin.*, **30**, 154.
FENEUILLE, S., 1977, *Rep. Prog. Phys.*, **40**, 1257.
FENG, Y.-P., and SPECTOR, H. N., 1987, *J. Phys. Chem. Solids*, **48**, 593.
FETTER, A. L., 1973, *Ann. Phys.* N.Y., **81**, 367; 1974, *Ibid.*, **88**, 1.
FLUEGEL, B., PEYGHAMBARIAN, N., OLBRIGHT, G., LINDBERG, M., KOCH, S. W., JOFFRE, M., HULIN, D., MIGUS, A., and ANTONETTI, A., 1987, *Phys. Rev. Lett.*, **59**, 2588.
FORK, R. L., GREENE, B. I., and SHANK, C. V., 1981, *Appl. Phys. Lett.*, **38**, 671.

FRANZ, W., 1958, *Z. Naturf* (a), **13**, 484.
FRIEDEL, J., 1952, *Phil. Mag.*, **43**, 153.
FROEHLICH, D., NOETHE, A., and REIMANN, K., 1985, *Phys. Rev. Lett.*, **55**, 1335.
FROEHLICH, D., WILLE, R., SCHLAPP, W., and WEIMANN, G., 1987, *Phys. Rev. Lett.*, **59**, 1748.
FU, Q., LEE, D., MYSYROWICZ, A., NURMIKKO, A. V., GUNSHOR, R. L., and KOLODZIEJSKI, L. A., 1988, *Phys. Rev.* B, **37**, 8791.
FU, Q., NURMIKKO, A. V., KOLODZIEJSKI, L. A., GUNSHOR, R. L., and WU, J., 1987, *Appl. Phys. Lett.*, **51**, 578.
FUMI, F. G., 1955, *Phil. Mag.*, **46**, 1007.
GALITSKII, V. M., GORESLAVSKII, S. P., and ELESIN, V. F., 1970, *Soviet Phys. JETP*, **30**, 117.
GAVORET, J., NOZIÈRES, P., ROULET, B., and COMBESCOT, M., 1969, *J. Phys., Paris*, **30**, 987.
GAY, J. G., 1971, *Phys. Rev.* B, **4**, 2567; 1972, *Ibid.*, **6**, 4884.
GIBBS, H. M., 1985, *Optical Bistability: Controlling Light with Light* (New York: Academic).
GIBBS, H. M., GOSSARD, A. C., MCCALL, S. L., PASSNER, A., WIEGMANN, W., and VENKATESAN, T. N. C., 1979, *Solid St. Commun.*, **30**, 271.
GLICK, M., PAVUNA, D., and REINHART, F. K., 1987, *Electron Lett.*, **23**, 1235.
GLICK, M., REINHART, F. K., and WEIMANN, G., 1985, *Helv. Phys. Acta*, **58**, 403.
GLICK, M., REINHART, F. K., WEIMANN, G., and SCHLAPP, W., 1986, *Herbsttagung Schweiz. phys. Gesellschaft*, **59**, 137.
GLOECKLE, W., 1983, *The Quantum Mechanical Few-Body Problem* (New York: Springer).
GOSSARD, A. C., and PINCZUK, A., 1985, *Synthetic Modulated Structures*, edited by L. L. Chang and B. C. Giessen (New York: Academic), p. 215.
GREENE, R. L., BAJAJ, K. K., 1983, *Solid St. Commun.*, **45**, 831.
GREENE, R. L., BAJAJ, K. K., and PHELPS, D. E., 1984, *Phys. Rev.* B, **29**, 1807.
GREENE, B. I., MÜLLER, J. F., ORENSTEIN, J., RAPKINE, D. H., SCHMITT-RINK, S., and THAKUR, M., 1988, *Phys. Rev. Lett.*, **61**, 325.
GREENE, B. I., ORENSTEIN, J., MILLARD, R. R., and WILLIAMS, L. R., 1987, *Phys. Rev. Lett.*, **58**, 2750.
GROSS, E. P., 1961, *Nuovo Cim.*, **20**, 454.
GUY, D. R. P., APSLEY, N., TAYLOR, L. L., BASS, S. J., and KLIPSTEIN, P. C., 1987, *Proc. SPIE*, **792**, 189.
HAINES, L. K., and ROBERTS, D. H., 1969, *Am. J. Phys.*, **37**, 1145.
HANAMURA, E., 1973, *Solid St. Commun.*, **12**, 951.
HANAMURA, E., and HAUG, H., 1977, *Phys. Rep.*, **33**, 209.
HARBICH, TH., and MAHLER, G., 1981, *Phys. Stat. sol.* B, **104**, 185.
HARTMANN, M., ZIMMERMANN, R., and STOLZ, H., 1988, *Phys. Stat. sol.* B, **146**, 357.
HARWIT, A., and HARRIS, J. S., 1987, *Appl. Phys. Lett.*, **50**, 685.
HARWIT, A., HARRIS, J. S., and KAPITULNIK, A., 1986, *J. appl. Phys.*, **60**, 3211.
HAUG, H., 1976, *Z. Phys.* B, **24**, 351; 1985, *J. Lumin.*, **30**, 171; (editor), 1988, *Optical Nonlinearities and Instabilities in Semiconductors* (New York: Academic).
HAUG, H., MÜLLER, J. F., and MEWIS, R., 1987, *J. Lumin.*, **38**, 239.
HAUG, H., and SCHMITT-RINK, S., 1984, *Prog. quant. Electron.*, **9**, 3; 1985, *J. opt. Soc. Am.* B, **2**, 1135.
HAWRYLAK, P., 1987, *Phys. Rev. Lett.*, **59**, 485.
HAWRYLAK, P., and QUINN, J. J., 1986, *Phys. Rev.* B, **33**, 8264.
HEGARTY, J., and STURGE, M. D., 1985, *J. opt. Soc. Am.* B, **2**, 1143.
HENNEBERGER, F., 1986, *Phys. Stat. sol.* B, **137**, 371.
HIROSHIMA, T., 1987, *Appl. Phys. Lett.*, **50**, 968.
HIROSHIMA, T., HANAMURA, E., and YAMANISHI, M., 1988, *Phys. Rev.* B, **38**, 1241.
HIROSHIMA, T., and LANG, R., 1986, *Appl. Phys. Lett.*, **49**, 639.
HIROSHIMA, T., and NISHI, K., 1987, *J. appl. Phys.*, **62**, 3360.
HOHENBERG, P. C., 1967, *Phys. Rev.*, **158**, 383.
HOLONYAK, JR, N., 1985, *Soviet Phys. Semicond.*, **19**, 943.
HONG, S., JAFFE, M., and SINGH, J., 1987, *IEEE J. quant. Electron.*, **23**, 2181.
HONG, S., and SINGH, J., 1986, *Appl. Phys. Lett.*, **49**, 331; 1987, *J. appl. Phys.*, **62**, 1994.
HOPFIELD, J. J., 1958, *Phys. Rev.*, **112**, 1555; 1969, *Comments Solid St. Phys.*, **2**, 40.
HORIKOSHI, Y., FISCHER, A., and PLOOG, K., 1985, *Phys. Rev.* B, **31**, 7859.
HUANG, D., CHU, H. Y., CHANG, Y. C., HOUDRE, R., and MORKOÇ, H., 1988, *Phys. Rev.* B, **38**, 1246.

HULIN. D., MYSYROWICZ, A., ANTONETTI, A., MIGUS, A., MASSELINK, W. T., MORKOÇ, H., GIBBS, H. M., and PEYGHAMBARIAN, N., 1986a, *Phys. Rev.* B, **33**, 4389.
HULIN, D., MYSYROWICZ, A., ANTONETTI, A., MIGUS, A., MASSELINK, W. T., MORKOÇ, H., GIBBS, H. M., and PEYGHAMBARIAN, N., 1986b, *Appl. Phys. Lett.*, **49**, 749.
IKONIC, Z., MILANOVIC, V., and TJAPKIN, D., 1987a, *J. Phys.* C, **20**, 1147; 1987b, *Ibid.*, **20**, L425.
INOSHITA, T., OHNISHI, S., and OSHIYAMA, A., 1986, *Phys. Rev. Lett.*, **57**, 2560.
IORIATTI, JR, L. C., and ISIHARA, A., 1981, *Z. Phys.* B, **44**, 1.
ISLAM, M. N., HILLMAN, R. L., MILLER, D. A. B., CHEMLA, D. S., GOSSARD, A. C., and ENGLISH, J. H., 1987, *Appl. Phys. Lett.*, **50**, 1098.
IWAMURA, H., SAKU, T., and OKAMOTO, H., 1985, *Jap. J. appl. Phys.*, **24**, 104.
JOFFRE, M., HULIN, D., and ANTONETTI, A., 1987, *J. Phys., Paris*, C5–537.
JOFFRE, M., HULIN, D., MIGUS, A., and COMBESCOT, M., 1989, *Phys. Rev. Lett.*, **62**, 74.
JOGAI, B., and WANG, K. L., 1987, *Phys. Rev.* B, **35**, 653.
JONSON, M., 1976, *J. Phys.* C, **9**, 3055.
JUANG, F., SINGH, J., BHATTACHARYA, P. K., BAJEMA, K., and MERLIN, R., 1986, *Appl. Phys. Lett.*, **48**, 1246.
KADANOFF, L. P., and BAYM, G., 1962, *Quantum Statistical Mechanics* (New York: Benjamin).
KAJZAR, F., ROTHBERG, L., ETEMAD, S., CHOLLET, P. A., GREC, D., BOUDET, A., and JEDJU, T., 1988, *Optics Commun.*, **66**, 55.
KAN, Y., NAGAI, H., YAMANISHI, M., and SUEMUNE, I., 1987, *IEEE J. quant. Electron.*, **23**, 2167.
KAN, Y., YAMANISHI, M., SUEMUNE, I., YAMAMOTO, H., and YAO, T., 1985, *Jap. J. appl. Phys.*, **24**, L589.
KAN, Y., YAMANISHI, M., USAMI, Y., and SUEMUNE, I., 1986, *IEEE J. quant. Electron.*, **22**, 1837.
KASH, J. A., MENDEZ, E. E., and MORKOÇ, H., 1985, *Appl. Phys. Lett.*, **46**, 173.
KELDYSH, L. V., 1958, *Soviet Phys. JETP*, **34**, 788; 1965, *Ibid.*, **20**, 1018; 1979, *JETP Lett.*, **29**, 658.
KELDYSH, L. V., and KOPAEV, YU. V., 1965, *Soviet Phys. Solid St.*, **6**, 2219.
KELDYSH, L. V., and KOZLOV, A. N., 1968, *Soviet Phys. JETP*, **27**, 521.
KHURGIN, J., 1987, *Appl. Phys. Lett.*, **51**, 2100.
KLEINMAN, D. A., 1983, *Phys. Rev.* B, **28**, 871; 1985, *Ibid.*, **32**, 3766; 1986, *Ibid.*, **33**, 2540.
KLEINMAN, D. A., and MILLER, R. C., 1985, *Phys. Rev.* B, **32**, 2266.
KLIPSTEIN, P. C., and APSLEY, N., 1986, *J. Phys.* C, **19**, 6461.
KLIPSTEIN, P. C., TAPSTER, P. R., APSLEY, N., ANDERSON, D. A., SKOLNICK, M. S., KERR, T. M., and WOODBRIDGE, K., 1986, *J. Phys.* C, **19**, 857.
KLYUCHNICK, A. V., and LOZOVIK, YU. E., 1978, *Soviet Phys. Solid St.*, **20**, 364.
KNOX, R. S., 1963, *Solid State Physics*, Suppl. 5, edited by H. Ehrenreich, F. Seitz and D. Turnbull, (New York: Academic).
KNOX, W. H., DOWNER, M. C., FORK, R. L., and SHANK, C. V., 1984, *Optics Lett.*, **9**, 552.
KNOX, W. H., FORK, R. L., DOWNER, M. C., MILLER, D. A. B., CHEMLA, D. S., SHANK, C. V., GOSSARD, A. C, and WIEGMANN, W., 1985, *Phys. Rev. Lett.*, **54**, 1306.
KNOX, W. H., HIRLIMANN, C., MILLER, D. A. B., SHAH, J., CHEMLA, D. S., and SHANK, C. V., 1986a, *Phys. Rev. Lett.*, **56**, 1191.
KNOX, W. H., MILLER, D. A. B., DAMEN, T. C., CHEMLA, D. S., SHANK, C. V., and GOSSARD, A. C., 1986b, *Appl. Phys. Lett.*, **48**, 864.
KNOX, W. H., STARK, J. B., CHEMLA, D. S., MILLER, D. A. B., and SCHMITT-RINK, S., 1988, *Phys. Rev. Lett.*, **62**, 1189.
KOHN, W., and SHAM, L. J., 1965, *Phys. Rev.* A, **140**, 1133.
KOREN, U., KOCH, T. L., PRESTING, H., and MILLER, B. I., 1987, *Appl. Phys. Lett.*, **50**, 368.
KOSTERLITZ, J. M., and THOULESS, D. J., 1973, *J. Phys.* C, **6**, 1181.
KURAMOTO, Y., and KAMIMURA, H., 1974, *J. phys. Soc. Japan*, **37**, 716.
LARSSON, A., YARIV, A., TELL, R., MASERJIAN, J., and ENG, S. T., 1985, *Appl. Phys. Lett.*, **47**, 866.
LE, H. Q., ZAYHOWSKI, J. J., and GOODHUE, W. D., 1987, *Appl. Phys. Lett.*, **50**, 1518.
LEDERMAN, F. L., and DOW, J. D., 1976, *Phys. Rev.* B, **13**, 1633.
LEE, H. C., DZURKO, K. M., DAPKUS, P. D., and GARMIRE, E., 1987, *Appl. Phys. Lett.*, **51**, 1582.
LEE, J. S. IWASA, Y., and MIURA, N., 1987, *Semicond. Sci. Technol.*, **2**, 675.
LEE, Y. C., and LIN, D. L., 1979, *Phys. Rev.* B, **19**, 1982.
LEE, Y. H., CHAVEZ-PIRSON, A., KOCH, S. W., GIBBS, H. M., PARK, S. H., MORHANGE, J., JEFFERY, A., PEYGHAMBARIAN, N., BANYAI, L., GOSSARD, A. C., and WIEGMANN, W., 1986, *Phys. Rev. Lett.*, **57**, 2446.

LEVI, A. F. J., HAYES, J. R., GOSSARD, A. C., and ENGLISH, J. H., 1987, *Appl. Phys. Lett.*, **50**, 98.
LIAO, P. F., and BJORKHOLM, J. E., 1976, *Optics Commun.*, **16**, 392.
LIEBLER, J. G., SCHMITT-RINK, S., and HAUG, H., 1985, *J. Lumin.*, **34**, 1.
LITTLE, J. W., WHISNANT, J. K., LEAVITT, R. P., and WILSON, R. A., 1987, *Appl. Phys. Lett.*, **51**, 1786.
LIVESCU, G., MILLER, D. A. B., CHEMLA, D. S., RAMASWAMY, M., CHANG, T. Y., SAUER, N., GOSSARD, A. C., and ENGLISH, J. H., 1988, *IEEE J. quant. Electron.*, **24**, 1677.
LOEWENAU, J. P., SCHMITT-RINK, S., and HAUG, H., 1982, *Phys. Rev. Lett.*, **49**, 1511.
LOUDON, R., 1959, *Am. J. Phys.*, **27**, 649.
LUNDQVIST, B. I., 1967a, *Phys. Kondens. Mat.*, **6**, 193; 1967b, *Ibid.*, **6**, 206.
LUTTINGER, J. M., 1956, *Phys. Rev.*, **102**, 1030.
LUTTINGER, J. M., and KOHN, W., 1955, *Phys. Rev.*, **97**, 869.
MAHAN, G. D., 1967a, *Phys. Rev.*, **153**, 882; 1967b, *Ibid.*, **163**, 612.
MAILHIOT, C., and SMITH, D. L., 1986, *J. vac. Sci. Technol.* B, **4**, 996; 1987, *Phys. Rev.* B, **35**, 1242.
MANZKE, G., HENNEBERGER, K., and MAY, V., 1987, *Phys. Stat. sol.* B, **139**, 233.
MASUMOTO, Y., TARUCHA, S., and OKAMOTO, H., 1986, *J. phys. Soc. Japan*, **55**, 57.
MATSUURA, M., and KAMIZATO, T., 1986, *Phys. Rev.* B, **33**, 8385.
MAY, R. M., 1967, *Phys. Lett.* A, **24**, 282.
MCILROY, P. W. A., 1986, *J. appl. Phys.*, **59**, 3532.
MENDEZ, E. E., BASTARD, G., CHANG, L. L., ESAKI, L., MORKOÇ, H., and FISCHER, R., 1982, *Phys. Rev.* B, **26**, 7101.
MENDEZ, E. E., AGULLO-RUEDA, F., and HONG, J. M., 1988, *Phys. Rev. Lett.*, **60**, 2426.
MERKULOV, I. A., and PEREL, V. I., 1973, *Phys. Lett.* A, **45**, 83.
MERKULOV, I. A., 1974, *Soviet Phys. JETP*, **39**, 1140.
MEYNADIER, M. H., NAHORY, R. E., WORLOCK, J. M., TAMARGO, M. C., and DE MIGUEL, J. L., 1988, *Phys. Rev. Lett.*, **60**, 1338.
MEYNADIER, M. H., ORGONASI, J., DELALANDE, C., BRUM, J. A., BASTARD, G., and VOOS, M., 1986, *Phys. Rev.* B, **34**, 2482.
MILLER, A., MILLER, D. A. B., and SMITH, S. D., 1981a, *Adv. Phys.*, **30**, 697.
MILLER, D. A. B., 1984, *J. opt. Soc. Am.* B, **1**, 857; 1985, U.S. Patent 4,546,244; 1987, *Opt. Engng*, **26**, 72.
MILLER, D. A. B., CHEMLA, D. S., EILENBERGER, D. J., SMITH, P. W., GOSSARD, A. C., and WIEGMANN, W., 1983a, *Appl. Phys. Lett.*, **42**, 925.
MILLER, D. A. B., CHEMLA, D. S., DAMEN, T. C., GOSSARD, A. C., WIEGMANN, W., WOOD, T. H., and BURRUS, C. A., 1984a, *Phys. Rev. Lett.*, **53**, 2173.
MILLER, D. A. B., CHEMLA, D. S., DAMEN, T. C., GOSSARD, A. C., WIEGMANN, W., WOOD, T. H., and BURRUS, C. A., 1984b, *Appl. Phys. Lett.*, **45**, 13.
MILLER, D. A. B. CHEMLA, D. S., DAMEN, T. C., GOSSARD, A. C., WIEGMANN, W., WOOD, T. H., and BURRUS, C. A., 1985a, *Phys. Rev.* B, **32**, 1043.
MILLER, D. A. B., CHEMLA, D. S., DAMEN, T. C., WOOD, T. H., BURRUS, C. A., JR, GOSSARD, A. C., and WIEGMANN, W., 1985b, *IEEE J. quant. Electron.*, **21**, 1462.
MILLER, D. A. B., CHEMLA, D. S., EILENBERGER, D. J., SMITH, P. W., GOSSARD, A. C., and TSANG, W. T., 1982b, *Appl. Phys. Lett.*, **41**, 679.
MILLER, D. A. B., CHEMLA, D. S., and SCHMITT-RINK, S., 1986a, *Phys. Rev.* B, **33**, 6976.
MILLER, D. A. B., CHEMLA, D. S., and SCHMITT-RINK, S., 1988, *Appl. Phys. Lett.*, **52**, 2154.
MILLER, D. A. B., CHEMLA, D. S., SMITH, P. W., GOSSARD, A. C., and WIEGMANN, W., 1982a, *Appl. Phys.* B, **28**, 96.
MILLER, D. A. B., CHEMLA, D. S., SMITH, P. W., GOSSARD, A. C., and WIEGMANN, W., 1983b, *Optics Lett.*, **8**, 477.
MILLER, R. C., and GOSSARD, A. C., 1983, *Appl. Phys. Lett.*, **43**, 954.
MILLER, R. C., KLEINMAN, D. A., GOSSARD, A. C., and MUNTEANU, O., 1982c, *Phys. Rev.* B, **25**, 6545.
MILLER, R. C., KLEINMAN, D. A., TSANG, W. T., and GOSSARD, A. C., 1981b, *Phys. Rev.* B, **24**, 1134.
MILLER, R. C., and KLEINMAN, D. A., 1985, *J. Lumin.*, **30**, 520.
MILLER, D. A. B., WEINER, J. S., and CHEMLA, D. S., 1986b, *IEEE J. quant. Electron.*, **22**, 1816.

MIYAZAWA, T., TARUCHA, S., OHMORI, Y., SUZUKI, Y., and OKAMOTO, H., 1986, *Jap. J. appl. Phys.*, **25**, L200.
MOLLOW, B. R., 1969, *Phys. Rev.*, **188**, 1969; 1972, *Phys. Rev.* A, **5**, 2217.
MOSELEY, A. J., SCOTT, M. D., WILLIAMS, P. J., WALLIS, R. H., DAVIS, J. I., and RIFFAT, J. R., 1987, *Electron. Lett.*, **23**, 516.
MOTT, N. F., 1974, *Metal–Insulator Transitions* (London: Taylor & Francis).
MÜLLER, J. F., MEWIS, R., and HAUG, H., 1987, *Z. Phys.* B, **69**, 231.
MÜLLER, J. F., and HAUG, H., 1987, *J. Lumin.*, **37**, 97.
MYSYROWICZ, A., HULIN, D., ANTONETTI, A., MIGUS, A., MASSELINK, W. T., and MORKOÇ, H., 1986, *Phys. Rev. Lett.*, **56**, 2748.
NAGAI, H., KAN, Y., YAMANISHI, M., and SUEMUNE, I., 1986b, *Jap. J. appl. Phys.*, **25**, L640.
NAGAI, H., YAMANISHI, M., KAN, Y., and SUEMUNE, I., 1986a, *Electron. Lett.*, **22**, 888.
NAGANO, S., SINGWI, K. S., and OHNISHI, S., 1984, *Phys. Rev.* B, **29**, 1209.
NAGANUMA, M., ISHIBASHI, T., and HORIKOSHI, Y., 1987, *J. appl. Phys.*, **62**, 644.
NEWSON, D. J., and KUROBE, A., 1987, *Electron. Lett.*, **23**, 439.
NISHI, K., and HIROSHIMA, T., 1987, *Appl. Phys. Lett.*, **51**, 320.
NOJIMA, S., 1988, *Phys. Rev.* B, **37**, 9087.
NOJIMA, S., KAWAGUCHI, Y., NAKASHIMA, K., and WAKITA, K., 1987, *Jap. J. appl. Phys.*, **26**, 1927.
NOYES, H. P., 1965, *Phys. Rev. Lett.*, **15**, 538.
NOZIÈRES, P., GAVORET, J., and ROULET, B., 1969, *Phys. Rev.*, **178**, 1084.
NOZIÈRES, P., and COMTE, C., 1982, *J. Phys., Paris*, **43**, 1083.
NOZIÈRES, P., and SAINT-JAMES, D., 1982, *J. Phys., Paris*, **43**, 1133.
NOZIÈRES, P., and SCHMITT-RINK, S., 1985, *J. low. temp. Phys.*, **59**, 195.
NOZIÈRES, P., and DE DOMINICIS, C. T., 1969, *Phys. Rev.*, **178**, 1097.
OGURA, I., YAMANISHI, M., KAN, Y., and SUEMUNE, I., 1987, *Jap. J. appl. Phys.* **26**, L1313.
OUDAR, J. L., HULIN, D., MIGUS, A., ANTONETTI, A., and ALEXANDRE, F., 1985, *Phys. Rev. Lett.*, **55**, 2074.
OVERHAUSER, A. W., 1970, *Phys. Rev.* B, **3**, 1888.
PARK, S. H., MORHANGE, J., JEFFERY, A., MORGAN, R. A., CHAVEZ-PIRSON, A., GIBBS, H. M., KOCH, S. W., PEYGHAMBARIAN, N., DERSTINE, M., GOSSARD, A. C., ENGLISH, J. H., and WIEGMANN, W., 1988, *Appl. Phys. Lett.*, **52**, 1201.
PEYGHAMBARIAN, N., and GIBBS, H. M., 1985, *J. opt. Soc. Am.* B, **2**, 1215.
PEYGHAMBARIAN, N., GIBBS, H. M., JEWELL, J. L., ANTONETTI, A., MIGUS, A., HULIN, D., and MYSYROWICZ, A., 1984, *Phys. Rev. Lett.*, **53**, 2433.
PFITZNER, M., and WÖLFLE, P., 1987, *Phys. Rev.* B, **35**, 4699.
PINCZUK, A., SHAH, J., MILLER, R. C., GOSSARD, A. C., and WIEGMANN, W., 1984, *Solid St. Commun.*, **50**, 735.
PITAEVSKII, L. P., 1959, *Soviet Phys. JETP*, **9**, 830; 1961, *Ibid.*, **13**, 451.
PLOOG, K., and DOEHLER, G. H., 1983, *Adv. Phys.*, **32**, 285.
POLLAND, H., SCHULTHEIS, L., KUHL, J., GOBEL, E. O., and TU, C. W., 1985, *Phys. Rev. Lett.*, **55**, 2610.
POLUEKTOV, I. A., POPOV, YU. M., and ROITBERG, V. S., 1975, *Soviet Phys. Usp.*, **17**, 673.
RABI, I. I., 1937, *Phys. Rev.*, **51**, 652.
RALPH, H. I., 1968, *J. Phys.* C, **1**, 378.
ROSELER, M., ZIMMERMANN, R., and RICHERT, W., 1984, *Phys. Stat. sol.* B, **121**, 609.
RORISON, J. M., 1987, *J. Phys.* C, **20**, L311.
ROULET, B., GOVORET, J., and NOZIÈRES, P., 1969, *Phys. Rev.*, **178**, 1072.
RUCKENSTEIN, A. E., SCHMITT-RINK, S., and MILLER, R. C., 1986, *Phys. Rev. Lett.*, **56**, 504.
RUCKENSTEIN, A. E., and SCHMITT-RINK, S., 1987, *Phys. Rev.* B, **35**, 7551.
SANDERS, G. D., and BAJAJ, K. K., 1987a, *Phys. Rev.* B, **35**, 2308; 1987b, *J. vac. Sci. Technol.* B, **5**, 1295.
SCHAEFER, W., BINDER, R., and SCHULDT, K.-H., 1988a, *Z. Phys.* B, **70**, 145.
SCHAEFER, W., BINDER, R., SCHULDT, K.-H., and TREUSCH, J., 1987, *Proceedings of the 18th International Conference on the Physics of Semiconductors*, edited by O. Engström (Singapore: World Scientific), p. 1449.
SCHAEFER, W., SCHULDT, K.-H., BINDER, R., and TREUSCH, J., 1988b, *J. Lumin.*, **40/41**, 569.
SCHAEFER, W., and TREUSCH, J., 1986, *Z. Phys.* B, **63**, 407.

SCHAEFER, W., 1988, *Festkörperprobleme/Advances in Solid State Physics*, volume 28, p. 63.
SCHMITT-RINK, S., 1988, AT&T preprint.
SCHMITT-RINK, S., and CHEMLA, D. S., 1986, *Phys. Rev. Lett.*, **57**, 2752.
SCHMITT-RINK, S., CHEMLA, D. S., and HAUG, H., 1988, *Phys. Rev.* B, **37**, 941.
SCHMITT-RINK, S., CHEMLA, D. S., and MILLER, D. A. B., 1985, *Phys. Rev.* B, **32**, 6601.
SCHMITT-RINK, S., and ELL, C., 1985, *J. Lumin.*, **30**, 585.
SCHMITT-RINK, S., ELL, C., KOCH, S. W., SCHMIDT, H. E., and HAUG, H., 1984, *Solid St. Commun.*, **52**, 123.
SCHMITT-RINK, S., ELL, C., and HAUG, H., 1986, *Phys. Rev.* B, **33**, 1183.
SCHMITT-RINK, S., MILLER, D. A. B., and CHEMLA, D. S., 1987, *Phys. Rev.* B, **35**, 8113.
SCHUDA, F., STROUD, JR, C. R., and HERCHER, M., 1974, *J. Phys.* B, **7**, L198.
SCHULTHEIS, L., KUHL, J., HONOLD, A., and TU, C. W., 1986a, *Phys. Rev. Lett.*, **57**, 1635.
SCHULTHEIS, L., KUHL, J., HONOLD, A., and TU, C. W., 1986b, *Phys. Rev. Lett.*, **57**, 1797.
SCHULTHEIS, L., KOEHLER, K., and TU, C. W., 1987, *Phys. Rev.* B, **36**, 6609.
SCHWARTZ, C., 1987, *Appl. Phys. Lett.*, **50**, 457.
SCHWEIZER, H., FORCHEL, A., HANGLEITER, A., SCHMITT-RINK, S., LOEWENAU, J. P., and HAUG, H., 1983, *Phys. Rev. Lett.*, **51**, 698.
SEEL, M., LIEGENER, C. M., FORNER, W., and LADIK, J., 1988, *Phys. Rev.* B, **37**, 956.
SEGALL, B., 1966, *Phys. Rev.*, **150**, 734.
SHAM, L. J., and SCHLÜTER, M., 1983, *Phys. Rev. Lett.*, **51**, 1888.
SHANK, C. V., FORK, R. L., YEN, R., SHAH, J., GREENE, B. I., GOSSARD, A. C., and WEISBUCH, C., 1983, *Solid St. Commun.*, **47**, 981.
SHEN, Y. R., 1984, *The Principles of Nonlinear Optics* (New York: Wiley).
SHIMIZU, A., 1988a, *Phys. Rev. Lett.*, **61**, 613; 1988b, *Phys. Rev.* B, **37**, 8527.
SHINADA, M., and SUGANO, S., 1966, *J. phys. Soc. Japan*, **21**, 1936.
SHORTHOSE, M. G., MACIEL, A. C., RYAN, J. F., SCOTT, M. D., MOSELEY, A., DAVIES, J. I., and RIFFAT, J. R., 1987, *Appl. Phys. Lett.*, **51**, 493.
SILIN, A. P., 1977, *Soviet Phys. Solid St.*, **19**, 77.
SINGH, J., 1986, *Appl. Phys. Lett.*, **48**, 434.
SINGH, J., and HONG, S., 1986, *IEEE J. quant. Electron.*, **22**, 2017.
SINGWI, K. S., TOSI, M. P., LAND, R. H., and SJOLANDER, A., 1968, *Phys. Rev.*, **176**, 589.
SKOLNICK, M. S., RORISON, J. M., NASH, K. J., MOWBRAY, D. J., TAPSTER, P. R., BASS, S. J., and PITT, A. D., 1987, *Phys. Rev. Lett.*, **58**, 2130.
SMITH, D. L., 1986, *Solid St. Commun.*, **57**, 919.
SMITH, D. L., and MAILHIOT, C., 1987, *Phys. Rev. Lett.*, **58**, 1264.
SMITH, P. W., SILBERBERG, Y., and MILLER, D. A. B., 1985, *J. opt. Soc. Am.* B, **2**, 1228.
SOORYAKUMAR, R., CHEMLA, D. S., PINCZUK, A., GOSSARD, A. C., WIEGMANN, W., and SHAM, L. J., 1985, *Solid St. Commun.*, **54**, 859.
SOORYAKUMAR, R., PINCZUK, A, GOSSARD, A. C., CHEMLA, D. S., and SHAM, L. J., 1987, *Phys. Rev. Lett.*, **58**, 1150.
STERN, F., and DAS SARMA, S., 1984, *Phys. Rev.* B, **30**, 840.
STERN, F., and HOWARD, W. E., 1967, *Phys. Rev.*, **163**, 816.
STOLZ, H., 1974, *Einführung in die Vielelektronentheorie der Kristalle* (Berlin: Akademie-Verlag).
STURGE, M. D., 1962, *Phys. Rev.*, **127**, 768.
TAI, K., HEGARTY, J., and TSANG, W. T., 1987b, *Appl. Phys. Lett.*, **51**, 86; 1987c, *Appl. Phys. Lett.*, **51**, 152.
TAI, K., JEWELL, J. L., TSANG, W. T., TEMKIN, H., PANISH, M., and TWU, Y., 1987a, *Appl. Phys. Lett.*, **50**, 795.
TAKEOKA, T., YAMANISHI, M., KAN, Y., and SUEMUNE, I., 1987, *Jap. J. appl. Phys.*, **26**, L117.
TARUCHA, S., IWAMURA, H., SAKU, T., and OKAMOTO, H., 1985, *Jap. J. appl. Phys.*, **24**, L442.
TARUCHA, S., KOBAYASHI, H., HORIKOSHI, Y., and OKAMOTO, H., 1984, *Jap. J. appl. Phys.*, **23**, 874.
TEMKIN, H., GERSHONI, D., and PANISH, M. B., 1987, *Appl. Phys. Lett.*, **50**, 1776.
THARMALINGAM, K., 1963, *Phys. Rev.*, **130**, 2204.
THUSELT, F., 1983, *Phys. Lett.* A, **94**, 93.
TOTSUJI, H., 1975, *J. phys. Soc. Japan*, **39**, 253.
TRAENKLE, G., LACH, E., FORCHEL, A., SCHOLZ, F., ELL, C., HAUG, H., WEIMANN, G., GRIFFITHS, G., KROEMER, H., and SUBBANNA, S., 1987b, *Phys. Rev.* B, **36**, 6712.

TRAENKLE, G., LEIER, H., FORCHEL, A., HAUG, H., ELL, C., and WEIMANN, G., 1987a, *Phys. Rev. Lett.*, **58**, 419.
TSANG, L., AHN, D., and CHUANG, S. L., 1987, *Appl. Phys. Lett.*, **52**, 697.
TSUI, D. C., STOERMER, H. L., and GOSSARD, A. C., 1982, *Phys. Rev. Lett.*, **48**, 1559.
URBACH, F., 1953, *Phys. Rev.*, **92**, 1324.
VALATIN, J. G., and BUTLER, D., 1958, *Nuovo Cim.*, **10**, 37.
VAN ECK, T. E., CHU, P., CHANG, W. S. C., and WIEDER, H. H., 1986, *Appl. Phys. Lett.*, **49**, 135.
VINA, L., COLLINS, R. T., MENDEZ, E. E., and WANG, W. I., 1986, *Phys. Rev.* B, **33**, 5939; 1987b, *Phys. Rev. Lett.*, **58**, 832.
VINA, L., MENDEZ, E. E., WANG, W. I., CHANG, L. L., and ESAKI, L., 1987a, *J. Phys.* C, **20**, 2803.
VINTER, B., 1976, *Phys. Rev.* B, **13**, 4447.
VISSCHER, P. B., and FALICOV, L. M., 1971, *Phys. Rev.* B, **3**, 2541.
VON LEHMEN, A., CHEMLA, D. S., ZUCKER, J. E., and HERITAGE, J. P., 1986b, *Optics Lett.*, **11**, 609.
VON LEHMEN, A., ZUCKER, J. E., HERITAGE, J. P., and CHEMLA, D. S., 1987, *Phys. Rev.* B, **35**, 6479.
VON LEHMEN, A., ZUCKER, J. E., HERITAGE, J. P., CHEMLA, D. S., and GOSSARD, A. C., 1986a, *Appl. Phys. Lett.*, **48**, 1479.
WAKITA, K., KAWAMURA, Y., NAKAO, M., and ASAHI, H., 1987, *IEEE J. quant. Electron.*, **23**, 2210.
WAKITA, K., KAWAMURA, Y., YOSHIKUNI, Y., and ASAHI, H., 1985a, *Electron. Lett.*, **21**, 338.
WAKITA, K., KAWAMURA, Y., YOSHIKUNI, Y., and ASAHI, H., 1985b, *Electron. Lett.*, **21**, 574.
WAKITA, K., KAWAMURA, Y., YOSHIKUNI, Y., ASAHI, H., and UEHARA, S., 1985c, *Electron. Lett.*, **21**, 951; 1986, *IEEE J. quant. Electron.*, **22**, 1831.
WAKITA, K., YOSHIKUNI, Y., NAKAO, M., KAWAMURA, Y., and ASAHI, H., 1987, *Jap. J. appl. Phys.*, **26**, L1629.
WATANABE, K., KARASAWA, T., KOMATSU, T., and KAIFU, Y., 1986, *J. phys. Soc. Japan*, **55**, 897.
WAUTELET, M., and LAUDE, L. D., 1978, *Phys. Stat. sol.* B, **89**, 275.
WEBER, C., KLINGSHIRN, C., CHEMLA, D. S., MILLER, D. A. B., CUNNINGHAM, J. E., and ELL, C., 1988, *Phys. Rev.* B, **38**, 12748.
WEINER, J. S., CHEMLA, D. S., MILLER, D. A. B., HAUS, H. A., GOSSARD, A. C., WIEGMANN, W., and BURRUS, C. A., 1985b, *Appl. Phys. Lett.*, **47**, 664.
WEINER, J. S., CHEMLA, D. S., MILLER, D. A. B., WOOD, T. H., SIVCO, D., and CHO, A. Y., 1985a, *Appl. Phys. Lett.*, **46**, 619.
WEINER, J. S., MILLER, D. A. B., and CHEMLA, D. S., 1987a, *Appl. Phys. Lett.*, **50**, 842.
WEINER, J. S., GOSSARD, A. C., ENGLISH, J. H., MILLER, D. A. B., CHEMLA, D. S., and BURRUS, C. A., 1987b, *Electron. Lett.*, **23**, 75.
WEINER, J. S., MILLER, D. A. B., CHEMLA, D. S., DAMEN, T. C., BURRUS, C. A., WOOD, T. H., GOSSARD, A. C., and WIEGMANN, W., 1985c, *Appl. Phys. Lett.*, **47**, 1148.
WEINER, J. S., PEARSON, D. B., MILLER, D. A. B., CHEMLA, D. S., SIVCO, D., and CHO, A. Y., 1986, *Appl. Phys. Lett.*, **49**, 531.
WEINERT, H., HENNEBERGER, F., WOGGON, U., URALTSEV, I. N., and BRUEHL, H.-G., 1987, *Physica scripta*, **35**, 76.
WEISBUCH, C., DINGLE, R., GOSSARD, A. C., and WIEGMANN, W., 1981, *Solid St. Commun.*, **38**, 709.
WHITEHEAD, M., PARRY, G., WOODBRIDGE, K., DOBSON, P. J., and DUGGAN, G., 1988, *Appl. Phys. Lett.*, **52**, 345.
WOOD, T. H., BURRUS, C. A., MILLER, D. A. B., CHEMLA, D. S., DAMEN, T. C., GOSSARD, A. C., and WIEGMANN, W., 1984, *Appl. Phys. Lett.*, **44**, 16.
WOOD, T. H., CARR, E. C., BURRUS, C. A., TUCKER, R. S., CHIU, T. H., and TSANG, W. T., 1987a, *Electron. Lett.*, **23**, 540.
WOOD, T. H., TKACH, R. W., and CHRAPLYVY, A. R., 1987b, *Appl. Phys. Lett.*, **50**, 798.
WU, F. Y., EZEKIEL, S., DUCLOY, M., and MOLLOW, B. R., 1977, *Phys. Rev. Lett.*, **38**, 1077.
WU, JI-WEI, and NURMIKKO, A. V., 1987, *Phys. Rev.* B, **36**, 4902.
XU WANG, XI, XIA LIANG, and KAN CHANG, 1988, *Solid St. Commun.*, **65**, 83.
YAMAMOTO, H., ASADA, M., and SUEMATSU, Y., 1985, *Electron. Lett.*, **21**, 579.

YAMANAKA, K., FUKUNAGA, T., TSUKADA, N., KOBAYASHI, K. L. I., and ISHII, M., 1986, *Appl. Phys. Lett.*, **48**, 840.
YAMANISHI, M., 1987, *Phys. Rev. Lett.*, **59**, 1014.
YAMANISHI, M., and SUEMUNE, I., 1983, *Jap. J. appl. Phys.*, **22**, L22.
YAMANISHI, M., USAMI, Y., KAN, Y., and SUEMUNE, I., 1985, *Jap. J. appl. Phys.*, **24**, L586.
YANG QING, and YANG CHU-LIANG, 1987, *J. Phys.* C, **20**, 5125.
YU, P. W., REYNOLDS, D. C., BAJAJ, K. K., LITTON, C. W., MASSELINK, W. T., FISCHER, R., and MORKOÇ, H., 1985, *J. vac. Sci. Technol.* B, **3**, 624.
ZIMMERMANN, R., 1976, *Phys. Stat. sol.* B, **76**, 191; 1988a, *Ibid.*, **146**, 371; 1988b, *Ibid.*, **146**, 545; 1988c, *Proceedings of the 19th International Conference on Semiconductors* (Warsaw) (to be published).
ZIMMERMANN, R., KILIMANN, K., KRAEFT, W. D., KREMP, D., and ROEPKE, G., 1978, *Phys. Stat. sol.* B, **90**, 175.
ZIMMERMANN, R., ROESLER, M., and ASNIN, V. M., 1981, *Phys. Stat. sol.* B, **107**, 579.
ZUCKER, J. E., and HENDRIKSON, T. L., 1988, *Appl. Phys. Lett.*, **52**, 945.